THE UNIVERSITY OF
SYDNEY

Hydrodeoxygenation of bio-oil model compounds on supported noble metal catalysts

A thesis submitted in partial fulfillment of the requirements for the degree of Master of Philosophy

By

Mengmeng Chen

School of Chemical and Biomolecular Engineering

The University of Sydney

March, 2013

Supervisor: Dr. Jun Huang

Declaration

I declare this thesis is to the best of my own knowledge, the entire work has not been submitted previously for any other degree.

Mengmeng Chen

March 2013

Abstract

This thesis focuses on understanding acidic effects on the mechanisms of Pt or Pd-catalyzed bio-oil model ketone or aldehyde hydrodeoxygenation (HDO) and application of nanocatalysts - supported Pt and Pd with different surface acidity in the hydrodeoxygenation of acetophenone and benzaldehyde.

The first part of the thesis addressed the understanding of bio-oil model ketone compound - acetophenone hydrodeoxygenation mechanism over alumina and silica-alumina supported Pt and Pd catalysts by in-situ attenuated total reflection infrared spectroscopy (ATR-IR) in combination with modulation excitation spectroscopy (MES) and phase sensitive detection (PSD). Experimental results indicated acidic supports promoted the hydrodeoxygenation of acetophenone (AP) to produce ethylbenzene (EB). Specially, on alumina supported Pt, AP was predominantly adsorbed on Pt via its η^1 (O) configuration and this species was hydrogenated with high chemoselectivity to 1-phenylethanol (PE). On silica-alumina supported Pd, hydrodeoxygenation of AP to EB involves transformation of a carbonyl group to PE via η^1 (O) configuration, followed by a dehydration producing styrene on acidic sites of supports, the styrene was further hydrogenated to EB on Pd.

The second part focused on the application of acidic supports supported catalysts Pt/Al-MCM-41 and Pt/SiO_2-Al_2O_3 on hydrodeoxygenation of acetophenone and benzaldehyde. Results indicated that Pt/Al-MCM-41 catalysts serve as bifunctional

catalysts in the hydrogenation of AP. The overall activity over the noble metal catalysts on acidic supports MCM-41 increased with the increase of surface acidity up to support Si/Al=20, further increase the surface acidity leads to the decrease of catalytic activity. The increase of surface acidity up to Si/Al=20 also promotes the hydrogenation of aromatic ring to produce CMK and CE. For hydrodeoxygenation of benzaldehyde, products toward hydrogenation of both carbonyl and aromatic ring can be produced on a reference Pt/Al_2O_3 catalyst at 80°C whereas when temperature was increased to 200°C, only toluene and benzene can be detected. SiO_2-doped Pt/SiO_2-Al_2O_3 catalysts showed 10%-20% higher catalytic activity than reference catalyst of Pt/Al_2O_3 under similar reaction condition. Acidity did also influence catalytic selectivity of benzaldehyde hydrodeoxygenation, toluene prefers to form on relative low acidic catalysts whereas methylcyclohexane was more easily formed on high acidic catalysts.

List of publications

Journal paper:

1. Chen, M., et al., *Molecular Insight into Pt-Catalyzed Chemoselective Hydrogenation of an Aromatic Ketone by In Situ Modulation–Excitation IR Spectroscopy.* ACS Catalysis, 2012. 2(9): p. 2007-2013.

2. Wang, Z., et al., *Palladium-doped silica–alumina catalysts obtained from double-flame FSP for chemoselective hydrogenation of the model aromatic ketone acetophenone.* Journal of Catalysis, 2013. **302**(0): p. 10-19.

Conference paper:

1. Chen, M., et al., *In Situ Modulation Excitation IR Study on the Dominant Product of Pt-Catalyzed Aromatic Ketone Hydrogenation*, Advanced Materials Research, 2013, 683, 271.

Acknowledgments

First, I would like to express my great thanks to my supervisor Dr. Jun Huang for his guidance, patience and for opportunities he has provided for me. I am particularly grateful to him for his support for my visiting a world leading lab at ETH Zürich.

I also would like to thank all of my colleagues. They help me out and give me a lot of encouragement throughout the whole project. Thanks Kevin for his help with experimental set-up and also for his assistance with X-ray diffractometer, BET surface area and TEM measurements. Thanks Alex for his help with NMR measurements.

Special thanks must go to Prof. Baiker and Dr. Nobutaka. Maeda at ETH Zürich for training me in-situ IR spectroscopy.

I am thankful to my family and friends for their constant support.

Table of Contents

List of figures

List of tables

List of schemes

1 Introduction

1.1 Bio-oil

Due to limited fossil-based resources, increased consumption for fuels as well as environmental concerns raised by the use of crude-oil, developing economical and energy-efficient processes for the sustainable production of fuels and chemicals has become an essential task.[1] Biomass is the only sustainable and renewable source of organic carbon for producing bio-fuels and valuable chemicals.[2] Biomass derived energy is almost carbon-neutral because the generated carbon dioxide during biomass conversion can be consumed by a new cycle of biomass growth.[3]

Generally, biomass can be classified into three groups (i) lignocellulosics (cellulosics) or woody biomass, (ii) amorphous sugars and (iii) triglycerides. Lignocellulosic biomass consists of three main units: cellulose, hemicellulose, and lignin[4] which is served as the cheapest, most abundant biomass. In addition, its regeneration costs relatively less time.[5]

Converting solid biomass into liquid product is of great importance. Generally, lignocellulosic (cellulosic) biomass can be converted to liquid product through hydrolysis (production of aqueous sugarsolutions), fast pyrolysis (bio-oil production) and liquefaction (bio-oil production).[6]

Bio-oils can be obtained through technologies of fast pyrolysis and direct high pressure liquefaction. Fast pyrolysis is a process with high temperature under inert atmosphere whereas high pressure liquefaction is a mild temperature process with solvent under high pressure.[7] Bio-oils are dark brown and fluid liquids which are a complex mixture of acids (acetic, propanoic), esters (methyl formate, butyrolactone, angelica lactone), alcohols (methanol, ethylene glycol, ethanol), ketones (acetone), aldehydes (acetaldehyde, formaldehyde, ethanedial), miscellaneous oxygenates (glycolaldehyde, acetol), furans (furfural alcohol, 5-hydroxymethylfurfural, furfural), phenols (phenol, dihydroxybenzene, methyl phenol, dimethyl phenol), guaiacols (isoeugenol, eugenol, 4-methyl guaiacol), and syringols (2,6-dimethoxyphenol, syringaldehyde, propyl syringol).[8-10] Sfetsas et al.[11] analyzed the composition of three different bio-oil samples. The composition of bio-oils can be summarized in the below figure 1.1.

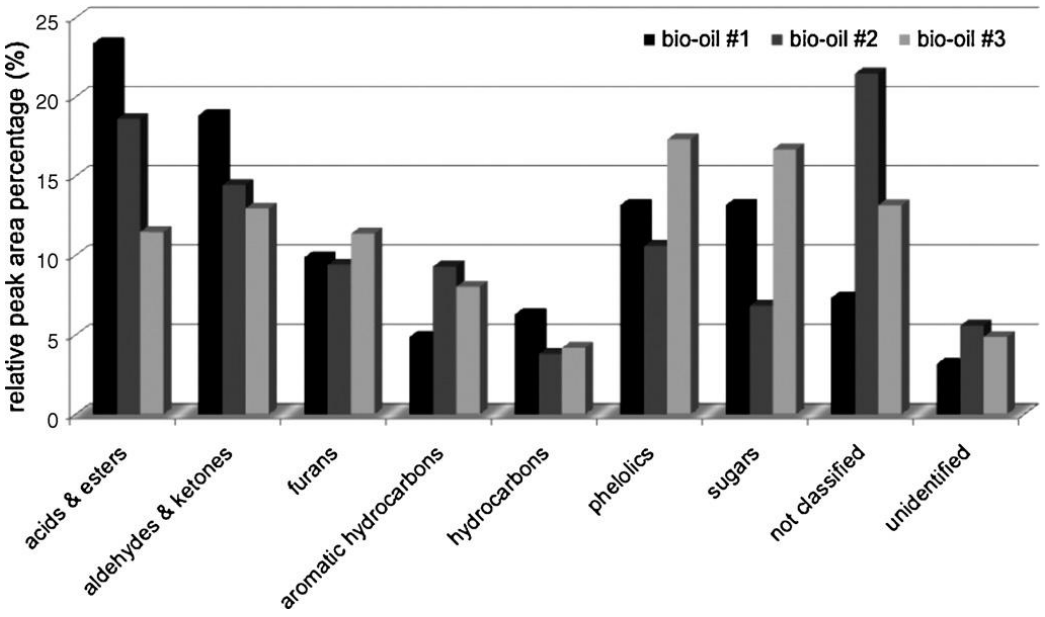

Figure 1.1 Compositions in bio-oil samples[11]

1.2 Bio-oil hydrodeoxygenation (HDO)

Bio-oil obtained from biomass fast pyrolysis or liquefaction is served as a promising second-generation source of renewable energy. However, high oxygen content in fast pyrolysis derived bio-oil results in the unsuitability of its direct application as liquid transportation fuel, because a high proportion of oxygen can cause problems such as thermal instability, low heating value, immiscibility with fossil fuels, tendency to polymerization and storage difficulties. The oxygen content of the primary liquids from pyrolysis may approach 50%, whereas that from liquefaction is less than 25%.[12-15] Based on above concerns, it is necessary to upgrade bio-oil before it can be used as a substitute for diesel and gasoline fuels. Generally, upgrading methods include physical and chemical processes, physical upgrading is to blend pyrolysis oil directly with petroleum diesel and chemical upgrading include catalytic cracking of pyrolysis vapors with zeolites[16, 17] and hydrodeoxygenation[18]. One of the most effective hydrotreating methods of removing oxygen is hydrodeoxygenation. Bio-oil hydrodeoxygenation is conventionally performed in the temperature range of 300 ℃ to 600 ℃ with high-pressure H_2 in the presence of heterogeneours catalysts. The process can be performed in bath or continuous system with catalysts.[19, 20] Regarding catalysts in bio-oil hydrodeoxygenation, sulfided CoMo and NiMo are most frequently applied. Except the use of sulfided CoMo and NiMo catalysts, supported noble catalysts such as Pt/SiO_2-Al_2O_3 and Ru-based have also been applied.[6] Conventional hydrotreating method with high temperature results in high levels of char/coke production that plug the reactor bed.[21, 22] To solve these problems, a two-step method was then developed that

a low temperature step was firstly performed below 573 K to remove oxygen containing compounds, followed by hydrodeoxygenation at conventional higher temperatures. The low temperature process was employed to avoid chemical instability of unsaturated double bonds such as olefins, aldehydes and ketones, thus achieving better storage and transport. This treatment could transform bio-oils into oils with a similar composition to high pressure oils. Afterwards, a higher temperature treatment between 350 ℃ and 425 ℃ was applied for elimination of phenolic and furanic oxygens. For both steps, a sulfided CoMo or NiMo-based catalyst is used. In comparison with single-step method, the two-step method is advantageous because it saves 13% hydrogen consumption for the production of equivalent gasoline yield.[23-26]

1.3 Hydrodeoxygenation of Bio-oil Model Compounds

Compared to hydrotreatment tests with derived pyrolysis oil, the use of model compounds possess several advantages. One of the advantages is that it gives more insight in the reaction mechanisms and pathways as well as in the way catalyst works. Another advantage is that catalytic model reactions are independent of competitive thermal polymerization reactions. Furthermore, it also permits to save much of the time and effort that would be required by the difficult analysis of pyrolytic oils.[27] Therefore, HDO study of oxygen-containing model compounds is of great importance. In bio-oil model hydrodeoxygenation, it is highly desirable to selectively hydrodeoxygenate

oxygenates because selective hydrodeoxygenation can reduce excessive energy consumption.[6]

1.3.1 Furanic and phenolic compounds

Furanic and phenolic compounds account for a large amount of bio-oil. Thus, most study of hydrodeoxygenation of oxygen-containing compounds has focused on furanic and phenolic groups. The hydrodeoxygenation of furanic groups has been widely discussed, furan and benzofuran have been commonly used as model compounds.[28-32] Among these studies, the effect of pretreatment on the HDO activity and distribution of products was examined. It is indicated that the sulfided catalyst showed much better catalytic performance than the reduced catalyst.[28] Hydrodeoxygenation mechanism of furanic groups was also investigated on conventional sulfide CoMo and NiMo catalysts, and details of this will be discussed in section 1.10.1.[28-31]

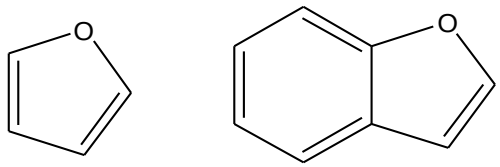

Furan Benzofuran

Figure 1.2 Furanic compounds

The hydrodeoxygenation of phenolic compounds has also been widely studied. Phenol and mono- and dimethyl substituted phenols have been used as model compounds. Conventional sulfided CoMo and NiMo catalysts were applied for the hydrodeoxygenation of these model compounds. Generally, catalytic reactivity of sulfided CoMo and NiMo on different models was examined, the promotion effect of Co

and Ni was also studied. Some authors investigated catalytic kinetics and proposed catalytic hydrodeoxygenation mechanism as well as reaction pathways.[33-39]

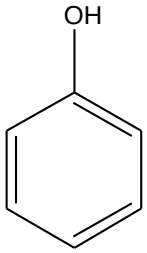

Phenol

Figure 1.3 Phenolic compound

1.3.2 Carbonyl, carboxylic groups

However, it is reported carboxylic acids, ketones and aldehydes have also been detected in significant amounts in bio-oils.[24, 40] The study of the hydrodeoxygenation of these groups is very important in the context of the upgrading of bio-oils because they are the main cause of instability, and polymerisation because of their high chemical reactivity. The deoxygenation of these compounds leads to the stabilisation of the oils. This stablisation could be the first step of a full refining process in order to avoid polymerisation at the standard hydrotreating temperatures or, another interesting possibility, the reaction could be stopped at this stage leading to the production of a partially deoxygenated oil useful for the electricity production in turbines or diesel engines.[27] However, the literature concerning the hydrodeoxygenation of these groups is very scarce. Maier et al.[41] studied the transformation of ketones in a methylene group over a metallic nickel catalyst. Weisser et al.[42] reported the hydrogenation of ketones over single metal sulphides. Concerning typical bimetallic hydrotreating catalysts,

only Durand et al.[43] worked on the hydrogenation of ketones over sulphided NiMo/alimiina. Delmon and co-workers studied sulfided CoMo catalyst on the hydrodeoxygenation of bio-oil model compounds contained phenolic, ketonic, carboxylic or furanic groups. It is suggested that the hydrogenation of the ketonic group is performed at a temperature 100− 200 ℃ lower than the temperature needed for the elimination of methoxy, phenolic and furanic oxygens. The carboxylic ester group has an intermediate reactivity.[12]

Acetophenone as one of the most simple and important aromatic ketones, its hydrogenation on supported noble catalysts has been widely investigated. AP hydrogenation has been studied on noble metals such as Pt and Pd.[44-46] Pt hydrogenates carbonyl and phenyl groups at similar rates producing comparable amounts of PE and CMK, PE and CMK products are then hydrogenated to CE.[44, 45] Palladium promotes selective hydrogenation of C=O bond of AP in the formation of PE and is also active for consecutively transforming PE to EB by hydrogenolysis.[46] AP hydrogenation has been also investigated on non-noble metals, especially on Ni-based catalysts. These studies show that nickel promotes the selective AP hydrogenation to PE, but variables quantities of CMK and CE are also formed. Moreover, Ni is active for producing EB by PE hydrogenolysis.[47-50]

Concerning the hydrogenation of unsaturated aldehydes, one important reaction is the hydrogenation of benzaldehyde. Southwick and Coven found Pd the most active by comparing benzaldehyde hydrogenation over Pd, Pt, Rh and Ru dispersed on carbon at

room temperature and atmospheric pressure.[51] Merabti et al.[52] studied benzaldehyde hydrogenation over activated carbon supported Cu and Ni catalysts. The obtained yields depend on the nature of the metal active phase and reaction temperature. Copper catalyst selectively formed benzylalcohol (50–100%) which gave toluene (up to 50%) at high temperature. Supported Ni catalyst strongly preferred benzaldehyde hydrogenolysis to benzene (about 50% of selectivity). At high temperature it also enhanced aromatic ring hydrogenation to methylcyclohexane (up to 50% of selectivity) at the expense of toluene. Pinna et al.[53] investigated benzaldehyde hydrogenation over active carbon, silica and alumina supported Pd catalysts, high selectivity to benzyl alcohol and toluene was obtained over Pd/C, it is also found that a strong decrease of turnover frequency (almost an order of magnitude) was observed for very small (around 1.5 nm) Pd particles, pointing to structure sensitivity of benzaldehyde hydrogenation over Pd. M. Albert Vannice[54] et al. learned benzaldehyde hydrogenation on Pt/TiO_2, $Pt/\eta\text{-}Al_2O_3$ and Pt/SiO_2 and $Pt/SiO_2\text{-}Al_2O_3$, it is proven that Pt/TiO_2 with high temperature reduction was the most active, and Pt/TiO_2 (HTR) retained 100% selectivity to benzyl alcohol at conversions up to at least 80% which is due to the enhancement of benzaldehyde with H_2 on special sites created at the metal–support interface. Also, both conversion and temperature affect the selectivity; benzyl alcohol was the only product at low conversions as reaction temperature ranged from 353K to 453K. Generally, the benzene hydrogenolysis product was usually observed as conversions increased and temperatures rose above 373 K, while toluene was formed at conversions greater than 50% and at temperatures near 423K or higher. For $Pt/SiO_2\text{-}Al_2O_3$, no benzyl alcohol was ever detected, and benzene was only produced at higher temperatures.

1.4 Disadvantages of conventional HDO catalysts for hydrodeoxygenation

The most commonly used catalysts for HDO reactions are conventional CoMo and NiMo catalysts in the oil refineries in hydrotreating processes.[34, 55] However, sulfur stripping from the surface of the catalyst occurs, causing deactivation of the catalyst and contamination of the products. Therefore, during the operation, sulfiding agents have to be added to avoid sulfur leaching from the surface thus maintaining the activity of the catalysts.[38, 56, 57] Furthermore, the Al_2O_3 support applied during hydrotreating processes is active for coke formation leading to catalyst deactivation. Due to above problems encountered, developing new catalysts which are active at low temperatures needed to prevent coke formation is desirable.[58] Finally, the potential of water poison is also one of the disadvantages of conventional sulfide CoMo and NiMo catalysts.[34]

1.5 Supports modification and development for conventional hydrotreating

Traditionally, Al_2O_3 is used as supports for hydrodeoxygenation reactions such as the hydrodeoxygenation of carbonyl, carboxylic and methoxyl groups. However, Al_2O_3 strongly adsorbs polycondensation products formed during hydrotreating, leading to coke formation. Therefore, experts try to modify Al_2O_3 or use other supports to improve catalytic performance. Centeno et al.[59] studied the influence of Pt-modified conventional $CoMo/Al_2O_3$ catalyst, it was shown that the addition of Pt accelerates the

hydrodeoxygenation of carbonyl group of 4-methylacetophenone. However, Pt-doping did not prevent the catalyst from coke formation.

Later on, neutral supports such as activated carbon was considered as an alternative. Then, activated carbon was used to substitute Al_2O_3 of sulfided $CoMo/Al_2O_3$ for hydrodeoxygenation reactions of 4-methylacetophenone, ethyl decanoate and 2-methoxyphenol representative of oxygenated functions of bio-oil under 280 ℃, almost no coking reactions were observed. However, sulfur agents still needs to be added.[60] Therefore, highly active and stable HDO catalysts that can perform under mild conditions need to be developed for hydrotreating process.

1.6 Supported noble catalysts

In recent years, efforts have been made on the development of noble catalysts to improve catalytic hydrodeoxygenation systems. By comparison with conventional metal sulfide catalysts, supported noble metal catalysts have a better hydrogenation performance at lower temperatures, which are very interesting candidates for bio-oil hydrogenation. Furthermore, supported metal catalysts do not require the addition of sulfur to maintain stability and are less prone to deactivation in the presence of water. The metals used as hydrogenation catalysts are also not prone to coke formation.[61] In addition, flexible catalyst design by tailoring active phase or support is also advantageous.[25, 58]

Noble catalysts have been used as a new generation catalysts for the hydrodeoxygenation of bio-oils. Gutierrez et al.[58] performed hydrodeoxygenation of guaiacol on noble catalysts such as supported monometallic Rh, Pd and Pt and bimetallic RhPd, PhPt and PdPt catalysts at 100 ℃ and 300 ℃. It is indicated that ZrO_2 supported noble catalysts showed high performance without contaminating products or being deactivated due to carbon deposition. A study by Lin et al.[62] compared Rh-based catalysts and conventional CoMo and NiMo catalysts for hydrodeoxygenation of guaiacol under temperature 300 ℃ to 400 ℃, it is demonstrated that Rh/ZrO_2 catalyst was the most effective catalyst among all catalysts used. Liu et al.[63] studied the hydrodeoxygenation of benzofuran on active carbon supported Pt, Pd and Pt-Pd bimetallic catalysts in temperature range from 300 ℃ to 360 ℃. The Pt-Pd bimetallic catalyst achieved highest deoxygenation with maximum 100% conversion and 65% selectivity to deoxygenated products under 340 ℃. Based on experimental results, a reaction pathway involving ketone isomerization was proposed. Overall, supported noble catalysts achieved very high catalytic performance in hydrodeoxygenation reactions.

1.6.1 Silica-alumina supports

It is generally accepted that the support properties can affect overall HDO activity. Addition of acids or acidic supports is often used to enhance the efficiency of catalysts for hydrogenation, hydrogenolysis, and hydrocracking processes.[64, 65] Silica-alumina supports are one kind of acidic supports in many applications. It is indicated the acidic support of silica-alumina increased the conversion of sorbitol.[66] Li et al. also reported

silica-alumina supported platinum achieved high performance in the hydrodeoxygenation of sorbitol.[20] Silica-alumina supported platinum was also applied for the aqueous-phase reforming of ethylene glycol, it was found that Pt/SiO_2-Al_2O_3 showed better catalytic activity in producing hydrogen that those CeO_2, ZnO_2 and SiO_2 supported Pt catalysts.[67] Lin et al. investigated a bio-oil model ketone – acetophenone hydrodeoxygenation on silica-alumina supported Pt catalyst and achieved high yield of desired product ethylbenzene.[68] Huang et al. reported a high catalytic activity in hydrodeoxygenation of bio-oil model ketone compound over a series of silica-alumina supported palladium catalysts with tunable surface acidity.[69]

1.6.2 MCM-41 and Al-MCM-41 supports

A new class of mesoporous silica material has been reported in recent years. MCM-41 as one of the M41S family members of ordered mesoporous silicates was first synthesized by Mobil scientists. MCM-41 containing one-dimensional channels with pore diameters in 15-100 A range possess a hexagonal arrangement of uniformly sized mesopores, large surface area (usually>1000m^2/g) and mild acidity.[70, 71] The high internal surface area, uniform pore channels and good thermal stabilities of this material attract significant attention in the application of adsorption and catalysis. However, purely silica MCM-41 materials have no Brønsted acidity. For the use as acid supports, much effort has been made on doping of Al into the framework of MCM-41 because the incorporation of tetrahedrally coordinated aluminum ions can create Brønsted acid sites by the thermal

decomposition of ammonium ions generating acidic protons at the Al-O(H)-Si bridges.[72]

The synthesis and characterization of Al-MCM-41 materials have been reported by several groups.[70, 73-75] Regarding Al-MCM-41, aspects such as the aluminium source in synthesis, the effect of aluminium incorporation on the structure of framework and the coordination state of aluminium in Al-MCM-41 materials have been investigated.[76-79] The influence of Al content on catalyst acidity was examined by a variety of tools such as temperature programmed desorption (TPD) and NMR.[72, 80] NMR spectroscopy was also demonstrated as a powerful tool for quantify catalyst acidity. Therefore, it was used to identify the amount of Brønsted acid sites of Al-MCM-41.[80-83] It is indicated that Al content influences the concentration of Brønsted acid sites. Weglarski et al.[82] observed an increase of Brønsted acidity up to a molar Si/Al ratio of 34. Mokaya et al.[83] reported about a constant Brønsted-to-Lewis site ratio up to a Si/Al ratio of 10.

1.6.3 Al-MCM-41 supported noble catalysts

Al-MCM-41 supported noble catalysts have been applied as bifunctional catalysts. One contribution can be considered as metal sites, the other one is acid sites generated by the incorporation of Al into MCM-41 framework. Al-MCM-41 supported noble catalysts have been used as efficient hydrogenation and hydrodeoxygenation catalysts. Among these studies, some researchers focused on the influence of the nature of metal, others investigated the effect of support acidity. Jacquin et al.[84] used novel supported Rh, Pt,

Ir and Ru mesoporous Al-MCM-41 as catalysts for the hydrogenation of naphthalene, ruthenium and iridium show highest selectivity towards hydrogenolysis and/or ring-opening products. Wang et al.[85] studied hydrogenation of benzene, toluene and *o*-xylene over a series of Al-MCM-41 supported platinum catalysts, it is suggested Al-MCM-41 supported platinum with moderate acidity produced beneficial result for hydrotreating benzene, toluene and *o*-xylene. Chatterjee et al.[86] performed hydrogenation of phenol in the presence of Al-MCM-41 supported palladium catalysts, this palladium catalyst is shown to be highly active and promotes the selective formation of cyclohexanone. Bejblova´ et al.[87] found that the hydrodeoxygenation yield of benzophenone to desire diphenylmethane on MCM-41 supported Pd is much higher than on alumina supported Pd.

1.7 HDO mechanism on conventional sulfide catalysts

Catalytic hydrodeoxygenation mechanisms are of great importance, and have been extensively studied on conventional sulfide catalysts.

1.7.1 HDO mechanism of furanic and phenolic compounds

Mechanisms of model compounds such as furanic compounds and phenolic compounds have been studied on conventional CoMo and NiMo catalysts.[24, 28, 36, 37, 88-92]

For mechanism study of hydrodeoxygenation of furanic compounds, furan is commonly used as a model compound. Furimsky[28] studied HDO mechanism of furan in the presence of a conventional cobalt molybdate catalyst at 8.4 kPa and 400 ℃, reaction pathway was proposed involving a rapid hydrogenation of butadiene as a possible primary product as well as a partial hydrogenation of the ring prior to the cleavage of one of the C-O bonds. Later on researchers also investigated the hydrodeoxygenation of benzofuran on a presulfided $CoMo/Al_2O_3$ catalyst at high H_2 pressure and in the temperature range of 220 ℃ to 260 ℃. A mechanism for the hydrodeoxygenation of benzofuran was proposed, requiring hydrogenation to o-ethylphenol prior to hydrodeoxygenation.[93] Overall, the products from HDO reactions of furanic model compounds result from dual reaction pathway mechanisms which include an initial partial hydrogenation of the oxygen-containing heterocyclic ring, followed by cleavage of one of the C-O bonds. The other parallel pathway can be concluded as direct elimination of oxygen without prior hydrogenation of the heterocyclic ring.[24, 28, 91-93] For mechanism study of hydrodeoxygenation of phenolic compounds, phenol, substituted phenols and dimethylphenol have been widely studied on conventional Al_2O_3 supported CoMo and NiMo catalysts at high H_2 pressure and in the temperature range of 200 ℃ to 400 ℃. Two reaction pathways of hydrodeoxygenation of all phenolic compounds have been proposed. One is the hydrogenation of aromatic ring followed immediately by an elimination process, leading to the removal of oxygen. The other one is the direct elimination of oxygen by a hydrogenolysis reaction which is ruptured by addition of hydrogen of the aromatic carbon-heteroatom bond.[34, 36, 37, 94]

1.7.2 HDO mechanism of ketones and aldehydes

The study of the hydrodeoxygenation of these groups is very important in the upgrading of bio-oils because they are the main cause of instability and polymerisation caused by their high chemical reactivity. The deoxygenation of these compounds leads to the stabilisation of the oils. It is also reported that bio-oils contain significant amount of ketones and aldehydes, carboxylic acids and esters, aliphatic and aromatic alcohols and ethers. Therefore, the elimination of these oxygenated groups is a necessary step for the full hydrorefining of bio-oils.[27, 89, 90]

However, the literature concerning the hydrodeoxygenation of these groups is very scarce. Durand et al. reported an efficient hydrodeoxygenation of ketones to corresponding hydrocarbons on sulfide NiMo catalyst at hydrogen pressure of 40 bar and 250 ℃.[43] Laurent and Delmon studied the hydrodeoxygenation of carbonyl group of an aromatic ketone 4-methylacetophenone on sulfide alumina supported CoMo and NiMo catalysts at temperatures higher than 200 ℃. 4-methylacetophenone was efficiently converted to ethylmethylbenzene without intermediate products detected which may be explained as alcohol product from 4-methylacetohphenone hydrogenation quickly dehydrated under high temperature and transformed to ethylmethylbenzene on dehydration catalyzed alumina support.[89]

The transformation of ketones to hydrocarbons is considered to undergo two possible mechanisms one can be concluded as a conversion of ketones to corresponding alcohols is considered as a first step, followed by a dehydration process to unsaturated ketones and

finally hydrogenated to saturated hydrocarbons. The other one is the conversion of ketones to corresponding alcohols as the first step. After ketones are converted to corresponding alcohols, C-OH bond of these alcohols can be directly hydrogenolyzed to hydrocarbons.[43, 89, 90]

1.7.3 Model compounds HDO mechanism on noble catalysts

Although supported noble catalysts have attracted increasing attention and showed promising catalytic activity for hydrodeoxygenation of bio-oils, experimental proof of mechanism investigation of hydrodeoxygenation of bio-oils on these catalysts is still limited.

1.7.3.1 Hydrodeoxygenation of furanic and phenolic compounds

For hydrodeoxygenation of furanic compounds on supported noble catalysts, only very few reports addressed mechanism. Liu et al.[63] studied hydrodeoxygenation of benzofuran over a series of silica-alumina supported monometallic Pt and Pd and alloyed Pt−Pd catalysts in a fixed-bed flow reactor at 280 ℃ and 3.0 MPa. Only one major route was found for the reaction network of HDO of benzofuran among the catalysts. First, benzofuran was transformed to 2,3-dihydrobenzofuran with the hydrogenation at the heterocyclic ring, followed by further conversion to octahydrobenzofuran at the benzene ring.

The mechanisms of phenolic compounds hydrodeoxygenation on noble catalysts have also been studied by several groups. The overall reaction pathway for the aqueous-phase hydrodeoxygenation of phenol to cyclohexane in the presence of a supported noble Pd/C catalyst proceeds by an initial metal-catalyzed hydrogenation of the aromatic ring followed by acid-catalyzed dehydration of cyclohexanol and metal-catalyzed hydrogenation of the cycloalkene.[88] J. Foster et al.[61] studied the hydrodeoxygenation of 3-methylphenol over a series of γ-Al_2O_3 and SiO_2 supported Pt catalysts at 533 K and 0.5 atm H_2, toluene and methylcyclohexane were detected as the main products. It was indicated that the reaction proceeds by a combination of Pt-catalyzed hydrogenation and acid-catalyzed dehydration reactions.

1.7.3.2 Hydrodeoxygenation of ketones and aldehydes

Concerning hydrodexoygenation of ketones and aldehydes, most of the existing reports focus on catalyst screening and optimization to improve catalytic properties in terms of their activity and selectivity,[69, 95-101] few studies have addressed the reaction kinetics and proposed mechanistic models.[102-106] However, mechanisms of the hydrodeoxygenation of ketones and aldehydes on noble catalysts have not been widely studied. Only very few reports addressed mechanisms of ketone hydrodeoxygenation at relatively high temperatures under working conditions. On the basis of in situ FT-IR spectroscopic study of the gas phase bio-oil model aromatic ketone - acetophenone (AP) hydrodeoxygenation on Pt/SiO_2, Chen et al.[45] concluded that the selectivity of AP hydrodeoxygenation strongly depends on the formation of fragments (CO, benzene,

toluene, and methane) originating from AP hydrogenolysis/decomposition and the strong adsorption of 1-phenylethanol (PE) on the Pt surface. These fragments were supposed to inhibit the bonding between the phenyl group and Pt surface, leading to a decrease in the rate the side reaction to 1-cyclohexylethanol (CE).[45] Since the hydrodeoxygenation of ketones on supported noble catalysts are usually operated at relatively low temperatures, it is essential to gain some insight into the mechanism of ketones hydrodeoxygenation at lower temperatures. Some researchers proposed the mechanism of hydrodeoxoygenation of ketones at relatively low temperature.[107] Procha´zkova´ et al.[108] studied hydrodeoxygenation of aldehydes such as benzaldehyde on a series of supported palladium catalysts (Pd/C, Pd/Beta and Pd/ZSM-5) in the temperature range from 30 to 130 ℃ and at pressure ranging from 1 to 6 MPa, it was proposed that the transformation of benzaldehyde to toluene proceeded by the hydrogenation-hydrogenolytic mechanism as well as by the direct hydrogenolysis of C=O bond. However, the lack of experimental evidence did not allow drawing an unambiguous conclusion.

1.8 Experimental spectroscopy techniques

Much information such as structure and orientation of adsorbates as well as on their interaction with the metal surface can be acquired from vibrational spectra from adsorbate layer. Therefore, vibrational spectroscopy is a powerful tool in fundamental studies of chemical reactions and catalysis at metal surfaces.[109] Techniques such as sum-frequency generation (SFG), electron energy loss spectroscopy (EELS) and infrared spectroscopy have been applied for the investigation of catalytic metal-gas interface. For

instance, the technique of sum-frequency spectroscopy has been successfully applied to the adsorption and oxidation of CO, hydrocarbon conversion such as ethylene hydrogenation and cyclohexene hydrogenation and dehydrogenation on Pt(111), active intermediates and their concentration has been detected.[110] Today, a great variety of spectroscopic methods[111] are applied in catalysis research, among which vibrational spectroscopies[112-114], particularly infrared spectroscopy, is probably the most versatile and most frequently employed.

1.8.1 Infrared spectroscopy

Infrared spectroscopy (IR) is based upon the interaction of electromagnetic radiation with species that possess a permanent or induced dipole moment and the excitation of different vibrational states. An IR spectrometer usually records the energy of the electromagnetic radiation which is transmitted through a sample as a function of the wavenumber or frequency.[115] IR has been used as a powerful tool in many research areas. IR spectroscopy was applied to catalysis at the end of the seventies. Very soon it appeared that a clearer vision of the investigated materials and mechanism of catalytic processes required operating conditions as close as possible to real application conditions for the catalysts.[116] The first in situ mechanism application was the study of the methanol synthesis over a $Cu/ZnAl_2O_4$ catalyst, at 523 K and under 1MPa of $CO+H_2$.[117]

IR techniques such as transmission IR spectroscopy (TIRS), diffuse reflectance IR Fourier transform spectroscopy (DRIFTS) and IR reflection-absorption spectroscopy

(IRRAS) and attenuated total reflection infrared spectroscopy (ATR-IR) are all suitable for in situ studies of the catalytic reaction system.

1.8.1.1 Diffuse reflectance infrared Fourier transform spectroscopy (DRIFTS)

Diffuse reflectance infrared Fourier transform spectroscopy (DRIFTS) was appeared and applied as a tool for monitoring adsorbed molecules at catalytic solid-gas interfaces.[118] Since its application, it was used for the mechanism investigation of gas phase catalytic reactions such as oxidation and hydrogenation and NOx storage-reduction.[119-122] Specially, Grunwaldt et al. studied CO oxidation on Au/TiO_2 and Au/ZrO_2. It was found that low coordinated gold sites are responsible for the adsorption of oxygen and carbon monoxide.[119] Weigel et al. also investigated CO and CO_2 hydrogenation over copper/zirconia to gain some insight into the mechanism of methanol synthesis. From the observed correlations it appears that adsorbed CO is the precursor to methanol. On the methanol synthesis catalyst, the adsorbed CO is further reduced to yield surface-bound formaldehyde and methylate, from which the desired methanol product is generated by hydrogenolysis or protolysis.[122]

1.8.1.2 Attenuated Total Reflection Infrared Spectroscopy (ATR-IR)

Conventional IR spectroscopy plays a key role for in situ solid-gas interfaces investigations.[123] However, in situ investigations for solid-liquid interfaces are still challenging. Recently, Attenuated total reflection infrared spectroscopy (ATR-IR) raised much attention because it possesses several features that are excellently suited for in situ

investigation of catalytic solid−liquid interfaces as encountered in heterogeneous catalysis.[124] It can provide information on the species adsorbed on the catalyst surface during reaction, such as intermediates, even in the presence of strongly absorbing solvents. In some cases, information about the catalyst itself can also be acquired. However, proper analysis of ATR-IR spectra of a multiphase system under working conditions is quite demanding because it simultaneously provides information about dissolved and adsorbed reactants and products, adsorbed intermediates, byproducts, and the catalyst itself as shown in Figure 1.4.[125]

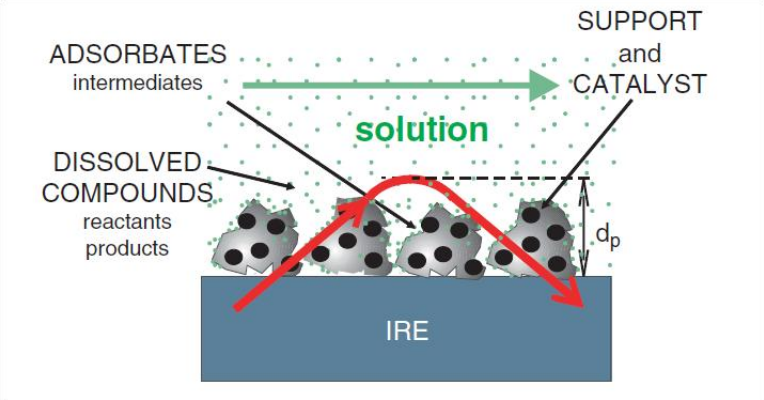

Figure 1.4 In situ ATR-FT-IR spectroscopy of heterogeneous solid–liquid catalytic reactions gives simultaneous information about dissolved species and species adsorbed on the catalyst

1.8.2 Attenuated Total Reflection Infrared Spectroscopy (ATR-IR) in combination with Modulation Excitation Spectroscopy (MES) and Phase Sensitive Detection (PSD)

Although ATR-IR shows significant potential for the investigation of solid-liquid interface, its limitations are not negligible. Too much information concerning solid-liquid interface obtained by ATR-IR raises difficulties in analyzing relevant spectra as shown in figure 1.4.[125] In order to solve this problem, much attention has been paid to the

combination of ATR-IR with modulation excitation spectroscopy (MES) and phase sensitive detection (PSD). Modulation technique can be applied when a system response reversibly or quasireversibly to a periodic external excitation such as temperature, pressure, concentration of a reactant. Consequently, all species in the system that are affected by this parameter will also change periodically at the same frequency as the stimulation.[126] Phase sensitive detection (PSD) is achieved by applying a mathematical treatment to modulation excitation spectroscopy (MES), this treatment enables significant enhancement of signal to noise ratio (S/N) and the extraction of kinetic information.[127-131] Thus, ATR-IR combined with MES and PSD can assist in obtaining very sensitive and selective signals as in figure 1.5 (iii).

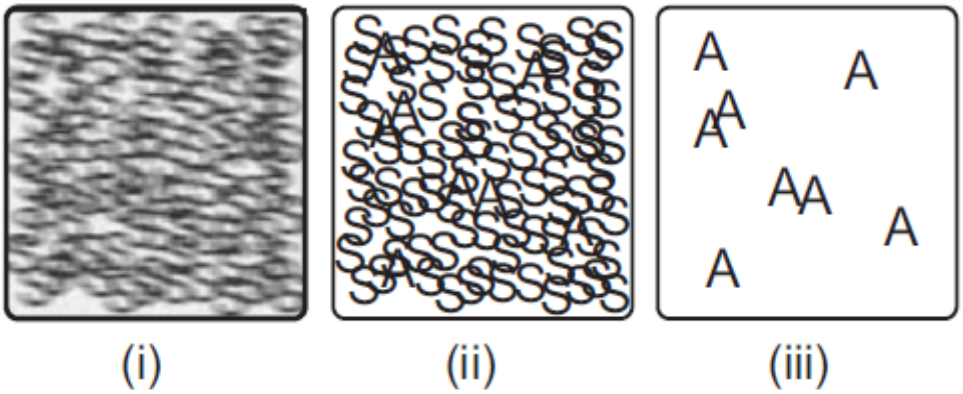

Figure 1.5 Three extreme situations of signals obtained by in situ spectroscopy of: (i) realistic; (ii) very sensitive; and (iii) very sensitive and selective methods. 'A' and 'S' represent active species and spectators, respectively

Very recently, the technique of ATR-IR in combination with MES and PSD was successfully applied for mechanism investigation of liquid phase catalytic reactions such as hydrogenation. Maeda et al.[129] applied this technique to investigate asymmetric hydrogenation of ketone on chirally modified Pt and found out the origin of involved

hydrogen atom of a typical an N–H–O type hydrogen bonding between the quinuclidine N atom of cinchonidine and the α-carbonyl O atom of the substrate which is hydrogen dissociated on Pt is involved in the interaction N–H–O between the chiral modifier, cinchonidine, and the ketone. Meemken et al.[132] used the combination of ATR-IR with MES and PSD to explore platinum-catalyzed asymmetric ketone hydrogenation. It indicates that the study extends the generally accepted model for enantiodifferentiation based on the formation of a H-bonding between the quinuclidine–N atom of the cinchona alkaloid and the oxygen of the a-carbonyl group of the ketone (N–H–O type H-bonding) and indicates that for some ketones the C9–O ··H ··O=C interaction has to be taken into account for explaining the enantiodifferentiation. It is again proved that ATR-IR in combination with MES and PSD is a powerful tool to explore the complex catalytic solid–liquid interface under reaction conditions.

2 Methodology

2.1 Introduction

In this chapter, experimental reagents and equipments will be described. Details of experimental procedures including catalysts preparation and characterization and catalytic tests will be introduced.

The technique process of attenuated total reflection infrared spectroscopy (ATR-IR) in combination with modulation excitation spectroscopy (MES) and phase sensitive detection (PSD) for mechanism investigation will be explained. Gas chromatography–mass spectrometry (GC-MS) was employed as the principal analytical method of catalytic tests.

2.2 Experimental and Methods

2.2.1 Chemicals

Acetophenone (AP) (Sigma-Aldrich, 99 %), 1-phenylethanol (PE) (Sigma-Aldrich, 98 %), 1-cyclohexylethanol (CE) (Sigma-Aldrich, 99 %), ethylbenzene (EB) (Sigma-Aldrich, 99 %), n-hexane (Sigma-Aldrich, 97 %), ethanol (Sigma-Aldrich, 99.8 %), benzaldehyde (Sigma-Aldrich, 99 %) and γ-Al_2O_3 (Umicore) were used as received.

2.2.2 Preparation of catalysts

2.2.2.1 Pt/Al_2O_3

Pt/Al_2O_3 catalyst was obtained from BASF-Engelhard 4759 with Pt dispersion of 0.27 and a BET surface area of 168 m^2/g.

2.2.2.2 Preparation of Pd/SiO_2-Al_2O_3

The catalysts were obtained by a flame spray pyrolysis (FSP) method according to the literature.[69] In brief, flame-made silica–alumina loaded with 5 wt% Pd nanoparticles (5 wt% Pd/SA) were prepared by dissolving the corresponding amounts of the precursor materials in a 1:1 (vol.%) mixture of acetic acid and methanol. The resulting solution was filtered over a glass filter, pumped through a capillary with 5 mL/min, and nebulized with 5 L/min O_2. The resulting spray was ignited by an annular supporting methane/oxygen flame (1.5/0.9 L/min) resulting in an approximately 6-cm-long flame. Particles were collected on a cooled Whatman GF6 filter (257 mm diameter). A Busch SV 1040C vacuum pump aided in particle recovery. The 5 wt% Pd/SA catalysts with different Si/Al ratio are denoted as Pd/SA-X, where X corresponds to the fraction of Al (Al at% = Al ×100 %/(Al + Si)) in the silica–alumina.[69]

2.2.2.3 Preparation of Pt/Al-MCM-41

Al-MCM-41 supports were used as obtained. $Pt(acac)_2$ (20 mg) diluted in toluene (7ml) was used as precursor for the impregnation. Each of 500 mg Al-MCM-41 supports with Si/Al ratio 10, 15, 20, 30, 40 and 50 was placed into the mixture of $Pt(acac)_2$ in toluene

for 24 h under magnetic stirring and room temperature. After impregnation, the derived mixtures were dried in ambient atmosphere at 25 ℃, followed by at 120 ℃ overnight and then calcinated at 350 ℃ in dry air stream for 2h.

2.2.2.4 Preparation of Pt/SiO_2-Al_2O_3

The catalysts were obtained according to the literature by a flame spray pyrolysis (FSP) method.[133] Specially, aluminum tri-sec-butoxide (Aldrich, >98%), hexamethyldisiloxane (HMDSO, Fluka, >98%) dissolved in 2-ethylhexanoic acid (Aldrich,>98%, 0.5 M) were used as aluminium and silicon precursors, respectively. The appropriate precursor amounts were mixed with diethyleneglycol - monobutylether (Fluka, >98%) and acetic anhydride (Aldrich, >98%) 1:1 by volume. The total support metal (Al + Si) concentration was kept constant at 0.6 M in these solutions. The nominal SiO_2 weight fraction in the product powder ranged from 0 to 100 wt%. As Pt precursor platinum(II)-bis(acetylacetonate) (Pt-70, Johnson Matthey) was added to the support solution to reach a nominal 4.7 wt.% Pt loading in the final powder product. The Pt/Al_2O_3–SiO_2 powders were produced in a laboratory scale FSP reactor described elsewhere[134]. The production rate ranged from 11 g/h for pure SiO_2 to 18.5 g/h for pure Al_2O_3. The powders were collected with the aid of a vacuum pump (Busch SV 1025 B) on a glass microfiber filter (Whatman GF/D, 257 mm in diameter).

2.2.3 Preparation of catalyst layer of Pt/Al_2O_3 and Pd/SiO_2-Al_2O_3

A thin film of pretreated catalyst was prepared for in situ IR measurements. A slurry of 90 mg catalyst in 10 ml ethanol was stirred overnight to achieve uniform suspension. Then, 1.6 ml of the slurry was brought onto a ZnSe internal reflection element (IRE, bevel of 45 º, 52 mm × 20 mm × 2 mm, Crystran Ltd.), and after complete evaporation of ethanol, the film was placed in a home-build stainless steel flow-through cell. The as-prepared catalyst layer adhered to the IRE so that no loss of catalyst was observed over the course of several hours under flow-through conditions. Prior to experiments, the Pt/Al_2O_3 and Pd/SiO_2-Al_2O_3 film layer was pretreated in situ by flowing hydrogen-saturated n-hexane for 3h at 323 K. In situ IR experiments were performed in the flow-through cell, which was mounted onto an ATR-IR attachment (OPTISPEC). The temperature of the cell was controlled by a thermostat (Julabo, F25).

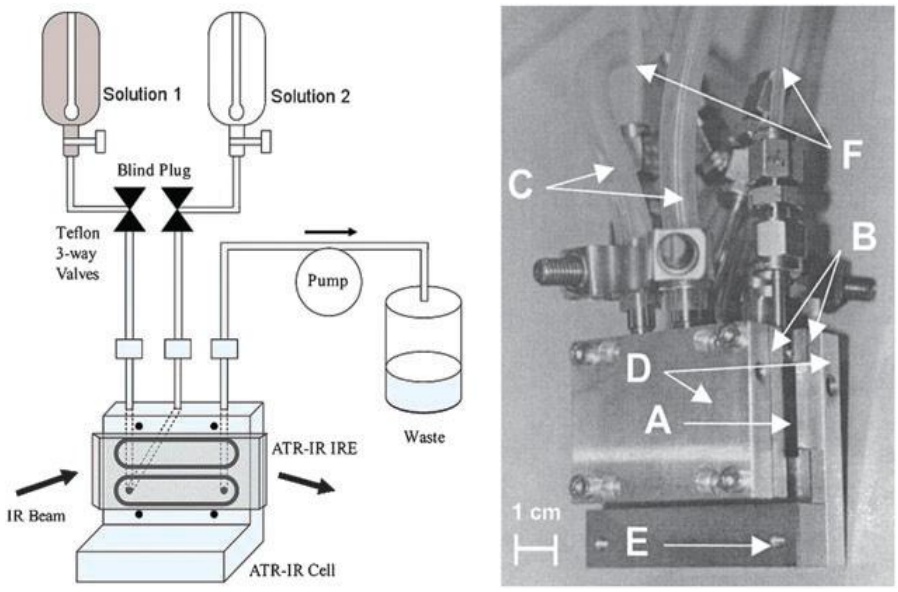

Figure 2.1 Experimental setup (left) (right) The picture shows the cell body (A) together with a Ge IRE (B) and the cooling system (C, water tubings and D, cooling jackets). E points to the location of the thermocouple. F is the in- and outlet

2.2.4 In situ ATR IR investigation of AP hydrogenation on Pt/Al_2O_3 and Pd/SiO_2-Al_2O_3

Infrared spectroscopy is performed by ATR-IR in combination with Modulation-excitation spectroscopy (MES) as shown in figure 2.1. ATR-IR spectra were recorded on a Bruker IFS-66/S spectrometer equipped with a liquid nitrogen cooled MCT detector at 4 cm^{-1} resolution. For Pt/Al_2O_3, modulation-excitation spectroscopy (MES) was carried out by periodically changing between two different solutions: (i) AP (2 mM) in n-hexane and neat n-hexane solution; (ii) AP (2 mM) and PE (2 mM) in n-hexane and neat n-hexane; (iii) AP (2 mM) and CE (2 mM) in n-hexane and neat n-hexane; (iv) AP (2 mM) and EB (2 mM) in n-hexane and neat n-hexane. For Pd/SiO_2-Al_2O_3, modulation-excitation spectroscopy (MES) was carried out by periodically changing between two different solutions: (i) AP (2 mM) in n-hexane and neat n-hexane solution; (ii) PE (2 mM) in n-hexane and neat n-hexane; The concentration of AP, PE, CE or EB was low enough to avoid IR absorption bands assignable to AP, PE, CE or EB in the liquid phase. Corresponding solutions were fed from two separate glass-made bubble tanks where the solutions can be saturated with gases such as He, H_2 and CO. The bubble tanks were connected to the flow-through cell via Teflon tubing. At the outlet a peristaltic pump (ISMATEC, Reglo 100) was installed for continuously admitting solutions with a flow rate of 0.5ml/min. Two interconnected pneumatically activated Teflon valves (PARKER, PV-1-2324) were synchronized with the acquisition of IR spectra by spectrometer software (Bruker Optics, OPUS). Specifically, one cycle consisted of admission of substrate (2 mM) in n-hexane for 187.5 s or both substrate (2 mM) and product (2 mM) in n-hexane for 187.5 s, followed by subsequent admission of n-hexane for 187.5 s (total

period of one cycle: 375 s). AP (saturated with He) concentration modulation was performed by admitting AP (2 mM) in n-hexane for 75 s followed by admission of n-hexane for 75 s (total period of one cycle: 150 s). Typically the experiments were carried out according to the following procedure. The initial three cycles were performed to obtain a stable response. Afterward, five cycles were repeated and averaged into one cycle to enhance the S/N ratio and time resolution. Phase sensitive detection (PSD) was used to further remove the noise and to obtain kinetic information of responding surface species. The phase-domain spectra were obtained by a mathematical treatment of the time-domain spectra according to the following equation:

$$A_k(\tilde{\nu}) \cos\left(\varphi_k + \varphi_k^{Delay}(\tilde{\nu})\right) = \frac{2}{T}\int_0^T A(t,\tilde{\nu}) \sin\left(k\omega t + \varphi_k\right) dt, \qquad (1)$$

where T is the length of a cycle, ω is the demodulation frequency, φ_k is the demodulation phase angle, k is the demodulation index (k = 1 in this study), and A(t, $\tilde{\nu}$) and $A_k(\tilde{\nu})$ are the active species responses in time- and phase-domain, respectively.

2.2.5 Pt/Al-MCM-41 characterization

2.2.5.1 X-Ray Diffraction (XRD)

X-ray diffraction (XRD) patterns of the prepared fresh catalysts were obtained on a SIEMENS D5000 in the range of 1–7 ℃ with a scanning step of 1°C using Cu Kα radiation (0.1542 nm wavelength). The surface area, average pore size, and total pore volume of the Pt/MCM-41 catalysts were determined by N_2 adsorption and desorption

isotherms on Quantachrome Autosorb-1. Before the isotherms analysis, 50 mg of each catalyst was degassed under vacuum at 110 ℃ for 12 h.

2.2.5.2 N_2 adsorption-desorption measurements

Nitrogen adsorption-desorption measurements were carried out at 77 K using a 4000e NOVA system to determine the specific surface areas. Before the measurements, 50 mg of the samples were degassed at 200 ℃ under vacuum to remove adsorbants from the surface. The primary particle size and specific surface areas were determined by BET measurement.

2.2.5.3 Transmission Electron Microscopy (TEM)

Pt/Al-MCM-41 catalysts were characterized by a Transmission electron microscopy (TEM) employed using a Philips CM120 BioFilter. For preparing the TEM samples, a small amount of the sample material was dispersed in 5 mL of ethanol (AR grade, Strem) in an ultrasonic bath and sonicated for 60 minutes. A drop of the colloidal suspension was placed on a copper grid coated with carbon film. The samples were dried in ambient air.

2.2.5.4 Diffuse reflectance infrared Fourier transform spectroscopy (DRIFTS)

Diffuse reflectance infrared Fourier transform spectroscopy (DRIFTS) combined with CO adsorption was used to gain some insight into the properties of the supported Pt

nanoparticles. The investigations were carried out at 297 K with an EQUINOX 55 spectrometer (Bruker Optics) equipped with a liquid nitrogen-cooled HgCdTe detector. The catalyst was introduced into a plug-flow DRIFTS cell and pretreated at 400 ℃ in a flowing (40 mL/min) mixture of 20 vol.% H_2 in He before CO adsorption. CO adsorption was carried out by flowing a mixture of 10 vol.% CO in He (40 mL/min) over the catalyst for 1 h and then switching to He (40 mL/min) till steady state was achieved. In situ IR spectra were collected by averaging 200 scans at 4 cm^{-1} resolution.

2.2.5.5 NMR measurements

^{1}H MAS NMR investigations were carried out on a Bruker Avance III 400 WB spectrometer at resonance frequencies of 400.1, 104.3, and 100.6 MHz with the sample spinning rate of 8 kHz using 4 mm MAS rotors. Spectra were recorded after single-pulse $\pi/2$ and $\pi/6$ excitation with repetition times of 20 s and 0.5 s for studying ^{1}H. Quantitative ^{1}H MAS NMR measurements were performed using zeolite H, Na-Y (35 % ion-exchanged) as an external intensity standard, which contains 58.5 mg zeolite H, Na-Y with 1.776 mmol protons/g.

2.2.6 Catalysts tests

2.2.6.1 Catalytic tests of AP hydrodeoxygenation on Pt/Al_2O_3, Pt/Al-MCM-41 and Pd/SiO_2-Al_2O_3

Prior to use, Pt/Al_2O_3, Pt/Al-MCM-41 and Pd/SiO_2-Al_2O_3 catalysts were reduced in a fixed-bed reactor by firstly heating under helium-flow from room temperature to 673 K (473K for Pd/SiO_2-Al_2O_3), followed by reduction in pure hydrogen for 1 hour at 673 K (473K for Pd/SiO_2-Al_2O_3), cooling down in hydrogen for another half an hour, and finally purging with helium-flow. The reduced catalysts were immediately transferred to a 50 ml stainless steel autoclave, which was purged with nitrogen followed by hydrogen for 3 times. For AP hydrogenation on Pt/Al_2O_3, Pt/Al-MCM-41 and Pd/SiO_2-Al_2O_3 acetophenone (AP) hydrogenation was carried out in a stainless steel autoclave. 20mg of freshly reduced catalyst, 0.5 mmol of acetophenone and 6 ml of n-hexane solvent were filled into the reactor and stirred magnetically at 500 rpm and 298K (333K for Pd/SiO_2-Al_2O_3). The reactor was purged three times with hydrogen to remove air, followed by pressurizing up to 1 bar.

2.2.6.2 Catalytic tests of benzaldehyde hydrodeoxygenation on Pt/Al_2O_3 and Pt/SiO_2-Al_2O_3

The catalytic hydrogenation reactions were conducted over Pt/Al_2O_3 and Pt/SiO_2-Al_2O_3. Prior to the hydrogenation reaction, the catalyst needed to be reduced with hydrogen. The reduction was carried out in a quartz reactor with introducing hydrogen (50 ml/min) for 1 hour at 400 ℃. Continuous reaction was carried out under atmosphere pressure. The pure benzaldehyde in gas phase was introduced into the reactor by nitrogen flow of 20 ml/min and being evaporated at 60 ℃. The hydrogenation was conducted in a U-tube reactor at different temperatures with hydrogen (15 ml/min). 50 mg freshly reduced catalyst was placed at the bottom of the reactor with the fix of quartz wool. The products were

collected by ice trap at the end of 15, 30, 60, 90, 120 and 180 min or 30, 60, 90, 120, 150 and 180 min, respectively.

2.2.7 Products analysis

The obtained products were analysed by gas chromatography-mass spectrometry (GC/MS-QP 2010, Shimadzu). The GC was equipped with an Rtx-5 column and an GC-FID detector. MS analysis was performed and equipped with an Rtx-5 MS column. Bicyclohexyl was used as an internal standard. The selectivity to specific products was calculated as $S(\%) = 100 \times (i)/[(\text{reactant})_0 - (\text{reactant})]$, where (i) is the molar concentration of the products and $(\text{reactant})_0$ and (reactant) correspond to the molar concentration of AP and benzaldehyde before and after reaction, respectively.

3 Mechanistic insight into Pt-catalyzed bio-oil model ketone hydrodeoxygenation

3.1 Introduction

Hydrodeoxygenation (HDO) of bio-oil model compounds is of great importance because model compounds study offers many advantageous features such as easy analysis, independent of competitive reactions and the insight into reaction mechanism. It is suggested expect phenols and furans served as the main oxygenated model compounds, esters, carboxylic acids, aliphatic and aromatic alcohols, ethers, ketones and aldehydes have also been detected in significant amounts in bio-oils.[24, 40] Therefore, it is also important to understand reaction pathway of these compounds and catalytic effects on these oxygen-containing compounds. Ketones representative one kind of important model compounds in bio-oil, its hydrogenation and hydrodeoxygenation on noble catalysts has been studied by several groups. Most of the existing reports focus on catalyst screening and optimization to improve catalytic properties in terms of their activity and selectivity,[69, 95-101] few studies have addressed the reaction kinetics and proposed mechanistic models.[102-106] Mechanism investigation of ketones hydrogenation and hydrodeoxygenation on noble catalysts has not been widely discussed.

In this chapter, acetophenone (AP) is used as a model ketone compound for the investigation of hydrodeoxygenation mechanism on a reference catalyst of supported noble catalyst of Pt/Al_2O_3. Acetophenone (AP) typical in the oxygenate fractions of bio-oils is one of the simplest aromatic ketones. Acetophenone (AP) containing both aromatic

ring and carbonyl group serves as an ideal simplest model ketone compound because in bio-oil upgrading, it is also desirable to only promote hydrogenolysis of carbonyl groups to saturated C-C bonds and avoiding hydrogenation of aromatic rings since the latter decreases the octane number of the produced fuels and results in undesired hydrogen consumption.[69] Competitive and consecutive hydrogenation of the carbonyl group and the aromatic ring give rise to a complex reaction network leading to several products and byproducts (Scheme 3.1).[95]

Based on in situ FT-IR spectroscopic study of the gas phase AP hydrogenation on Pt/SiO_2, Chen et al.[135] concluded that the selectivity of AP hydrogenation strongly depends on the formation of fragments (CO, benzene, toluene, and methane) originating from AP hydrogenolysis/decomposition and the strong adsorption of PE on the Pt surface. These fragments were supposed to inhibit the bonding between the phenyl group and Pt surface, leading to a decrease in the rate of the side-reaction to 1-cyclohexylethanol (CE). It is desirable to perform the aromatic ketone hydrogenation and hydrodeoxygenation at low temperatures due to environmental and energy concerns. Furthermore, the hydrogenation and hydrodeoxygenation of ketones on supported noble catalysts are usually operated at relatively low temperatures, it is essential to gain some insight into the mechanism of ketones hydrodeoxygenation at lower temperatures. Therefore, the question arises whether this behavior is also true under liquid-phase conditions.

Attenuated total reflection infrared (ATR-IR) spectroscopy possesses several features which are excellently suited for in situ investigation of catalytic solid-liquid interfaces as

encountered in heterogeneous catalysis.[136] It can provide information on the species adsorbed on the catalyst surface during reaction, such as intermediates even in the presence of strongly absorbing solvents. In some cases, information about the catalyst itself can be also acquired. However, proper analysis of ATR-IR spectra of a multiphase system under working conditions is quite demanding because it simultaneously provides information about dissolved and adsorbed reactants and products, adsorbed intermediates, byproducts, and the catalyst itself.[137] In order to solve the difficulties of conventional ATR-IR in assigning absorption bands and analyzing kinetics, ATR-IR spectroscopy in combination with modulation excitation spectroscopy (MES) and phase sensitive detection (PSD) has gained increasing attention. The most favorable features of this technique are the enhanced signal-to-noise ratio (S/N ratio) and the discrimination between active and spectator species at catalytic solid-liquid interfaces.[138-140] Here, we used this technique to gain some molecular insight into the adsorption and reaction steps occurring during the platinum-catalyzed liquid-phase hydrogenation of AP.

3.2 Results and discussion

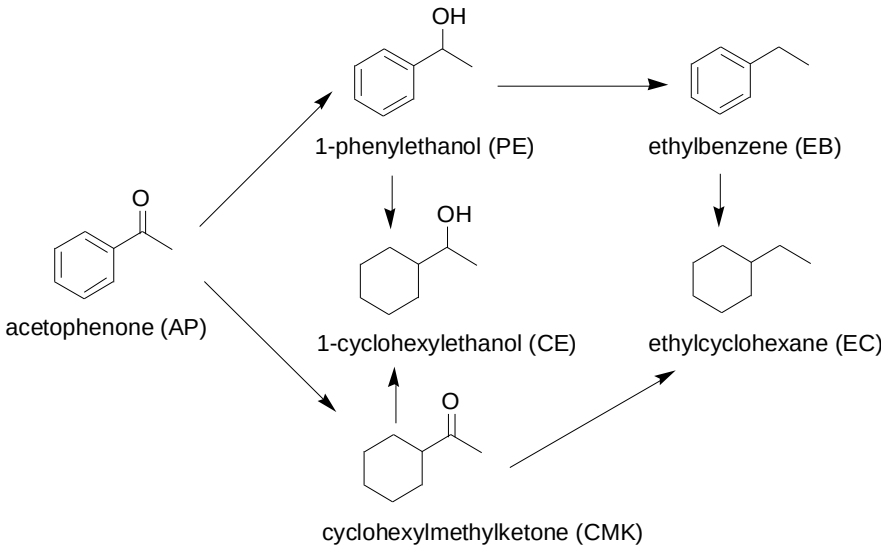

Scheme 3.1 Reaction pathway of AP hydrogenation

3.2.1 AP hydrogenation on Pt/Al_2O_3

Table 3.1 Acetophenone (AP) hydrogenation at PH_2 = 1 bar and 298 K on reduced Pt/Al_2O_3

Reaction time	Selectivity (%)					Total conversion (%)
	EC	EB	CMK	CE	PE	
5mins	0	0	17.5	0	82.5	9.0
20mins	0	0	20.7	4.8	74.5	29.2
40mins	0	0	21.6	5.7	72.7	45.9
1h	0	0	21.9	6.5	71.6	61.0

3.2.2 Pt-catalyzed AP hydrogenation mechanism investigation

3.2.2.1 Adsorption of acetophenone

In a first step we used in situ ATR-IR in combination with MES and PSD to investigate AP adsorption-desorption in He-saturated n-hexane on Pt/Al_2O_3 and Al_2O_3 at 298 K. As shown in Fig. 3.1a (phase-domain) and 3.1c (time-domain), splitting bands at 1697 cm^{-1} and 1672 cm^{-1} were observed for the C=O stretching vibration (1682 cm^{-1} for the neat AP as shown in Fig. A1, in the Appendix) after AP adsorption on Pt/Al_2O_3. The band at 1672 cm^{-1} was identified as the C=O stretching vibration of AP adsorbed on Al_2O_3, as shown in Fig. 3.1b and 3.1d, while the band at 1697 cm^{-1} can be assigned to the C=O stretching vibration of AP adsorbed on Pt (Fig. 3.1a and 3.1c).

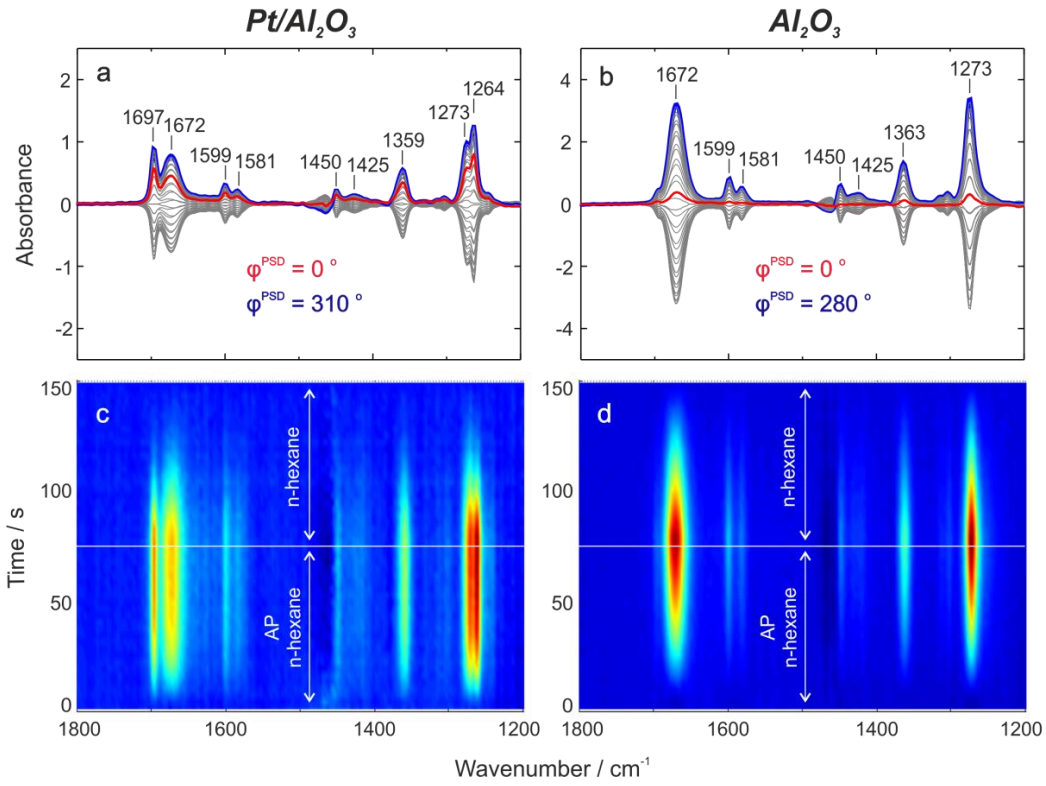

Figure 3.1 (a, b) Phase-domain and (c, d) time-domain ATR-IR spectra during adsorption and desorption of AP (2 mM) in He-saturated n-hexane on (a, c) Pt/Al_2O_3 and (b, d) Al_2O_3 at 298 K.

Similarly, the band at 1262 cm^{-1} attributed to X-sensitive benzene mode[141] of neat AP (Fig. A1 in appendix) was split into two bands at 1273 and 1264 cm^{-1}, respectively, in Fig. 3.1a and 3.1c. Figures 3.1b and 3.1d indicate that the adsorption of AP on Al_2O_3 caused a shift of the X-sensitive benzene mode[141] of AP from 1262 to 1273 cm^{-1}. This C-C stretching vibration was shifted to 1264 cm^{-1} in Fig. 3.1a and 3.1c, when AP adsorbed on Pt. Bands at 1359cm^{-1} in Figs. 3.1a and 3.1c and the band at 1363 cm^{-1} in Figs. 3.1b and 3.1d are due to the bending mode of CH_3.[141, 142] Bands at 1599, 1581, and 1450 cm^{-1} in Figs. 3.1c and 3.1d were assigned to the C=C stretching vibrations of the phenyl group[45, 141], and showed no band shift.

From the above findings, we conclude that AP adsorbed not only on Pt but also on the Al_2O_3 support. AP adsorption on Al_2O_3 occurred most likely via coordination to Lewis acid sites through one of the oxygen lone pairs, which might explain the significant red shift of the C=O stretching vibration (from 1682 cm^{-1} in liquid phase to 1672 cm^{-1} on Al_2O_3).[143] On Pt, two adsorption configurations, η^1 (O) and η^2 (C, O), were proposed for AP adsorption. According to Greenler's surface selection rule, any vibrational modes involving the dipole moment change parallel to the metal surface[144] cannot be observed; the dipole moment change of the η^2 (C, O) configuration should be cancelled out, hence the corresponding IR band disappears. Because the C=O band was clearly observable at 1697 cm^{-1}, AP was likely adsorbed on Pt surface in the η^1 configuration.

Interestingly, the band intensity (1672 cm^{-1}) of C=O stretching vibration of AP on Al_2O_3 (7.0 milliabsorbance) is much higher than that on Pt/Al_2O_3 (1.6 milliabsorbance).

Moreover, the adsorption-desorption of AP was significantly slower on Al_2O_3 compared to that on Pt/Al_2O_3, as emerges from comparison of their phase-domain spectra presented in Figs. 3.1a and 3.1b. In Fig. 3.1a, the in-phase angle of absorption bands is $\varphi = 310°$ with a phase-delay of 50 °(360 °-310 °), while in Fig. 3.1b, the in-phase angle of bands is $\varphi = 280°$ with a phase-delay of 80 °(360 °-280 °).

3.2.2.2 Adsorption of 1-phenylethanol (PE)

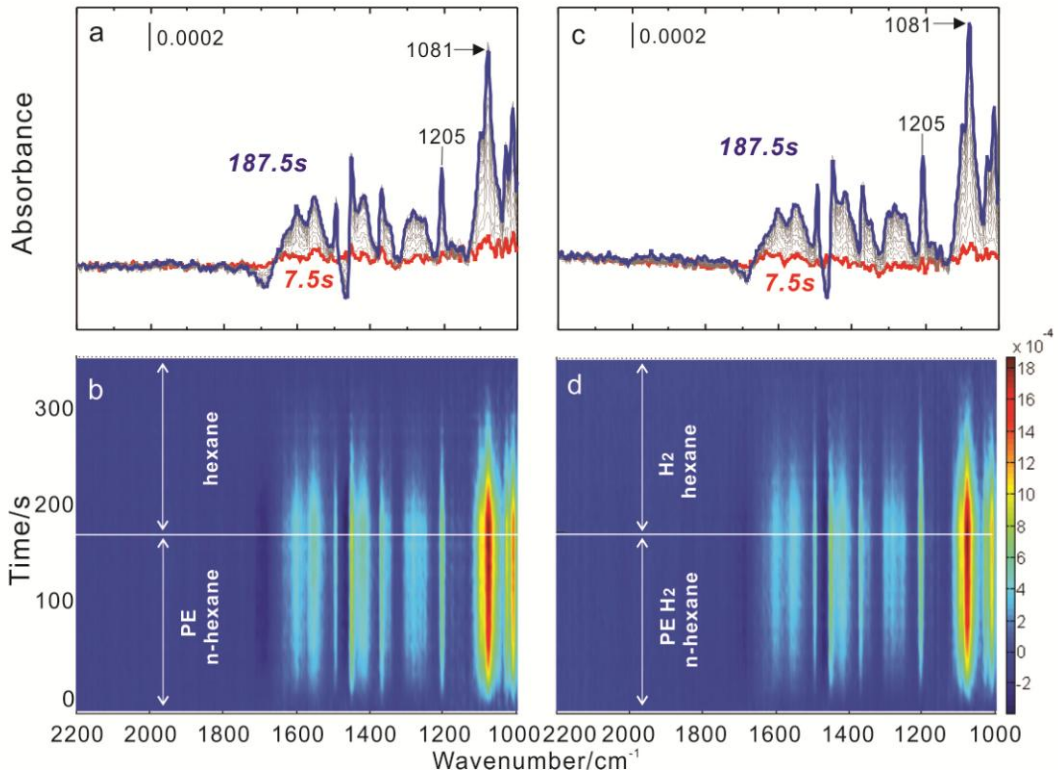

Figure 3.2 Time-domain ATR-IR spectra during adsorption and desorption of PE (2 mM) (a, c) He- and (b, d) H_2-saturated n-hexane on Pt/Al_2O_3 at 298 K.

1-phenylethanol (PE) is one of the potential main products of AP hydrogenation. Therefore, it is necessary to monitor the role of PE adsorption on Pt/Al_2O_3. As shown in the above Fig. 3.2, a band at 1205cm^{-1} assigned to deformation of phenyl ring whereas a

peak at 1081cm^{-1} is due to C-O stretching vibration (υ(C-O) mode).[145] It can be seen PE adsorption on Pt/Al_2O_3 gradually increased from 7.5s to 187.5s.

3.2.2.3 Hydrogenation

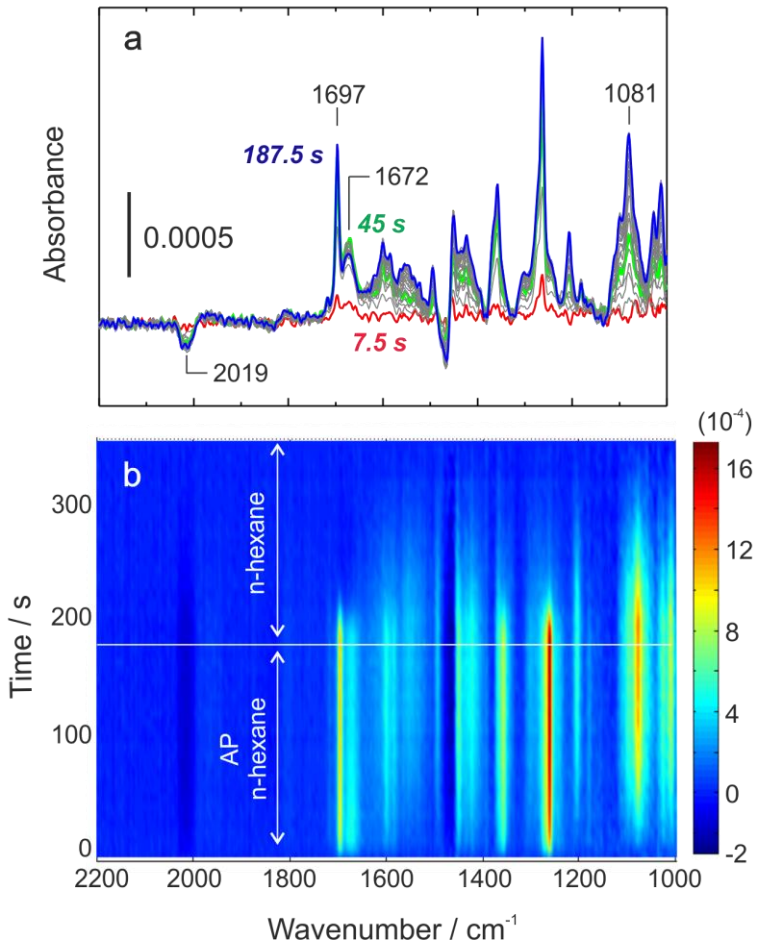

Figure 3.3 Time-domain ATR-IR spectra during hydrogenation of AP (2 mM) in H_2-saturated n-hexane on Pt/Al_2O_3 at 298 K.

When the solutions were saturated with H_2, the hydrogenation of AP started and the reaction pathway was followed by in situ ATR-IR. As shown in Fig. 3.3, new absorption bands at 1012, 1027 and 1081 cm^{-1} emerged due to C=C stretching, in-plane C-H

bending, and C-O stretching vibration (υ(C-O) mode)[145] of the product, 1-phenylethanol (PE), which also gave rise to two other new bands at 1204 and 1494 cm^{-1} assigned to deformation of phenyl ring[145] and phenyl C=C stretching vibration.[45] The slight blue shifts of 6 cm^{-1} for υ(C-O) of PE in the reaction compared with neat liquid phase PE (1075 cm^{-1} in Fig. A2) were probably caused by its adsorption on the Al_2O_3 support.

Interestingly, the band at 1672 cm^{-1} of AP υ(C=O) adsorbed on the Al_2O_3 support quickly reached maximum intensity at 45 s and gradually decreased while the characteristic band of PE at 1081cm^{-1} increased continuously. At the same time, the band at 1273 cm^{-1} of AP υ(C-C) on Al_2O_3 almost disappeared. However, the band intensity at 1697 and 1264 cm^{-1} due to υ(C=O) and X-sensitive benzene mode of AP adsorbed on Pt still gradually increased with time until 187.5 s. The above observation suggests that PE originating from the selective hydrogenation of AP on Pt partially replaced AP pre-adsorbed on the Al_2O_3, indicating its stronger adsorption on the support. The AP desorbed from the support could either desorb to the bulk liquid phase or re-adsorb on Pt in η^1 (O) configuration and undergo hydrogenation. This scenario is strikingly different from that proposed earlier for the gas-phase hydrogenation[45] where the strong adsorption and accumulation of PE on Pt were considered to be responsible for the high selectivity due to suppression of the formation of CE.[45]

The above in situ ATR-IR investigation shows that AP was adsorbed on Pt in its η^1 (O) mode and PE was produced due to the favored hydrogenation of the carbonyl group. This

behavior is also reflected by the results of experiments performed under the same conditions in a batch reactor (Table 3.1). PE was the dominant product with a selectivity of 82.5%. Only a relative small fraction of the AP probably underwent aromatic ring hydrogenation via π-bonded complex.[146]

Interestingly, the decomposition/hydrogenolysis of AP observed in the gas-phase hydrogenation which leads to various fragmentation products (CO, benzene, toluene, methane) is strongly suppressed in the liquid-phase hydrogenation. Only a small negative band appeared at 2019cm^{-1} which gradually decreased with increasing AP adsorption on Pt. Furthermore, this band was hardly discernible in the IR spectra, when products PE, CE, and EB were introduced into AP solution. Tentatively we assign this band to low coverage of atop-bounded CO on Pt steps, which is in the range of 2009 cm^{-1} to 2030 cm^{-1}.[147] CO observed during the gas-phase hydrogenation of AP was attributed to the decomposition of η^2 (C, O) adsorbed AP on Pt.[45] In our liquid-phase experiments no evidence for AP adsorbed in η^2 (C, O) configuration could be found. Furthermore, no other decomposition products such as benzene and toluene were detected (see Table 3.1). The above results indicate that decomposition of AP possibly only occurred on few specific active sites at the beginning of the liquid-phase hydrogenation (no band at 2019 cm^{-1} during AP adsorption in Fig. 3.1). During the whole hydrogenation process, AP η^1 (O) was dominant on the Pt and is therefore assumed to be at the origin of the selective production of PE as shown in Fig. 3.3 and Table 3.1.

3.2.2.4 CO adsorption

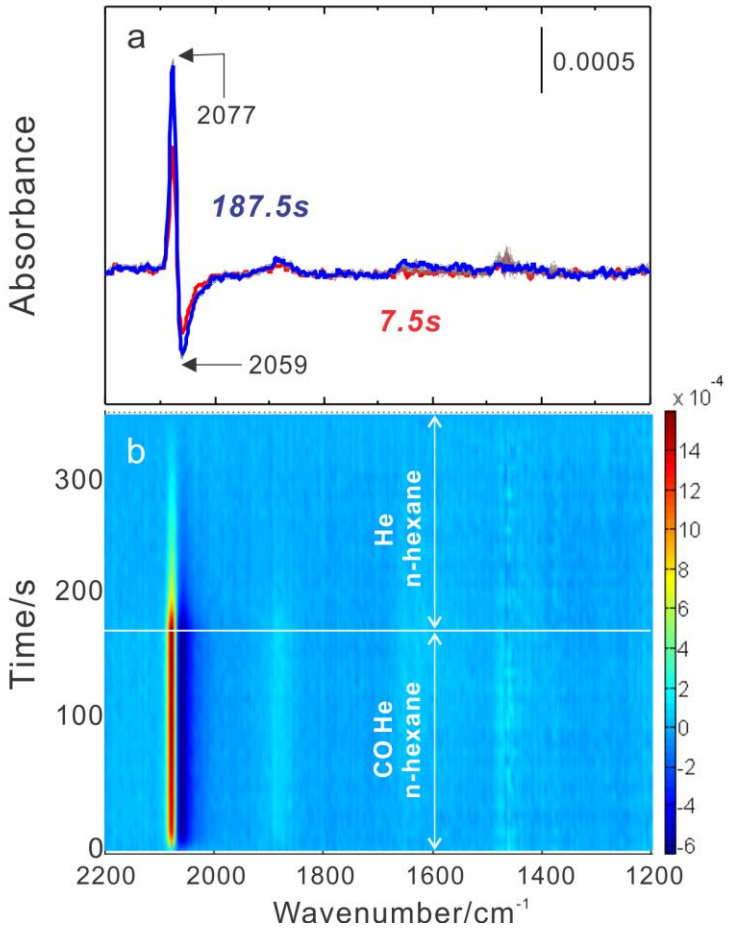

Figure 3.4 Time-domain ATR-IR spectra during adsorption and desorption of CO in CO and He saturated n-hexane and He saturated n-hexane.

It was suggested trace amount of CO was detected from AP decomposition during AP hydrogenation. Therefore, we deliberately performed in situ CO adsorption and desorption on Pt/Al_2O_3. As shown in Fig. 3.4, a positive band at 2074 cm^{-1} and a negative one at 2055 cm^{-1} due to linearly bounded CO appeared in the IR spectrum.

3.2.2.5 CO influence on AP hydrogenation

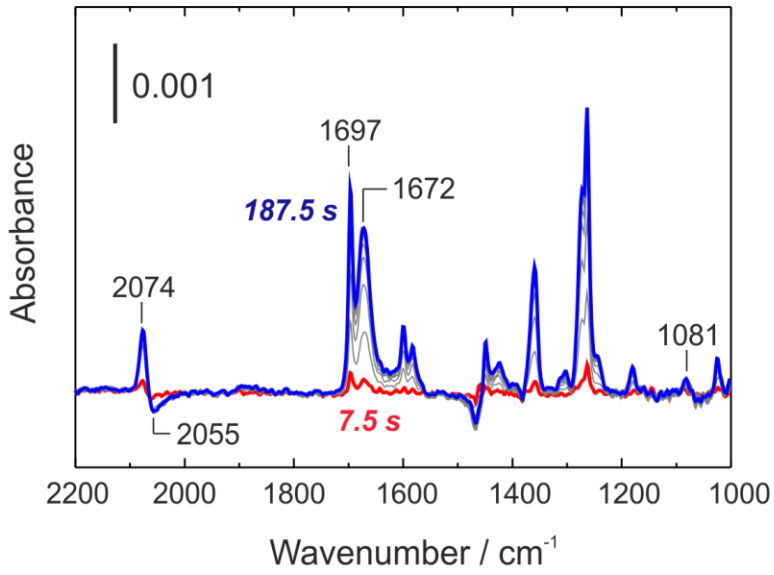

Figure 3.5 Time-domain ATR-IR spectra during hydrogenation of AP (2 mM) in H_2- and CO-saturated n-hexane on Pt/Al_2O_3 at 298 K.

To gain further information about the influence of CO in this reaction network, CO was deliberately introduced during in situ IR investigations of AP hydrogenation. As shown in Fig. 3.5, a positive band at 2074 cm^{-1} and a negative one at 2055 cm^{-1} appeared in the IR spectrum, due to CO linearly bound to Pt. No band at 2019 cm^{-1} is discernible in Fig. 3.5. This indicates that the band 2019 cm^{-1} in Fig. 3.3 might stem from minor AP fragmentation on specific active sites. In addition, no competition between CO and AP adsorption on the catalyst surface was observed. Even in the presence of CO, AP could still strongly adsorb on the catalyst surface as a comparison of the spectra in Fig. 3.5 and Fig. 3.1 reveals.

However, AP hydrogenation was significantly inhibited in the presence of CO, as the characteristic absorption band of PE at 1081 cm^{-1} almost disappeared in Fig. 3.5. Therefore, CO and H_2 were competitively adsorbed on the Pt sites, and CO completely blocked the adsorption of hydrogen on Pt for the further hydrogenation, while AP adsorption was barely affected by the presence of CO. The hydrogenolysis (decomposition) of AP on few specific active sites likely occurred between AP η^2 (C, O) and nearby dissociated hydrogen. Without adsorbed H_2 in Figs. 3.1 and 3.5, no CO band at 2019 cm^{-1} was detected from AP hydrogenolysis/decomposition. It seems that once CO covered these specific active sites, hydrogen adsorption was blocked and no further decomposition of AP was detected (the negative band at 2019cm^{-1}) as shown in Fig. 3.3. Therefore, AP hydrogenolysis/decomposition as observed in the gas-phase reaction under vacuum conditions only occurred in the beginning of the liquid-phase hydrogenation and stopped due to blocking of these active sites by the fragmentation products.

3.2.2.6 CO influence on PE adsorption

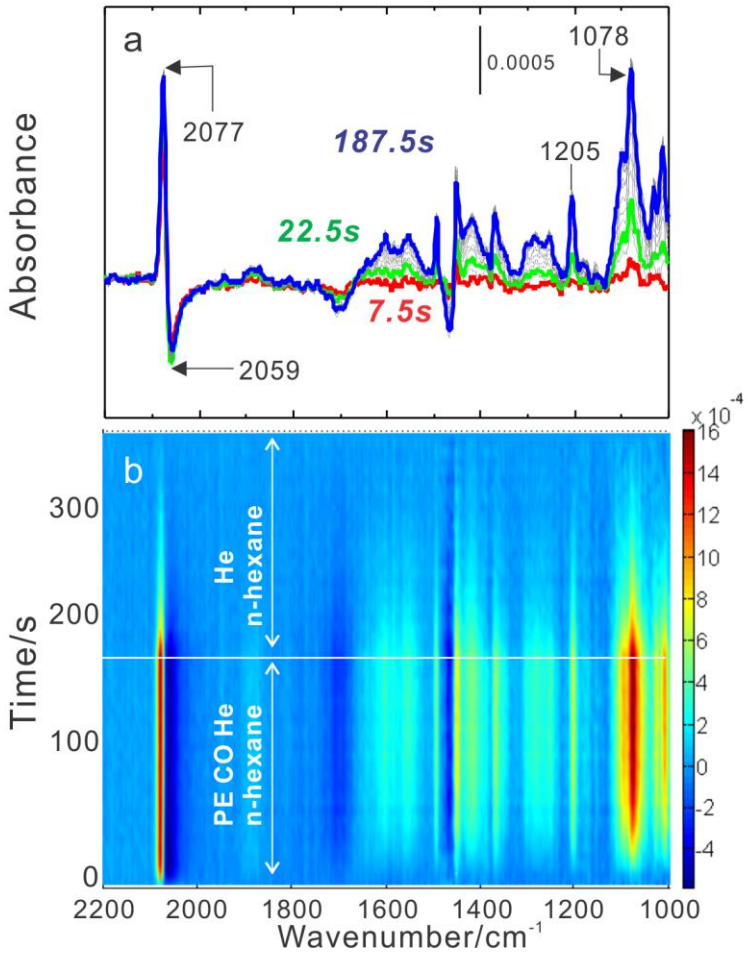

Figure 3.6 Time-domain ATR-IR spectra during PE adsorption and desorption in CO and He saturated n-hexane and He saturated n-hexane

CO can be linearly bounded to Pt as shown in Fig. 3.4. The potential influence of CO on the product of PE was still unclear. Based on this concern, it is interesting to perform co-adsorption of PE and CO to exam the influence of CO on the product of PE during AP hydrogenation. Fig. 3.6 clearly shows that CO barely inhibited PE adsorption and desorption on Pt/Al_2O_3 because characteristic bands of PE continually grew from 7.5s to

187.5s and no significant intensity difference can be observed in comparison with PE adsorption with CO in the absence.

In particular, the roles of CO, originating from AP decomposition/hydrolysis and the strong adsorption of the dominant product 1-phenylethanol (PE) have been elucidated. PE was found to be more strongly adsorbed on Al_2O_3 than on Pt. CO from AP decomposition/hydrogenolysis only weakly affected PE adsorption. The strong adsorption and accumulation of PE on the support seems to play a beneficial role by maintaining Pt accessible to the reactant AP, a necessary prerequisite for high performance of the Pt-catalyzed hydrogenation.

3.2.2.7 Reaction Pathway

Scheme 3.1 shows the general reaction scheme previously proposed for the Pt-catalyzed AP hydrogenation. According to this scheme AP hydrogenation can lead to four other products beside PE. While CMK is only produced from AP, CE can either be produced from PE or CMK. EB is only produced from PE while EC could be produced from EB and CE. In order to clarify the significance of the different reactions, co-adsorption experiments of substrate and main products were carried out. Fig. 3.7 shows ATR-IR spectra obtained by co-adsorption of AP and PE saturated either with helium or hydrogen. As emerges from Figs. 3.7a and 3.7c, upon admission of AP and PE in He-saturated n-hexane, the signals at 1264, 1273, 1358, 1585 and 1601 cm^{-1} belong to AP (Figure 3.1) and the bands at 1012, 1078, 1204 and 1494cm^{-1}, which appeared on the same time scale, correspond to PE. AP preferably adsorbed on the Pt surface via η^1 (O) (1697 cm^{-1}), and

PE was largely adsorbed on the Al_2O_3 support (1078 cm^{-1}). Interestingly, the adsorption band at 1672cm^{-1} quickly became saturated at 37.5 s and significantly decreased while the characteristic band at 1078 cm^{-1} grew. This phenomenon corroborated the observation made in Fig. 3.3 that there was competitive adsorption of AP and PE on the Al_2O_3 support.

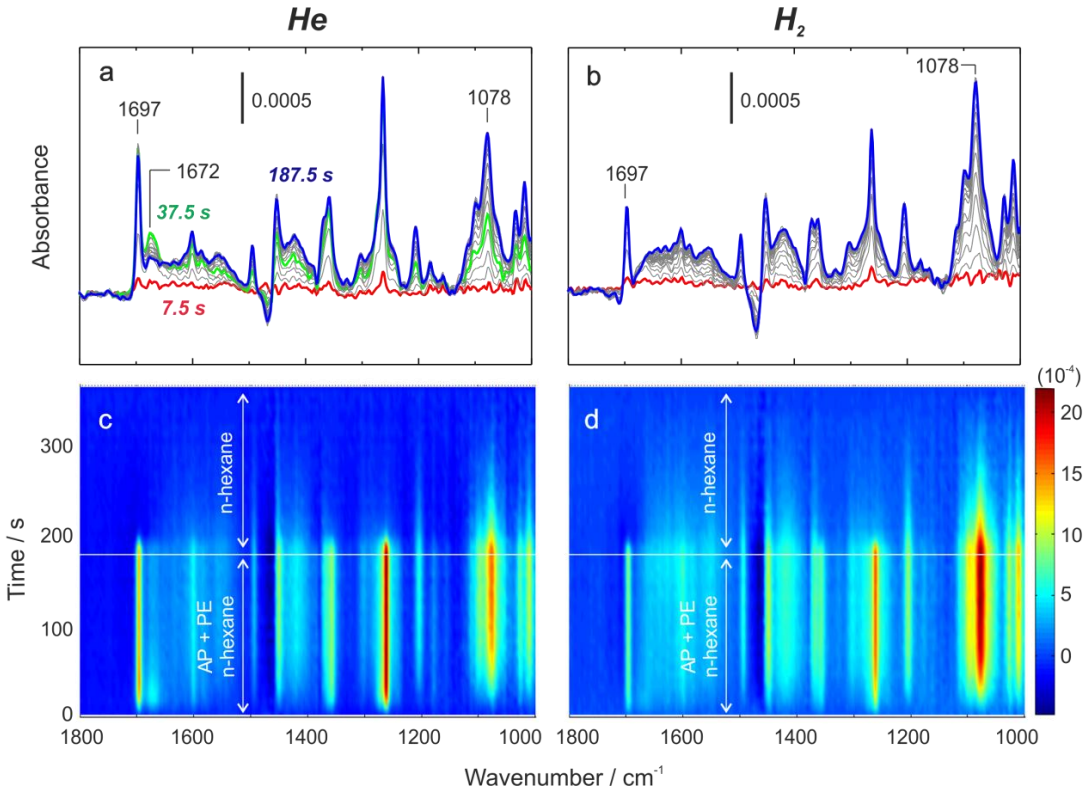

Figure 3.7 Time-domain ATR-IR spectra during adsorption and desorption of AP (2 mM) + PE (2 mM) in (a, c) He- and (b, d) H_2-saturated n-hexane on Pt/Al_2O_3 at 298 K.

Upon replacing He- by H_2-saturated AP and PE in n-hexane, the adsorbed η^1 (O) AP was hydrogenated to PE. As shown in Figs. 3.7b and 3.7d, the band at 1697 cm^{-1} of AP η^1 (O) on Pt decreased while the band at 1078 cm^{-1} of PE adsorbed on Al_2O_3 increased. During hydrogenation, the band at 1672 cm^{-1} of AP on Al_2O_3 almost disappeared due to the

competitive adsorption from the newly produced PE. Apparently the different adsorption properties of AP and PE significantly affected the processes occurring at the catalyst surface. For PE, no further reaction was detected because PE adsorbed on Al_2O_3 rather than on Pt. This is probably the reason that EB was hardly produced even after AP hydrogenation in 1 h (Table 3.1).

The results shown in Fig. 3.7 provide further evidence for the strikingly different behaviour of the chemoselective hydrogenation of AP in liquid-phase and gas-phase. It was proposed that in the gas-phase the selectivity of AP hydrogenation strongly depended on the fragmentation products (CO and benzene) from AP decomposition/hydrogenolysis and the strong adsorption of PE on Pt. As emerges from Fig. 3.7, in liquid-phase, PE adsorbed mainly on Al_2O_3 and less on Pt, and no significant band at 2019 cm^{-1} indicative of CO originating from AP fragmentation was discernible. Thus it appears that fragmentation hardly occurs in the liquid phase, while it is significant in the gas-phase.

CE was not detected in the above IR investigation as it was not produced in the first few minutes during hydrogenation (see Table 3.1). However, with longer reaction time formation of CE was significant, as shown in Table 1. In order to check whether the presence of CE affects AP hydrogenation, adsorption/desorption of AP and CE in He- and H_2-saturated n-hexane was studied (Fig. 3.8). Upon admission of AP and CE in He (Figs. 3.8a and 3.8c), bands at 1263, 1358, 1450, 1585, 1601, 1672 and 1697 cm^{-1} due to AP and bands in the range 1000 – 1200 cm^{-1} assigned to CE appeared. The bands of AP υ(C=O) on Al_2O_3 at 1672 cm^{-1} and η^1 (O) AP on Pt at 1697 cm^{-1} quickly reached

maximum intensity at 37.5 s. With growing bands in the range 1000 – 1200 cm^{-1} (more adsorbed CE), the band at 1672 cm^{-1} (AP υ(C=O) on Al_2O_3) gradually decreased until 187.5 s, while the band at 1697 cm^{-1} (AP η^1 (O) on Pt) remained nearly at its maximum intensity from 37.5 s to 187.5 s. This behaviour corroborates that CE and AP competitively adsorbed on Al_2O_3, and the absorption of CE on Al_2O_3 was not as strong as that of PE.

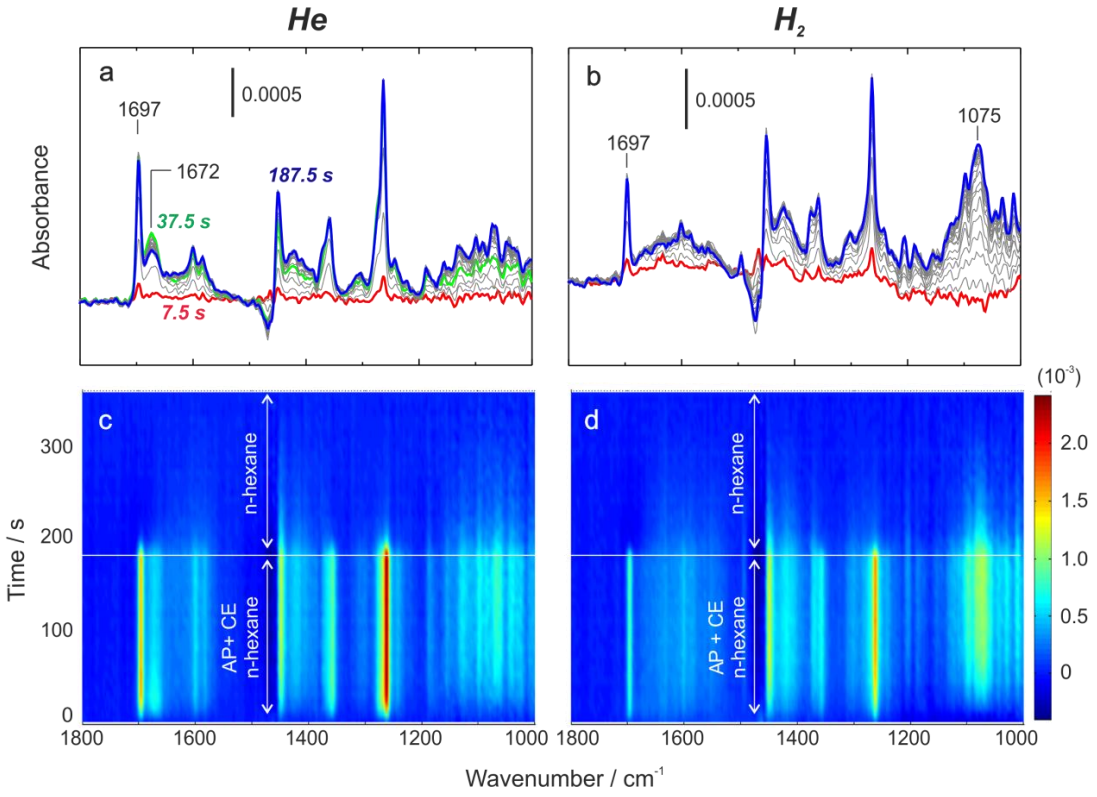

Figure 3.8 Time-domain ATR-IR spectra during adsorption and desorption of AP (2 mM) + CE (2 mM) in (a, c) He- and (b, d) H_2-saturated n-hexane on Pt/Al_2O_3 at 298 K.

Upon replacing H_2 by He in solvent (Figs. 3.8b and 3.8d), the band of η^1 (O) AP on Pt at 1697 cm^{-1} decreased, while new bands appeared. The band at 1075 cm^{-1} due to PE υ(C-O) on the Al_2O_3 support gradually increased and overlapped with characteristic signals of CE

in the region of 1000 – 1200 cm^{-1}. The band of AP υ(C=O) on Al_2O_3 at 1672 cm^{-1} disappeared, indicating that PE formed replaced AP on the support. The hydrogenation of AP to PE was hardly affected by the presence of CE, since CE did apparently not replace or block the AP η^1 (O) and hydrogen adsorption/dissociation on Pt.

At the beginning of the hydrogenation, CMK and PE were the only products as shown in Table 3.1. CMK could only be produced through hydrogenation of the phenyl group of AP. In order to elucidate whether hydrogenation of the aromatic ring competed with the carbonyl group during AP hydrogenation, co-adsorption and hydrogenation experiments of AP and EB were performed (Fig. 3.9). During co-adsorption of AP and EB in He-saturated n-hexane, characteristic bands of AP (1264, 1273, 1450, 1585, 1601, 1672 and 1697 cm^{-1}) appeared on the same time scale. Bands of AP υ(C=O) on Al_2O_3 and AP η^1 (O) on Pt (1672 and 1697 cm^{-1}) increased with time until 187.5 s, similar as observed in the investigation without EB (Fig. 3.1). AP adsorption on both Pt and Al_2O_3 via its carbonyl group consistently increased and was barely affected by EB.

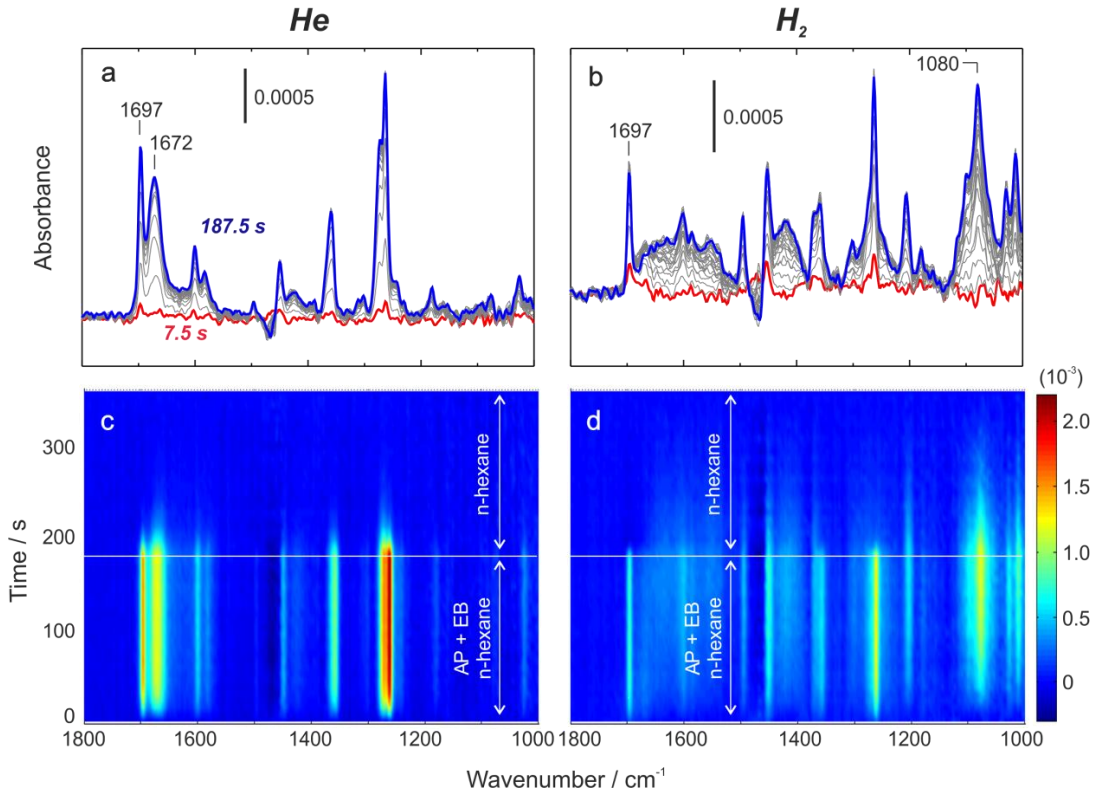

Figure 3.9 Time-domain ATR-IR spectra during adsorption and desorption of AP (2 mM) + EB (2 mM) in (a, c) He- and (b, d) H_2-saturated n-hexane on Pt/Al_2O_3 at 298 K.

Upon replacing He-saturated AP and EB by H_2-saturated AP and EB, new bands appeared at 1012, 1080 and 1204 cm^{-1} due to PE formation. The band at 1672 cm^{-1} assignable to υ(C=O) of AP on Al_2O_3 again significantly decreased due to the competitive adsorption of newly produced PE strongly adsorbed on Al_2O_3. The band at 1697cm^{-1} corresponding to AP η^1 (O) on Pt did hardly change compared to the experiments without EB (Fig. 3.3). Obviously, the presence of EB had only a minor effect on the adsorption behavior of AP.

3.3 Conclusions

In situ ATR-IR in combination with MES and PSD was applied to elucidate the surface processes occurring during the liquid-phase hydrogenation of AP on Pt/Al_2O_3. AP was predominantly adsorbed on Pt in its η^1 (O) configuration and this species was hydrogenated with high chemoselectivity to PE. The produced PE was more strongly adsorbed on the Al_2O_3 support than on Pt, which may have lead to enhanced desorption of PE from Pt. A smaller fraction of adsorbed AP probably also interacted with Pt via π-bonding of the aromatic ring forming cyclohexylmethylketone (CMK). Co-adsorption experiments of AP with CO, PE, CE, and EB, revealed that AP adsorbed in η^1 (O) configuration was always the prevalent adsorption mode of AP on Pt. This behavior is strikingly different from that that observed previously for AP hydrogenation in the gas-phase, where the fragmentation of AP by decomposition/hydrogenolysis and the strong adsorption of PE on Pt were reported to affect the chemoselectivity to PE.[45] Such behavior could not be observed in the liquid-phase, where decomposition of AP played only a minor role in the beginning of the hydrogenation, indicated by the formation of some CO. Co-adsorption experiments of AP and CO showed that the presence of CO hardly affected the adsorption of AP, but significantly inhibited AP hydrogenation since CO blocked H_2 adsorption and dissociation on the Pt surface. The whole mechanism was summarized in the below Scheme 3.2.

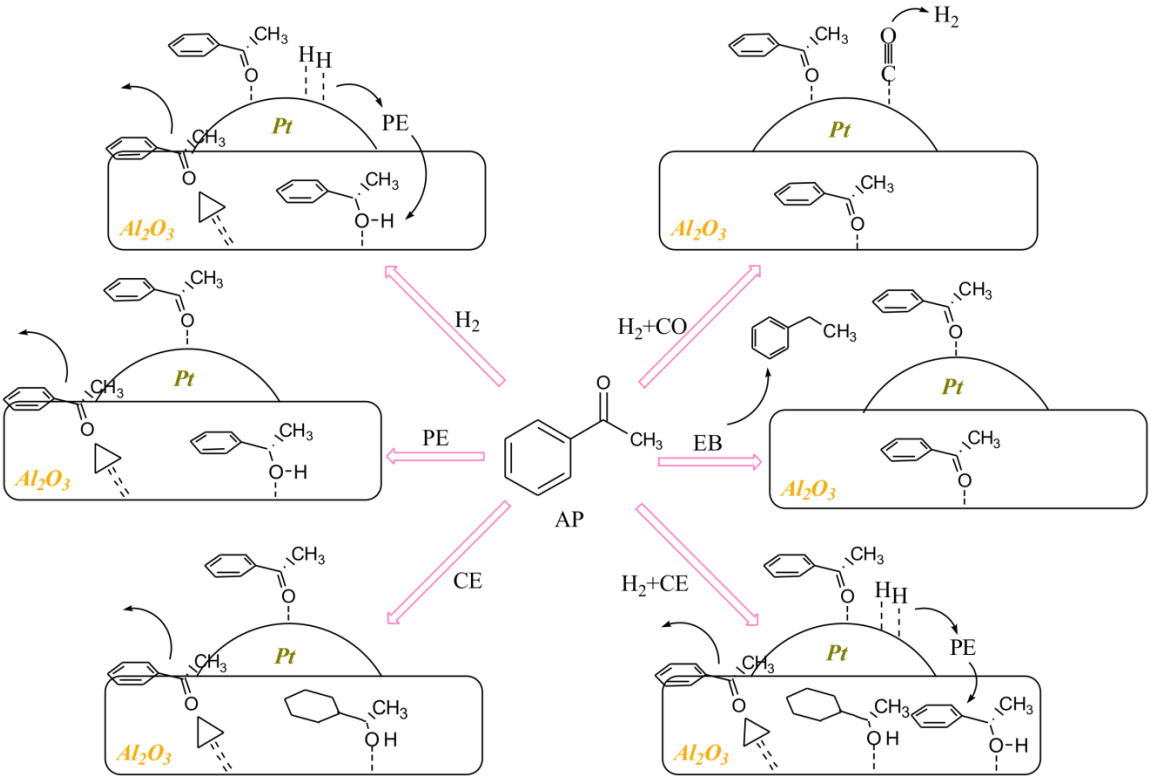

Scheme 3.2 Catalytic mechanism of AP hydrogenation on Pt/Al_2O_3

4 Mechanism study of acidic effects on hydrodeoxygenation of bio-oil model ketone

4.1 Introduction

Generally, support composition can affect catalytic activity and selectivity of supported metal catalysts commonly applied in hydrogenation and hydrodeoxygenation reactions.[148] The addition of acidic supports usually promotes catalytic processes of hydrogenation, hydrogenolysis and hydrocracking. Silica-alumina (SA) supports are one of excellent supports in hydrogenation reactions, and the acidity can be tuned with doping alumina into silica, thereby offering efficient catalysis.[6, 149] The chemoselective hydrogenation and hydrodeoxygenation of unsaturated keotnes on Pt, Pd and other noble metal catalysts can be controlled by support acid-base properties.[69, 150, 151] It has been proposed that the support properties can affect electronic properties of Pt metal particles. Specifically, a higher Pt-H bond strength was caused by basic supports while acidic supports result in the weakness of Pt-H bond.[152]

Acetophenone (AP) serves as an ideal simplest model ketone compound containing both aromatic ring and carbonyl group for hydrodeoxygenation of bio-oil because in bio-oil upgrading undesired hydrogen consumption and decrease of octane number will be generated if aromatic rings and carbonyl group are reduced at the same time.[6] In other words, it is highly desirable to hydrodeoxygenate carbonyl group of AP in producing ethylbenzene (EB).

Lin et al. investigated vapor-phase AP hydrogenation on SA supported Pt catalyst and achieved high yield to ethylbenzene (EB), proposing a bifunctional reaction including PE dehydration to styrene on acidic support followed by a hydrogenation step on Pt.[68] Recently, we have used flame spray pyrolysis (FSP) to generate palladium nanoparticles on silica-alumina (Pd/SA) with tunable surface acidity, these acidic solid catalysts also showed high chemoselectivity for AP hydrogenation to EB under solvent free conditions.[69] The details of FSP method can be found in the literatures.[153, 154]

It was suggested that the transformation of carbonyl group to methylene might occur through three mechanisms as shown in Scheme 4.1. For hydrogenation-dehydration mechanism, it includes transformation of a carbonyl compound to alcohol, followed by a dehydration producing C=C and further hydrogenation of the C=C double bond. In the case of hydrogenation-hydrogenolytic mechanism, hydrogenation of carbonyl compound to alcohol occurs, followed by the hydrogenolytic splitting of the bond C–O producing hydrocarbon (C–C=O→C–C–OH→C–C). The third mechanism is a direct hydrogenolysis of C=O bond (C–C=O→C–C).[108]

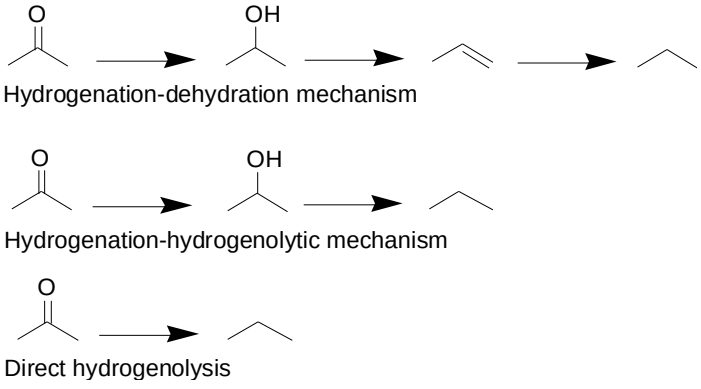

Scheme 4.1 Mechanism of transformation of carbonyl group to methylene

However, the mechanism regarding the activity and selectivity enhancement of these SA supported Pd nanoparticles in AP hydrodeoxygenation[69] still lacks experimental proof due to limited techniques under working conditions, especially highlighted for liquid phase reaction.

Herein, we used in situ attenuated total reflection infrared (ATR-IR)[126] in combination with modulation excitation spectroscopy (MES) and phase sensitive detection (PSD) to investigate AP hydrodeoxygentaion on SA supported Pd nanoparticles with tunable surface acidity, providing new insight into the increasing surface acidity effect in the selectivity enhancement for AP hydrogenation. The technique of combining ATR-IR and MES significantly enhances the signal to noise (S/N) ratio and also allows the discrimination of acitve surface species and spctators.[127, 128, 155] The details of ATR-IR in combination with MES and PSD were discussed in 1.8.3.

4.2 Results and discussion

4.2.1 AP hydrodeoxygenation on Pd/SiO_2-Al_2O_3

Table 4.1 AP hydrodeoxygenation with P_{H2} = 1bar at 333K on reduced Pd/SiO_2

reaction time	selectivity (%)					total conversion (%)
	EC	EB	CMK	CE	PE	
5min	0	0	0	0	100	2.9
20min	0	4.8	0	0	95.2	35.2
40min	0	10.8	0	0	89.2	74.1
1h	0	18.3	0	0	81.7	94.6
2h	0	41.8	0.9	2.2	55.1	99.2
3h	0	76.0	0.6	3.3	20.1	100

Table 4.2 AP hydrodeoxygenation with P_{H2} = 1bar at 333K on reduced Pd/SA-15

reaction time	selectivity (%)					total conversion (%)
	EC	EB	CMK	CE	PE	
5min	0	9.1	0	0	90.9	15.8
20min	2.2	23.9	0	0	73.9	49.4
40min	3.3	33.9	0	2.9	59.9	76.6
1h	3.1	38.8	0	2.7	55.5	100
2h	3.1	70.3	0	3.4	23.1	100
3h	3.6	85.2	0.9	3.7	6.5	100

Table 4.3 AP hydrodeoxygenation with P_{H2} = 1bar at 333K on reduced Pd/SA-70

reaction time	selectivity (%)					total conversion (%)
	EC	EB	CMK	CE	PE	
5min	0	0	0	0	100	11.9
20min	0	15	0	0	85	50.5
40min	0	34.4	0	0	65.6	86.7
1h	0	55.9	0	1.5	42.6	97.1
2h	0.2	87.5	1	3	8.3	99.0
3h	1.5	93.3	1.4	3.8	0	100

Tables 4.1, 4.2 and 4.3 described AP hydrodeoxygenation on Pd/SiO_2, Pd/SA-15 and Pd/SA-70. In table 4.1, total conversion of AP on Pd/SiO_2 was only 2.9% after 5min and increased to 100% after reaction time of 3h. In table 4.2, total conversion of AP on Pd/SA-15 reached 15.8% after 5 min and was 100% after 3h. In table 4.3, total conversion of AP on Pd/SA-70 was 11.9% after 5 min and increased to 100% after 3h. Clearly, compared to Pd/SiO_2, Pd/SA-15 and Pd/SA-70 showed an increase in catalytic activity of AP hydrodeoxygenation. Specially, total conversion of AP on Pd/SA-15 after 20 min was 49.4% and on Pd/SA-70 after 20 min was 50.5% whereas the conversion of AP on Pd/SiO_2 after 20 min was only 35.2%. Regarding catalytic selectivity, the initial main product of AP hydrogenation on Pd/SiO_2 was PE with selectivity of 100% after 5min (2.9% conversion). PE selectivity gradually decreased from 100% after 5min (2.9% conversion) to 20.1% after 3h (100% conversion) whereas EB selectivity increased from

0% after 5min to 76% after 3h. On Pd/SA-15, the initial PE selectivity after 5min (15.8% conversion) was 90.9%, it decreased to 6.5% after 3h (100% conversion). On the contrary, the selectivity of EB increased from 9.1% after 5min to 85.2% after 3h. On Pd/SA-70, the initial PE selectivity was 100% after 5min (11.9%), it gradually decreased to 0% after 3h (100% conversion) while selectivity of EB increased from 0% after 5min to 93.3% after 3h. Results show EB (the most valuable hydrodeoxygenation product) was formed with high selectivity on acidic catalysts. Results show EB (the most valuable hydrodeoxygenation product) was produced from PE, which causes the decrease of PE and the increase of EB in the final product solution. As shown in Scheme 4.1, two reaction pathways involved in EB production from PE.

4.2.2 Mechanism investigation

4.2.2.1 Adsorption of Acetophenone (AP) on Pd/SiO_2, Pd/SA-15 and Pd/SA-70

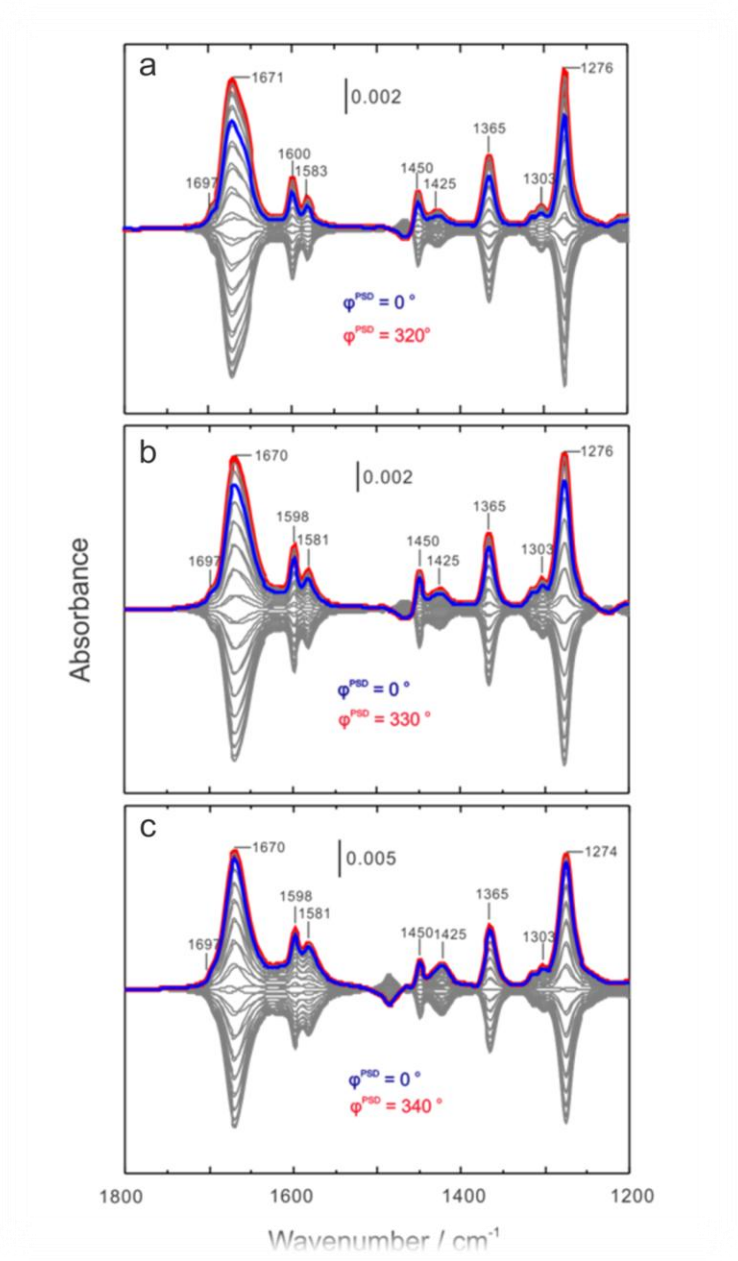

Figure 4.1 Phase-domain ATR-IR spectra during adsorption and desorption of AP (2 mM) in He-saturated n-hexane on (a) Pd/SiO_2 (b) Pd/SA-15 and (c) Pd/SA-70 at 333 K.

In situ ATR-IR in combination with MES and PSD was applied to monitor the adsorption-desorption kinetics of AP at catalysts surface with tunable acidity. Figure 4.1 shows phase-domain in situ ATR-IR spectra during adsorption and desorption of AP (2mM) in He-saturated n-hexane on Figure 4.1a (Pd/SiO_2), 4.1b (Pd/SA-15) and 4.1c (Pd/SA-70) at 333K. Bands at 1697 cm^{-1} and 1670 cm^{-1} in Figure 4.1a, 4.1b and 4.1c were observed and assigned to C=O stretching vibration of AP (1682cm^{-1} for the neat AP) The band at 1670 cm^{-1} was identified as the C=O stretching vibration of AP adsorbed on the support, whereas the band at 1697 cm^{-1} should be assigned to the C=O stretching vibration of AP adsorbed on Pd in the η^1 (O) configuration as proved in chapter 3. The band at 1276 cm^{-1} is attributed to X-sensitive benzene mode of AP on the support. Bands at 1365 cm^{-1} in Figure 4.1 is due to bending mode of CH_3.[141, 142] Bands at 1600 cm^{-1}, 1583 cm^{-1} and 1450 cm^{-1} in Figure 4.1a and bands at 1598 cm^{-1}, 1581 cm^{-1}, and 1450 cm^{-1} in Figure 4.1b and 4.1c were assigned to the C=C stretching vibrations of the phenyl group.[45]

In Figure 4.1a, the in-phase angle of absorption bands is $\varphi^{PSD} = 320°$ with a phase-delay of 40 ° (360 °-320 °) whereas in Figure 4.1b, in-phase angle of absorption bands is $\varphi^{PSD} = 330°$ with a phase-delay of 30 ° (360 °-330 °). The adsorption bands in Figure 4.1c show an in-phase angle of $\varphi^{PSD} = 340°$ with a phase delay of 20 ° (360 °-340 °). Chemical species with positive absorbance at $\varphi^{PSD} = 0°$ follow the same kinetics as the change in the solution and indicate that there is no time delay, i.e., phase delay 0 ° in the adsorption−desorption process. On the other hand, positive absorption bands at $\varphi^{PSD} = 320°$ indicate that the rate of adsorption and desorption processes is slower than that of

species at φ^{PSD} = 0 ° and results in a time delay, i.e., phase delay 40° (360° − 320 °).[130] Therefore, the rate of AP adsorption on catalysts is concluded as Pd/SA-70>Pd/SA-15>Pd/SiO_2.

4.2.2.2 AP hydrogenation, PE adsorption and hydrodeoxygenation on Pd/SiO_2, Pd/SA-15 and Pd/SA-70

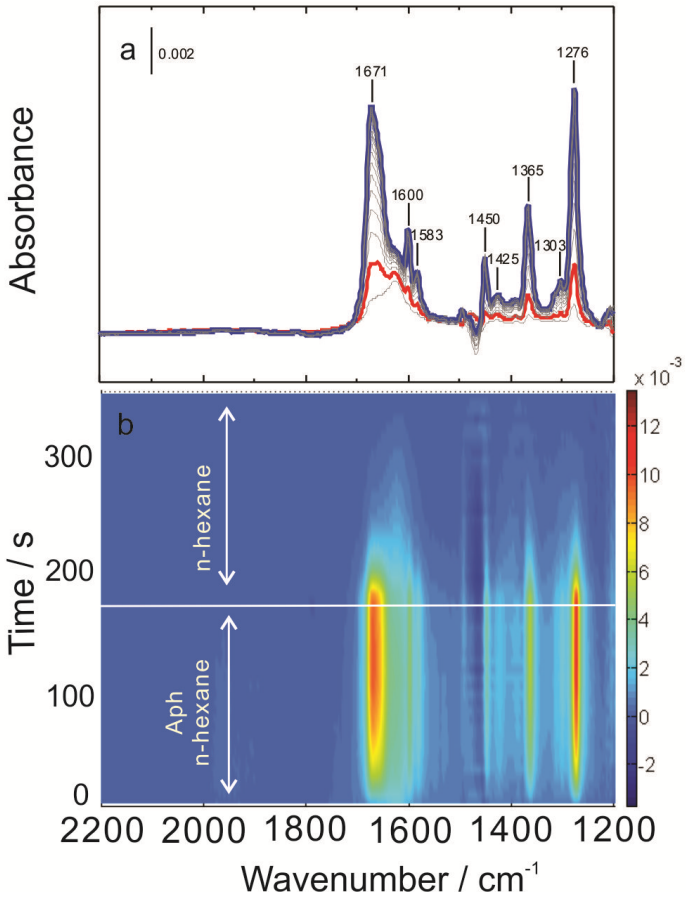

Figure 4.2 Time-domain spectra during hydrogenation of AP (2 mM) in H_2-saturated n-hexane on Pd/SiO_2 at 333 K.

In a first step, Pd/SiO_2 without doping alumina (with almost no acidic sites) was chosen as a reference catalyst for mechanism investigation of AP hydrogenation. Figure 4.2 showed time domain IR spectra of AP hydrogenation on Pd/SiO_2 at 333K. Notably, when

AP hydrogenation was started and tracked by in situ ATR-IR, bands at 1671cm^{-1}, 1600cm^{-1}, 1583cm^{-1}, 1450cm^{-1}, 1425cm^{-1}, 1365cm^{-1}, 1303cm^{-1} and 1276cm^{-1} assignable to AP continually grew until 187.5s. Almost no bands assignable to the products can be observed, indicating the initial AP hydrogenation rate on Pd/SiO_2 was relatively slow, which was in accordance with the reaction result in Table 4.1, the conversion of AP hydrogenation on Pd/SiO_2 was only 2.9% after 5 min. It is worth noting that, band of 1697 cm^{-1} assignable to the C=O stretching vibration of AP adsorbed on Pd in the η^1 (O) configuration was hardly observable in Figure 4.2 which might be caused by the following reasons: (i) very low concentration of C=O (η^1 (O)) mode of AP on can be detected on Pd (1697cm^{-1}). (ii) the adsorbed small amount of AP on Pd was reacted with H_2. (iii) and the initial main product PE from AP reacted with H_2 on Pd (100% selectivity after 5min) was hardly adsorbed on SiO_2. These reasons lead to difficulties in detecting AP η^1 (O) configuration on Pd.

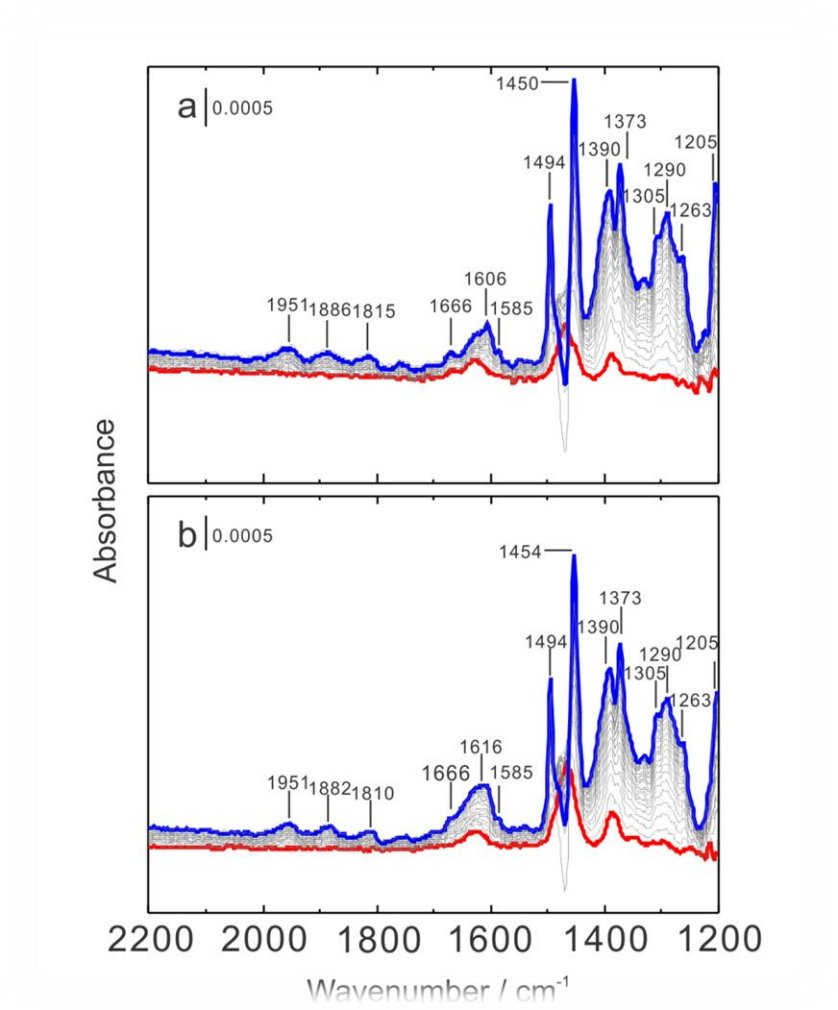

Figure 4.3 (a) Time-domain ATR-IR spectra during adsorption of PE (2 mM) in He-saturated n-hexane on Pd/SiO_2 at 333 K. (b) Time-domain ATR-IR spectra during hydrogenation of PE (2 mM) in H_2-saturated n-hexane on Pd/SiO_2 at 333 K.

As shown in Table 4.1, PE was the main product during AP hydrogenation on Pd/SiO_2 within 2h, it is also necessary to understand the adsorption and hydrogenation of PE. In order to monitor the behaviour of main product on the catalyst surface, PE adsorption and hydrogenation on Pd/SiO_2 were performed. Figure 4.3 showed PE adsorption (3a) and hydrogenation (3b) on Pd/SiO_2 at 333K. In Figure 4.3a, the band at 1494 cm^{-1} is due to C=C stretching vibration, 1205 cm^{-1} is due to deformation mode of phenyl ring of PE[45,

145], signals at 1951 cm^{-1}, 1882 cm^{-1} and 1810 cm^{-1} are assigned to C-H out of plane mode of benzene ring of PE.[156] Interestingly, aromatic ring of PE was also adsorbed on the catalyst surface due to above finding. Absorption bands at 1666cm^{-1}, 1606cm^{-1} and 1585cm^{-1} were considered to belong to PE because these peaks can also be observed in liquid phase PE (Figure A2 in appendix). When replacing He-saturated n-hexane (Figure 4.3a) by H_2 saturated n-hexane (Figure 4.3b), almost no difference can be observed.

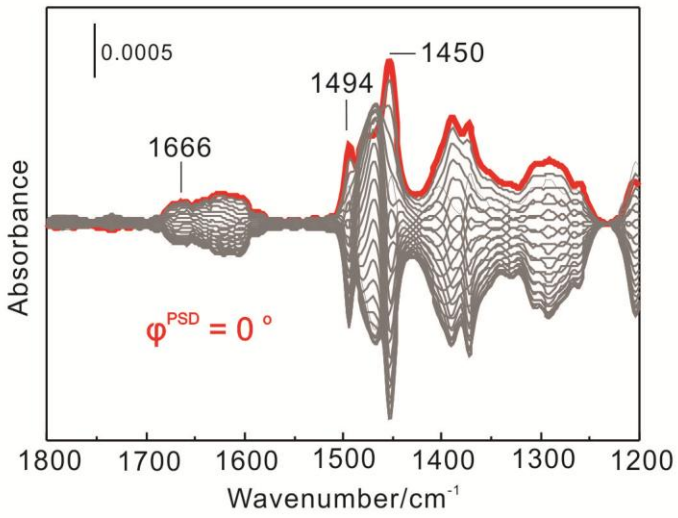

Figure 4.4 Phase-domain ATR-IR spectra during adsorption of PE (2 mM) in He-saturated n-hexane on Pd/SiO_2 at 333 K.

As different species should possess different kinetics and in-phase angles[130], in order to prove that no new species were produced during PE adsorption on He-saturated n-hexane on Pd/SiO_2, phase-domain ATR-IR spectra was applied and shown in Figure 4.4. All adsorption bands in above figure follow the same in-phase angle φ = 0 º, therefore, new species was not detected during adsorption of PE on He-saturated n-hexane.

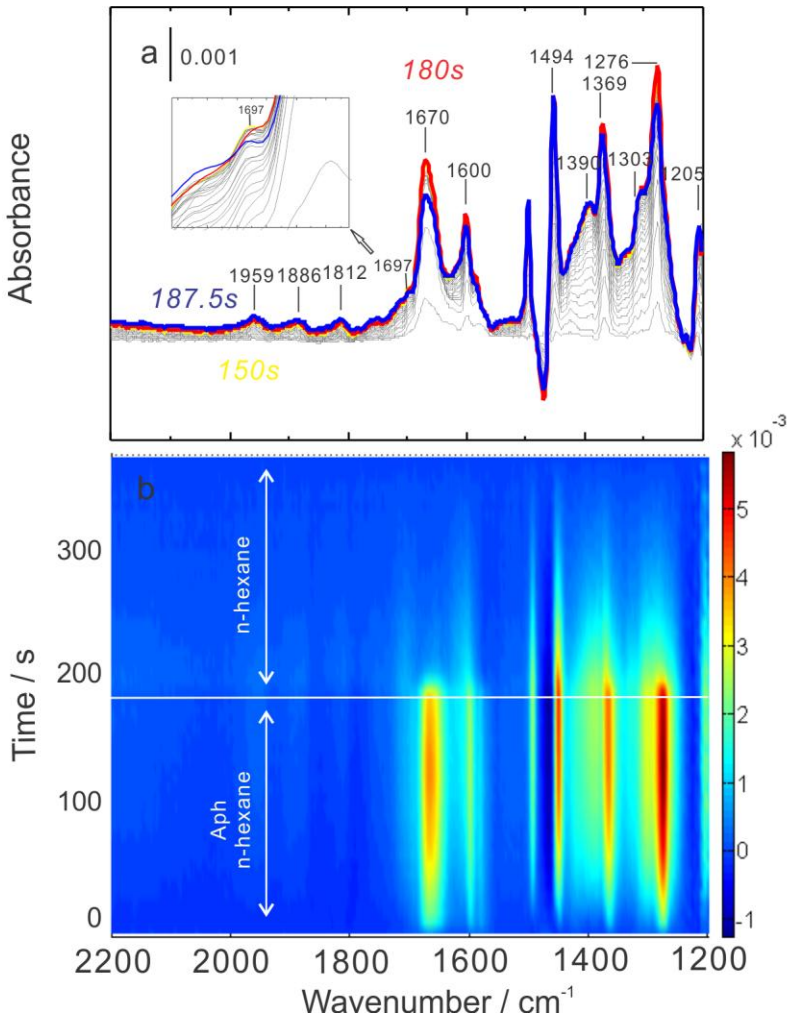

Figure 4.5 Time-domain spectra during hydrogenation of AP (2 mM) in H_2-saturated n-hexane on Pd/SA-15 at 333 K.

To clarify the AP hydrogenation mechanism differences caused by surface acidity, we investigated AP hydrogenation on surface acidity enhanced catalyst.(doping 15wt% alumina into silica support). AP hydrogenation was then carried out on Pd/SA-15, absorption bands emerging at 1207 cm^{-1}, 1812 cm^{-1}, 1886 cm^{-1} and 1959 cm^{-1} belong to AP hydrogenation product of PE (Figure 4.5) whereas bands at 1812 cm^{-1}, 1886 cm^{-1} and 1959 cm^{-1} are due to combination bands of C-H bending modes of aromatic ring of

PE.[156] It is worth noting that bands at 1812 cm^{-1}, 1886 cm^{-1} and 1959 cm^{-1} (C-H bending modes of aromatic ring of PE) gradually increases until 187.5s while band at 1670 cm^{-1} (C=O stretching vibration of AP adsorbed on the support) reached maximum intensity at 180s and significantly decreased with increasing bands at 1812 cm^{-1}, 1886 cm^{-1} and 1959 cm^{-1} until 187.5s. Moreover, band at 1697 cm^{-1} (Pd in the η^1 (O) configuration) saturated at 150s and slightly decreased with increasing bands at 1812 cm^{-1}, 1886 cm^{-1} and 1959 cm^{-1} (C-H bending modes of aromatic ring of PE). The observed phenomenon suggests an amount of PE product competitively adsorbed on Pd/SA-15 support with AP.

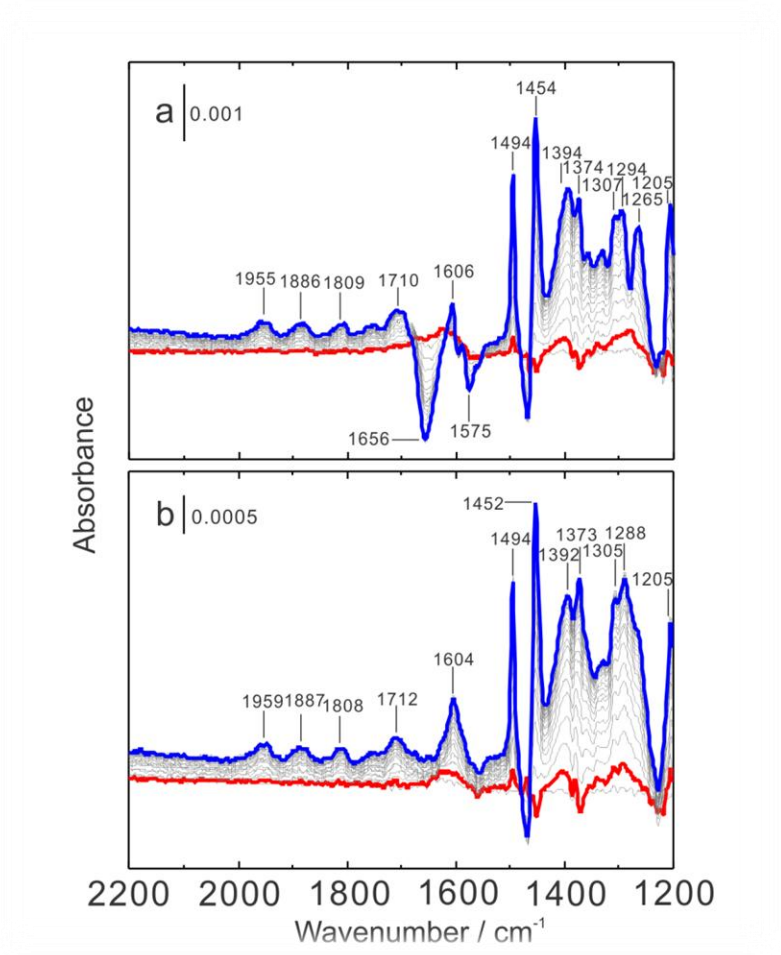

Figure 4.6 (a) Time-domain ATR-IR spectra during adsorption of PE (2 mM) in He-saturated n-hexane on Pd/SA-15 at 333 K. (b) Time-domain ATR-IR spectra during hydrogenation of PE (2 mM) in H_2-saturated n-hexane on Pd/SA-15 at 333 K.

In Table 4.2, the selectivity of EB on Pd/SA-15 significantly increased, becoming the main product after 2h (Selectivity achieved 70.3%). On the contrary, the selectivity of PE decreased to 23.1% after 2h. As PE is the initial dominant product, most of PE was transformed into EB due to reaction pathway Scheme 3.1. It is proved that alcohol products have the potential to be dehydrated on support acid sites. In order to elucidate whether PE dehydrated on acid sites contribute to the formation of EB on Pd/SA-15 catalyst surface, ATR-IR of PE adsorption on Pd/SA-15 at 333K was applied and the spectra was shown in Figure 4.6a. The band at 1494 cm^{-1} is due to C=C stretching vibration of phenyl group, band at 1454 cm^{-1} is assigned to CH_3 asymmetric stretching vibration, band at 1205 cm^{-1} is due to deformation mode of phenyl ring of PE, bands below 1200 cm^{-1} were overlapped with strong absorption bands of SiO_2 (C-O stretching vibration of PE at 1080cm^{-1} was also overlapped with bands of SiO_2).[145] Bands at 1955 cm^{-1}, 1886 cm^{-1} and 1809 cm^{-1} are due to combination bands of C-H out of plane bending mode of benzene ring.[156] Negative bands at 1656 cm^{-1} and 1575 cm^{-1} corresponding to styrene[157] grew with the increase of bands at 1955 cm^{-1}, 1886 cm^{-1} and 1809 cm^{-1}. This indicates styrene was generated by the consumption of PE on the catalyst support. In Figure 4.6b, characteristic peaks of styrene at 1656cm^{-1} and 1575cm^{-1} disappeared, which proved, styrene was produced by PE dehydration on acidic sites of the support and was further hydrogenated on Pd to produce EB. In Table 4.2, EB became the main product after reaction time of 2h, the selectivity was 70.3% at 2h which can be explained as the initial dominant product PE became abundant on the support and

dehydrated to styrene, more and more styrene then re-adsorb on Pd, further hydrogenated to EB.

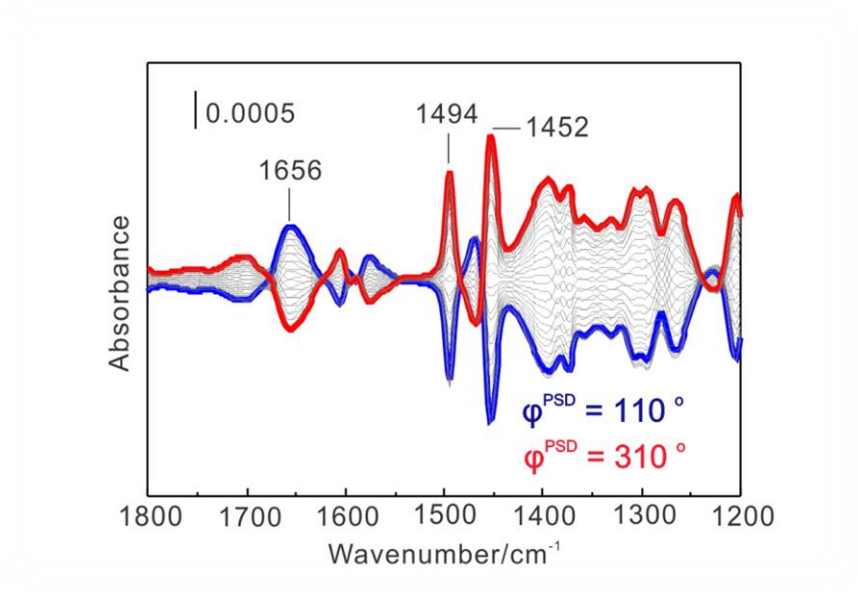

Figure 4.7 Phase-domain ATR-IR spectra during adsorption of PE (2 mM) in He-saturated n-hexane on Pd/SA-15 at 333 K.

To gain further information of styrene which was formed on Pd/SA-15, phase-domain spectra are shown in Figure 4.7. Clearly, the phase delay of band at 1656 cm^{-1} assignable to C=C stretching vibration of styrene is 250 º(360 º-110 º) whereas characteristic bands of PE at 1494cm^{-1} and 1452cm^{-1} possess a phase delay of 50 º(360 º-310 º). It is indicated that chemical species with positive absorbance at φ^{PSD} = 0 ° follow the same kinetics as the change in the solution and indicate that there is no time delay, i.e., phase delay 0 ° in the adsorption−desorption process.[130] Therefore, styrene was produced on Pd/SA-15 after the adsorption of PE on Pd/SA-15. This evidence further supports styrene formation was originally from PE dehydration on Pd/SA-15.

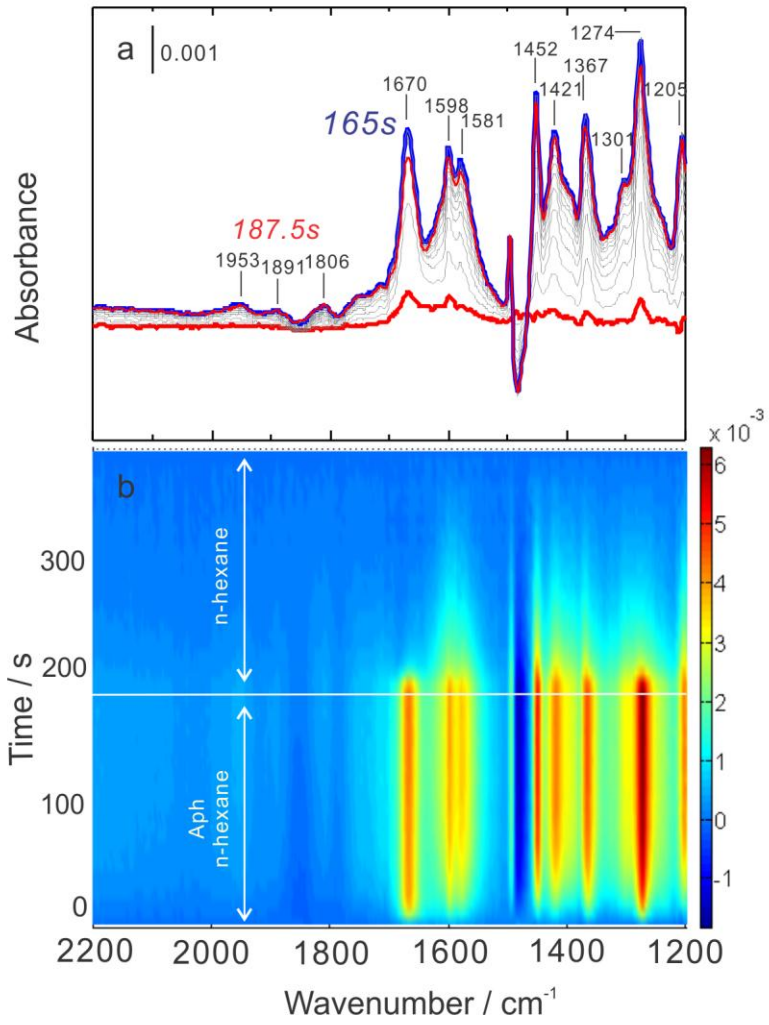

Figure 4.8 Time-domain spectra during hydrogenation of AP (2 mM) in H_2-saturated n-hexane on Pd/SA-70 at 333 K.

AP hydrogenation on Pd/SA-15 (Doping 15wt% Al_2O_3 into SiO_2) achieved significant increase in EB selectivity compared to the hydrogenation on Pd/SiO_2. (by comparing with Table 4.1 and Table 4.2)Taking this finding into account, we further increased catalyst surface acidity, doping 70wt% Al_2O_3 into SiO_2, followed by performing ATR-IR of AP hydrogenation on Pd/SA-70. Figure 4.8 showed AP adsorption and hydrogenation on Pd/SA-70. Bands appeared at 1205 cm^{-1}, 1806 cm^{-1}, 1891 cm^{-1} and 1953 cm^{-1} belong

to the product of PE (PE is the initial product with selectivity of 100% after 5 min as shown in Table 4.3). As described above, bands at 1953 cm^{-1}, 1891 cm^{-1} and 1806 cm^{-1} are due to C-H out of plane mode of benzene ring of PE,[156] these bands continuously grew until 187.5s whereas the band at 1670 cm^{-1} (C=O stretching of AP on the support) reached maximum intensity at 165s and significantly decreased until 187.5s, which indicates some newly produced PE replaced few AP on the support, aromatic ring of PE again adsorbed on the support of Pd/SA-70.

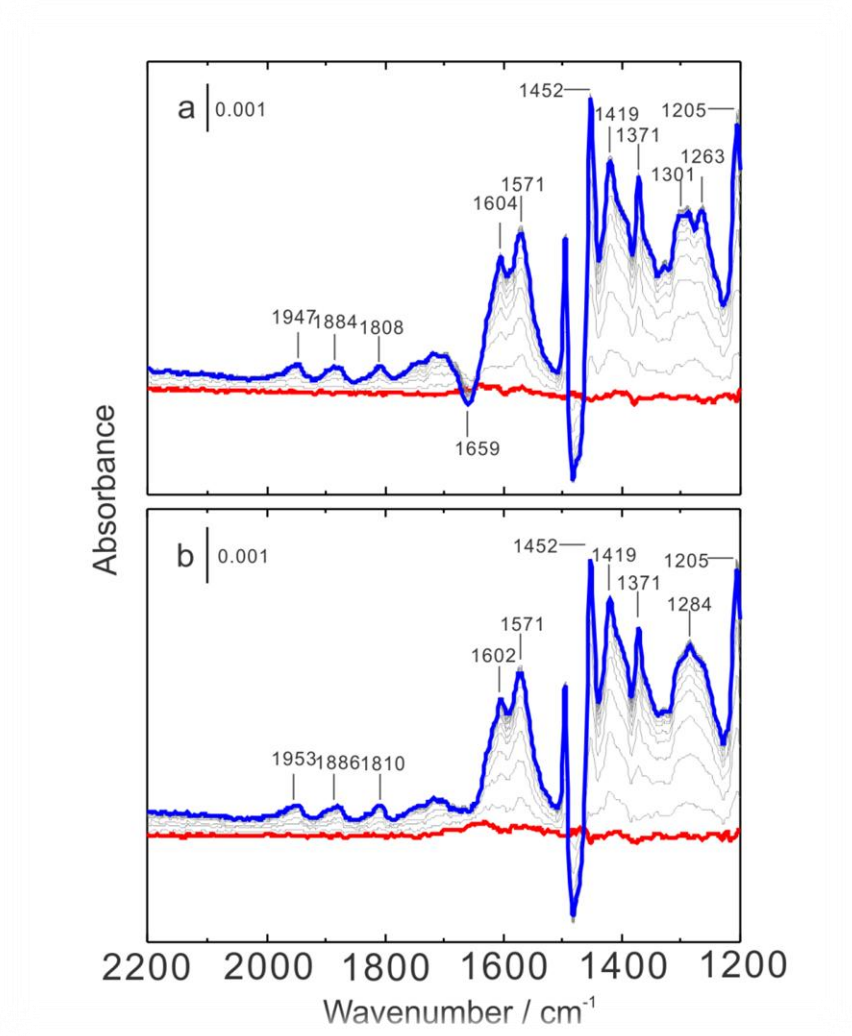

Figure 4.9 (a) Time-domain ATR-IR spectra during adsorption of PE (2 mM) in He-saturated n-hexane on Pd/SA-70 at 333 K. (b) Time-domain ATR-IR spectra during hydrogenation of PE (2 mM) in H_2-saturated n-hexane on Pd/SA-70 at 333 K.

As PE is also the initial dominant product of AP hydrogenation on Pd/SA-70, it is necessary to understand the formation process of PE on Pd/SA-70. Therefore, PE adsorption and hydrogenation was performed on Pd/SA-70. Figure 4.9 showed PE adsorption and hydrogenation on Pd/SA-70, the negative band at 1659 cm^{-1} is due to C=C stretching vibration of styrene, which is produced by PE dehydration on SA-70 support. Interestingly, the band intensity at 1659 cm^{-1} in Figure 4.9a is much lower than the band intensity at 1656 cm^{-1} in Figure 4.6a. Theoretically, PE dehydration should occur more intensely on high acidic support, which means more styrene should be formed on Pd/SA-70 than on Pd/SA-15. However, Figure 4.9a and Figure 4.6a showed reverse results. This could possibly be caused by the preferable protonation of styrene on strong acid sites to generate hydrocarbon cations. Hydrocarbon cations can hardly be detected by infrared spectroscopy.

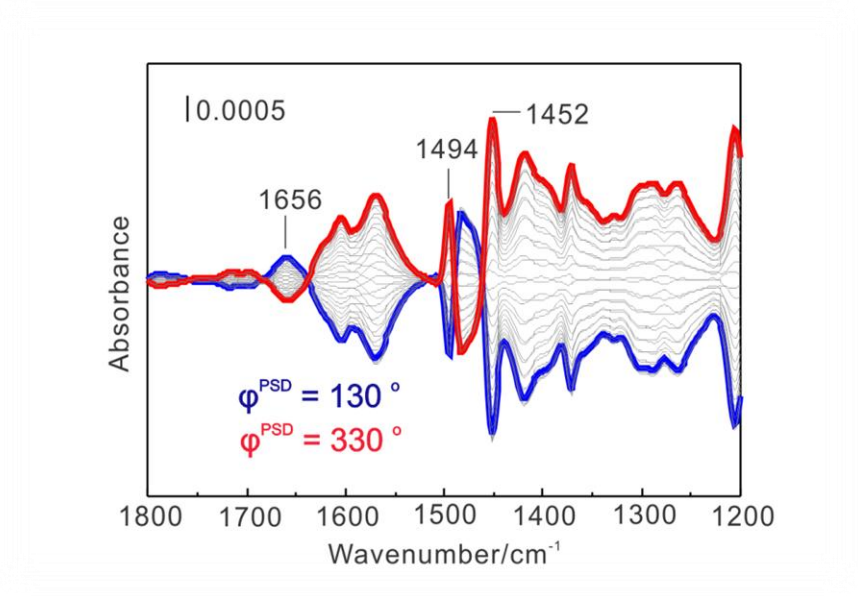

Figure 4.10 Phase-domain ATR-IR spectra during adsorption of PE (2 mM) in He-saturated n-hexane on Pd/SA-70 at 333 K.

To further elucidate kinetics of styrene formation on Pd/SA-70, phase-domain spectra are shown in Figure 4.10. Clearly, the phase delay of band at 1656cm^{-1} assignable to C=C stretching vibration of styrene is 230 º(360 º-130 º) whereas characteristic bands of PE at 1494cm^{-1} and 1452cm^{-1} possess a phase delay of 30 º (360 º-330 º). The observed information confirmed that small amount of styrene can also be generated by the consumption of PE on Pd/SA-70. In comparison with Pd/SA-15, PE adsorption was faster on Pd/SA-70 because the phase-delay of PE on Pd/SA-70 is 30 ºwhereas on Pd/SA-15 is 50 º. Although PE adsorption on Pd/SA-70 is faster than on Pd/SA-15, the formation of styrene from PE dehydration occurs more intensely on Pd/SA-15 than on Pd/SA-70. The moderate increase of acidic content on supports can promote PE dehydration and form dehydration product PE. However, strong acidity potentially hinders PE dehydration to produce styrene, but to increase the possibility in the production of hydrocarbon cations.

4.3 Conclusions

For AP hydrodeoxygenation on Pd/SA, this chapter addresses the understanding of mechanism differences of AP hydrodeoxygenation on supported palladium nanoparticles arose by the tuning of surface acidity. In situ ATR-IR spectroscopy combined with MES and PSD was applied to indentify tunable surface acidity effects on AP hydrodeoxygenation. The interaction of reactant AP or the reaction pathway component PE with supported palladium nanoparticles was studied. AP hydrodeoxygenation on SA supported nanoparticles showed an increase in EB selectivity with the increase of surface

acidity. In situ ATR-IR combined with MES and PSD proved that the initial AP hydrogenation product PE dehydrated on acidic sites of supports to produce styrene. The produced styrene can either desorb to liquid phase or further hydrogenated to EB. It is therefore concluded that styrene was only served as an intermediate during the formation of EB on acidic Pd/SA catalysts. The transformation of AP to EB on acidic catalysts undergo hydrogenation-dehydration mechanism, it includes hydrogenation of carbonyl bond of AP to produce alcohol product PE, followed by a dehydration in the production of styrene and further hydrogenation of the double bond of styrene to produce EB as summarized in Scheme 4.2.

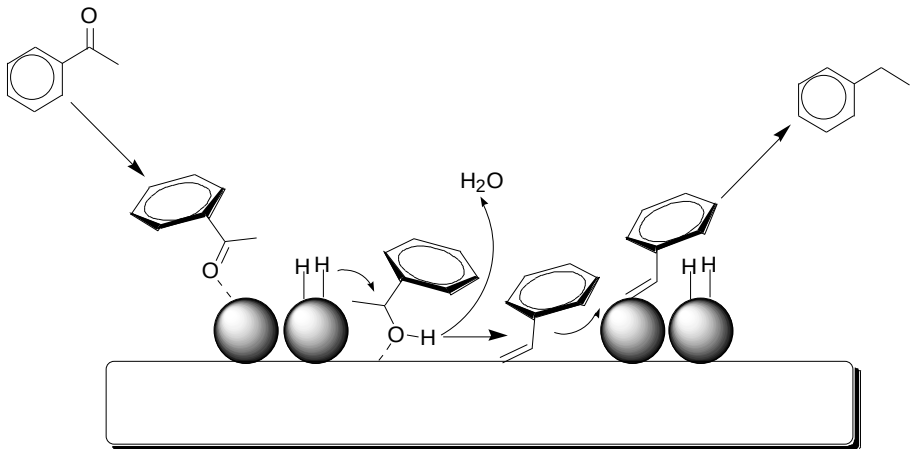

Scheme 4.2 AP hydrodeoxygenation mechanism on Pd/SA catalysts

5 Acetophenone (AP) hydrodeoxygenation (HDO) on Pt/Al-MCM-41

5.1 Introduction

Hydrogenation and hydrodeoxygenation of bio-oil model compounds has been studied over supported noble catalysts.[20, 88, 158, 159] Efforts have also been made on the development and modification of supports of noble catalysts to improve catalytic performance.[58, 62, 160] For the modification of supports, it has been proved that acidic supports showed much better performance than non-acidic ones in hydrogenation. For instance, the increasing of surface acidity of supported palladium catalyst can significantly improve catalytic hydrogenation activity and selectivity.[69] One of the possible reasons for the improvement would be tuning of support acid-base properties leading to the change of electronic properties of noble metal particles.[148, 151] However, problem concerning whether strong acid sites played a key role during hydrogenation of bio-oil model ketones was not addressed. Another possible reason for the catalytic activity difference, some authors suggested the effect of particle size may also be involved in catalytic hydrogenation performance.[133] Therefore, it is essential to clarify acid function of supported noble catalysts with uniform particle size in the hydrogenation of bio-oil model compounds.

MCM-41 as one of the M41S family members of ordered mesoporous silicates containing one-dimensional channels possess many advantageous features such as hexagonal

arrangement of uniformly sized mesopores, large surface area (usually>1000m^2/g) and mild acidity.[70, 71] This material has been widely used as catalyst supports for hydrogenation and hydrodeoxygenation. Since MCM-41 material possesses uniform mesoporous structure, metal nano-particles located in the channels of this support should have uniform particle size.

However, purely siliceous MCM-41 has no Brønsted acidity. Acidity could be generated through isomorphous substitution of Si by Al.[80] The amount and acid strength of the hydroxyl groups may be tuned with the incorporation of different amounts of Al atoms into the MCM-41 framework.[161-163] It is also reported that the mesoporous aluminosilicate MCM-41 is a suitable support for preparing noble metal based catalysts.[164] Furthermore, MCM-41 supported noble catalysts possess advantageous features and have been widely used in hydrogenation reactions. Therefore, it is interesting to study how the MCM-41 Si/Al ratio will affect the hydrogenation performance of Pt-based noble catalysts. Due to above concern, we use MCM-41 supported Pt catalysts with controlled particles size to identify the acid function during acetophenone (AP) hydrogenation, aiming to rule out the effect of particle size in AP hydrogenation over acid MCM-41 supported Pt catalysts.

In this chapter, we describe the synthesis and characterization of a series of Pt/Al-MCM-41 samples with different Si/Al ratios, followed by catalytic performance tests of bio-oil model compound – acetophenone (AP) hydrogenation on these catalysts. The structural properties of derived Pt/MCM-41 were determined by X-ray diffraction (XRD). N_2

adsorption and desorption and transmission electron microscopy (TEM) were used to identify physical properties of Pt/MCM-41 catalysts. TEM results confirmed that Pt particles were uniformly distributed inside MCM-41 channels. The structural and electronic properties were analyzed by CO adsorption on Pt/Al-MCM-41 by diffuse reflectance infrared Fourier transform spectroscopy (DRIFTS). Nuclear magnetic resonance (NMR) spectroscopy was used to identify the Brønsted acid sites of Pt/Al-MCM-41 catalysts.

5.2 Results and discussion

5.2.1 Catalyst synthesis and characterization

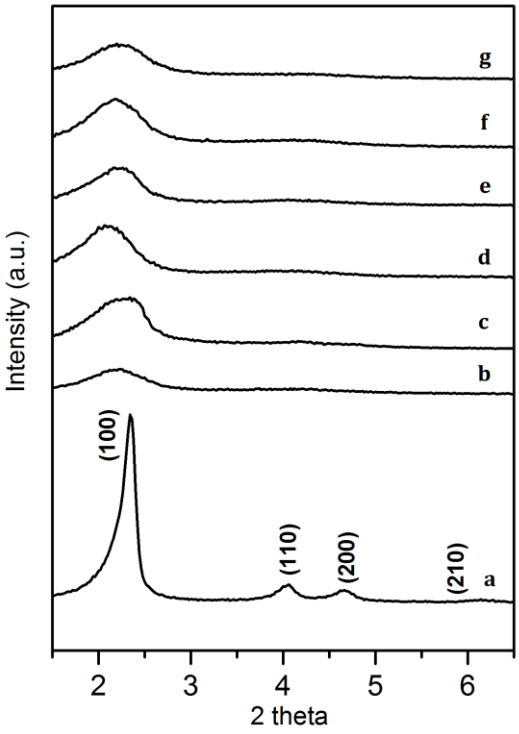

Figure 5.1 Small angles XRD patterns of (a) Pt/MCM-41 (b) Pt/MCM-41-50 (c) Pt/MCM-41-40 (d) Pt/MCM-41-30 (e) Pt/MCM-41-20 (f) Pt/MCM-41-15 and (g) Pt/MCM-41-10.

XRD patterns of small angles in the region 2θ = 1.5° - 6.5 ° of Pt/Al-MCM-41 with different Si/Al ratio are shown in Figure 5.1. The typical hexagonal lattice structure is observed for Pt/MCM-41 in Figure 5.1 (a) with the appearance of strong peak (100) at low angle and weak peaks (110), (200) and (210) at 4.1 °, 4.7 ° and 6.3 °. These peaks are characteristic peaks of long range order of crystallinity of the materials.[165] With increasing aluminum content, weak peaks (110), (200) and (210) became very small and broad as shown in Figure 5.1 (b), (c), (d), (e), (f) and (g). Furthermore, XRD patterns show a decrease in the intensity and broadening of peak (100), which might be caused by the distortion of the long-range ordering of the hexagonal structure as a consequence of the aluminum incorporation into the framework of MCM-41.[74, 166]

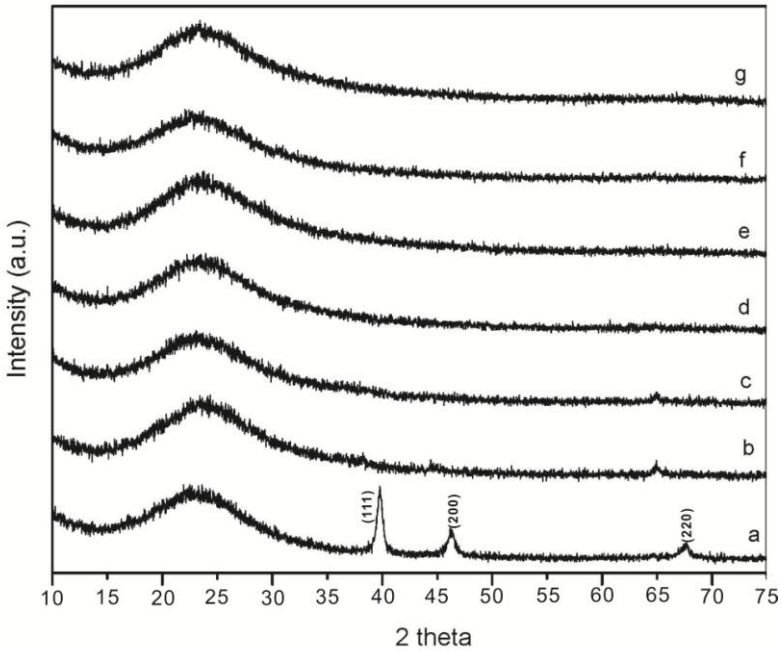

Figure 5.2 Large angles XRD patterns of (a) Pt/MCM-41 (b) Pt/MCM-41-50 (c) Pt/MCM-41-40 (d) Pt/MCM-41-30 (e) Pt/MCM-41-20 (f) Pt/MCM-41-15 and (g) Pt/MCM-41-10.

Figure 5.2 shows large angles XRD patterns in 2θ = 10 ° - 80 °. Characteristic reflections peaks at 2θ = 39.9°, 46.7° and 67.8° in figure 5.2 (a) to the reflection of (111), (200) and (220) appeared, which indicates big Pt particles occurred on the external surface (particle size=14.9nm at 2θ = 39.9° based on Scherrer equation) may form on Pt/MCM-41. However, in Figure 5.2 (b), (c), (d), (e), (f) and (g), no peaks at 2θ = 39.9°, 46.7° and 67.8° were clearly observed, suggesting no big crystal particles were formed. Thus, small Pt particles (3-6nm) were formed on supports of Pt/Al-MCM-41-50, Pt/Al-MCM-40, Pt/Al-MCM-41-30, Pt/Al-MCM-41-20, Pt/Al-MCM-41-15 and Pt/Al-MCM-41-10.

Table 5.1 N_2 physical adsorption and desorption of Pt/Al-MCM-41 with different Si/Al ratio

Pt/Al-MCM-41	Surface area (m^2/g)	Total pore volume (cm^3/g)	Average pore size (nm)
0Al	1313.603	1.111	3.38
Si/Al=10	1006.432	1.058	4.2
Si/Al=15	942.126	0.915	3.886
Si/Al=20	1040.827	0.878	3.37
Si/Al=30	970.922	0.84	3.46
Si/Al=40	958.935	0.899	3.75
Si/Al=50	1014.792	1.664	6.564

Table 5.1 displays the physical properties of Pt/Al-MCM-41 samples. 0Al, Si/Al=50, Si/Al=40, Si/Al=30, Si/Al=20, Si/Al=15 and Si/Al=10 in above figure represent Pt/MCM-41, Pt/Al-MCM-41-50, Pt/Al-MCM-41-40, Pt/Al-MCM-41-30, Pt/Al-MCM-41-15 and Pt/Al-MCM-41-10. It can be seen Pt/Al-MCM-41 with different Si/Al ratio possess variable physical properties. Specifically, BET surface areas of all Pt/Al-MCM-41 samples are above $940m^2/g$, Pt/Al-MCM-41 with 0Al shows maximum BET surface area of $1313.603m^2/g$. With Al incorporated into the framework of MCM-41, BET surface areas exhibit a decrease trend. Pore volumes of Pt/Al-MCM-41 samples are in the range of 0.84 to $1.664cm^3/g$. The average pore sizes distribute from around 3nm to 6nm as shown in the above table.

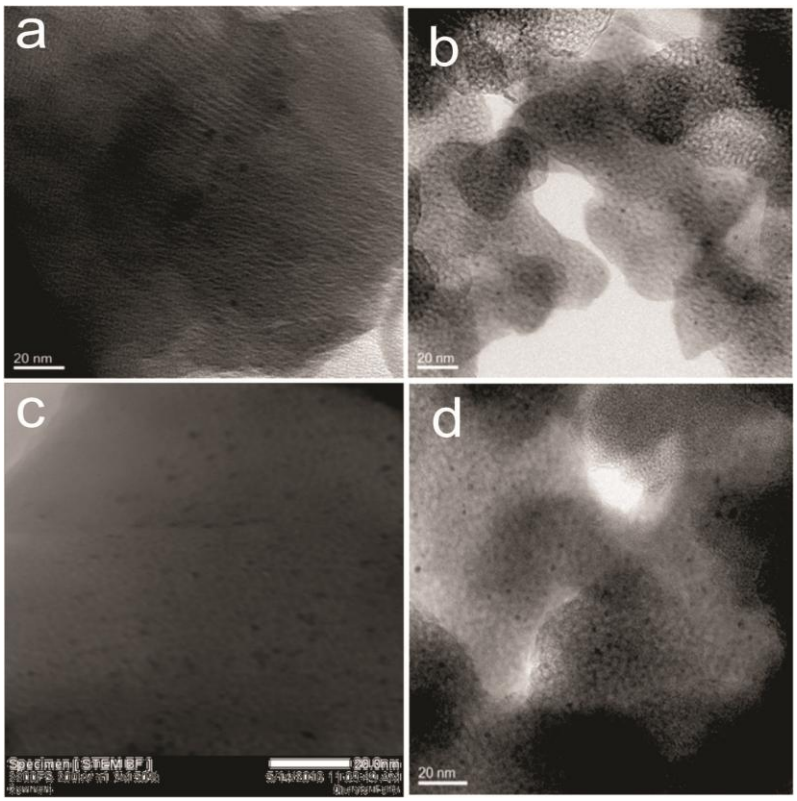

Figure 5.3 Transmission electron micrographs (TEM) images of (a) Pt/MCM-41 (b) Pt/Al-MCM-41-50 and (c) Pt/Al-MCM-41-20 (STEM) and (d) Pt/Al-MCM-41-10.

Figure 5.3 shows transmission electron micrographs (TEM) images of Pt/MCM-41, Pt/Al-MCM-41-50 and Pt/Al-MCM-41-20 and Pt/Al-MCM-41-10. For Pt/MCM-41 in Figure 5.3 (a), a typical regular mesoporous hexagonal pore channels structure can be clearly observed.[167] Most Pt particles loaded were uniformly distributed inside MCM-41 one-dimensional channels although XRD results in Figure 5.2 (a) show some Pt may form big particles distributed outside MCM-41 channels. When aluminum was introduced into the framework of MCM-41, TEM images of Pt/Al-MCM-41-50 of Figure 5.3(b)and Pt/Al-MCM-41-20 in Figure 5.3(c) and Pt/Al-MCM-41-10 in 5.3(d)exhibit irregular though hexagonal porous arrangement. It is thus apparent that incorporation of aluminum into the framework of MCM-41 seems to affect the long-range order of the

mesopores. However, the incorporation of aluminum did not damage the essentially mesoporous structure of the material.[74, 166] For Pt/Al-MCM-41-50, Pt/Al-MCM-41-20 and Pt/Al-MCM41-10 catalysts, Pt particles are still uniformly distributed inside MCM-41 channels as nanoparticles even with the incorporation of aluminium into the framework.

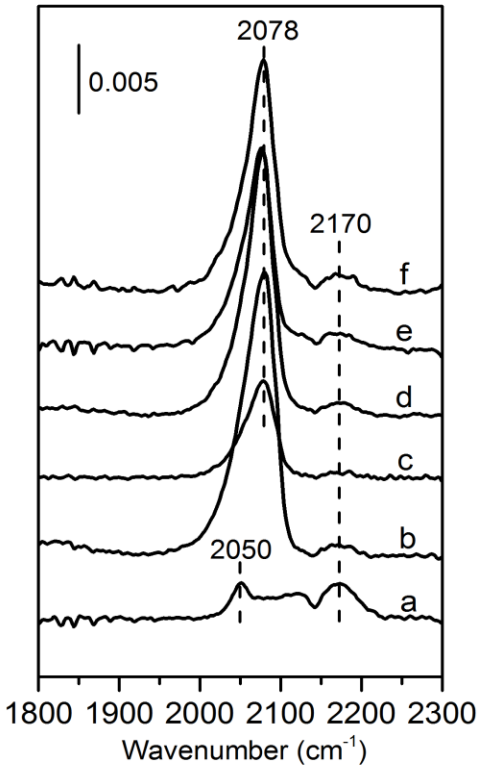

Figure 5.4 DRIFTS spectra of CO adsorption on (a) Pt/MCM-41 (b) Pt/Al-MCM-41-50 (c) Pt/Al-MCM-41-40 (d) Pt/Al-MCM-41-30 (e) Pt/Al-MCM-41-20 and (f) Pt/Al-MCM-41-15

Infrared spectroscopy of CO adsorption on supported metal clusters can assist in obtaining both structural and electronic properties of Pt nanoparticles. Specifically, the stretching frequencies and relative intensities of CO bands of CO adsorbed on supported Pt catalysts by IR spectroscopy are sensitive to oxidation state, particle size and metal-

support interaction.[168-172] On the basis of metal carbonyl spectra, bands in the region of 1950 cm^{-1} to 2100 cm^{-1} are usually assigned to linearly adsorbed CO species while bands between 1750 cm^{-1} and 1950 cm^{-1} are due to multibonded, bridged and threefold CO species.[173] Figure 5.4 shows DRIFTS spectra of CO adsorbed on a series of Pt/Al-MCM-41 samples. For Pt/Al-MCM-41, a band at 2050 cm^{-1} and a band at around 2170 cm^{-1} were observed which can be assigned to linear CO on Pt, almost no bridged coordination CO was detected. The band at 2050 cm^{-1} is considered to be assigned to CO adsorbed on Pt (100)[174, 175] whereas band at 2170 cm^{-1} can be assigned to CO adsorbed on Pt ions (such as oxidated state or interface between support and Pt or defects).[176] When Al was introduced into MCM-41, bands of linearly coordinated CO shifted from 2050 cm^{-1} (Pt/MCM-41) to around 2078 cm^{-1} (Pt/Al-MCM41-50, Pt/Al-MCM-41-40, Pt/Al-MCM-41-30, Pt/Al-MCM41-20 and Pt/Al-MCM-41-15). Studies have demonstrated that CO adsorbed on Pt particles inside zeolite channels leads to an increase in the stretching wavenumber (15 cm^{-1} to 23 cm^{-1}) because of the decrease of the electron density on the particles raised from interaction with strong Brønsted sites of highly acidic HZSM-5.[177, 178] Therefore, the shift from 2050 cm^{-1} to 2078 cm^{-1} might stem from the interaction of Pt particles inside MCM-41 channels with Brønsted acid sites generated by the incorporation of aluminium into MCM-41 framework. Moreover, bands intensity of 2078 cm^{-1} of Pt/Al-MCM41-50, Pt/Al-MCM-41-40, Pt/Al-MCM-41-30, Pt/Al-MCM41-20 and Pt/Al-MCM-41-15 significantly increased in comparison with the band at 2050 cm^{-1} of Pt/Al-MCM-41. This indicates more active sites were formed on the catalysts, leading to the increase of adsorption strength.

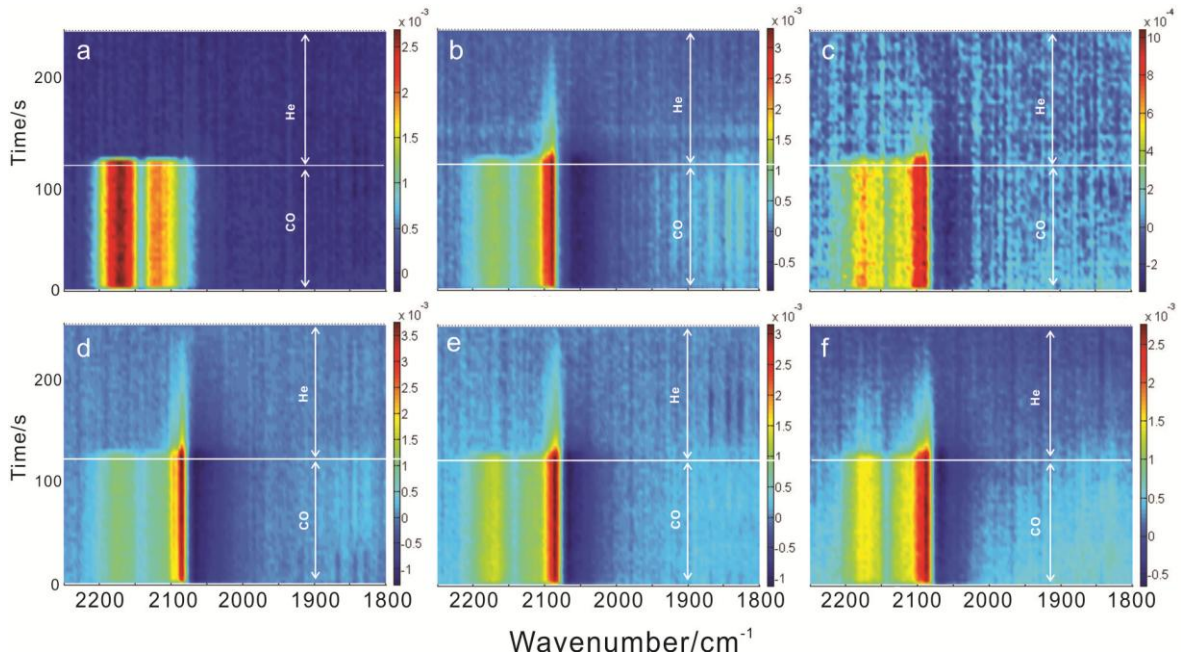

Figure 5.5 Time-domain IR spectra during CO adsorption and desorption on (a) Pt/MCM-41, (b) Pt/Al-MCM-41-50, (c) Pt/Al-MCM-41-40, (d) Pt/Al-MCM-41-30, (e) Pd/Al-MCM-41-20 and (f) Pd/Al-MCM-41-15 in mixture of CO, He and pure He.

Conventional infrared spectroscopy (IR) spectra can provide structural and electronic information of catalysts. A significant shortcoming of this technique is, however, the difficulty in monitoring catalytic kinetics. A combination of infrared spectroscopy (IR) and modulation excitation spectroscopy (MES) appeared and demonstrated its ability as a powerful tool for kinetics investigation.[129, 130] Therefore, we use diffuse reflectance infrared Fourier transform spectroscopy (DRIFTS) in combination with MES to monitor catalytic kinetics during CO adsorbed on Pt/Al-MCM-41 catalysts. IR spectra during CO adsorption and desorption on Pt/Al-MCM-41 are shown in Figure 5.5. Figure 5.5 (a) exhibited CO adsorption and desorption on Pt/MCM-41, a peak at around 2050 cm^{-1} indicates CO was mainly linearly bonded to Pt. Band at around 2170 cm^{-1} in Figure 5.5 (a) was probably due to CO adsorbed on Pt ions. After switching to pure He, bands at 2050

cm^{-1} and 2170 cm^{-1} immediately disappeared. For Pt/Al-MCM-41-50, Pt/Al-MCM-41-40, Pt/Al-MCM-41-30, Pd/Al-MCM-41-20 and Pd/Al-MCM-41-15, linearly bonded CO species appeared at around 2078 cm^{-1}. It is worth noting that desorption of bands at 2078 cm^{-1} in Figure 5.5 (b), 5.5 (c), 5.5 (d), 5.5 (e) and 5.5 (f) was delayed in comparison with band at around 2050 cm^{-1} in Figure 5.5 (a). The stronger CO adsorption due to delays observed in Figure 5.5 (b), (c), (d), (e) and (f) indicates more active sites were formed when Al was incorporated into MCM-41 framework.

In order to further understand kinetic information during CO adsorption and desorption on Pt/Al-MCM-41 catalysts, phase-domain spectra are shown below in Figure 5.6-5.10. Chemical species with positive absorbance at $\varphi^{PSD} = 0°$ (360°) follow the same kinetics as the change in the gas and indicate that there is no time delay while positive absorption bands at $\varphi^{PSD}<360°$ indicate that the rate of adsorption and desorption processes is slower than that of species at $\varphi^{PSD} = 0°$.[130]

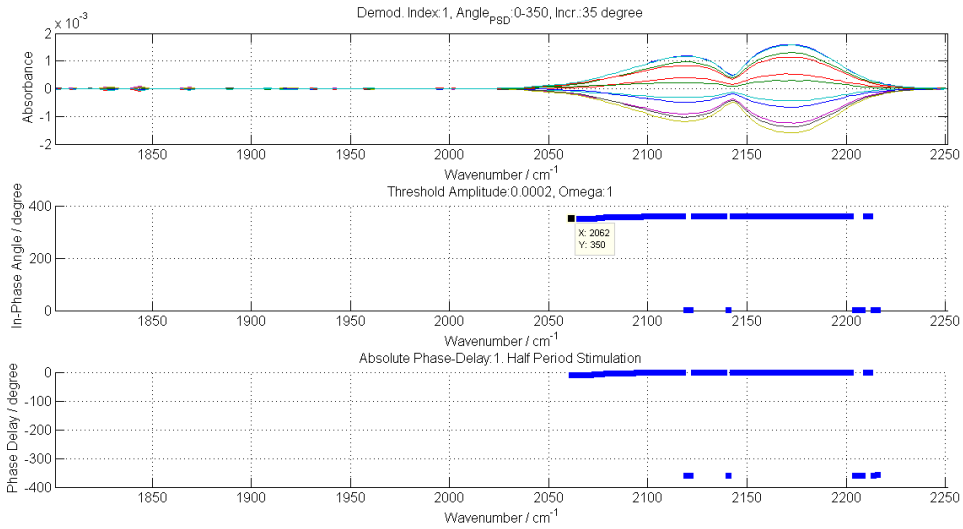

Figure 5.6 Phase-domain IR spectra during CO adsorption and desorption on Pt/MCM-41

Figure 5.6 shows phase domain spectra of CO adsorption and desorption on Pt/MCM-41. Absorption band at 2050cm^{-1} assignable to CO adsorption on Pt showed a phase-delay at around 10 º(360 º350 º).

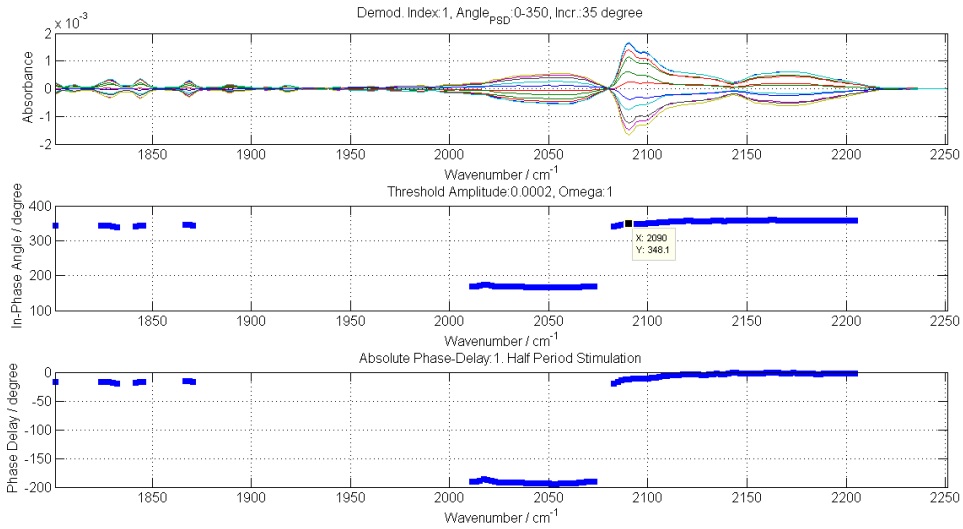

Figure 5.7 Phase-domain IR spectra during CO adsorption and desorption on Pt/Al-MCM-41-50

Figure 5.7 shows phase domain spectra of CO adsorption and desorption on Pt/Al-MCM-41-50. Absorption band at 2078cm^{-1} assignable to CO adsorption on Pt showed a phase-delay at around 11.9 º(360 º348.1 º).

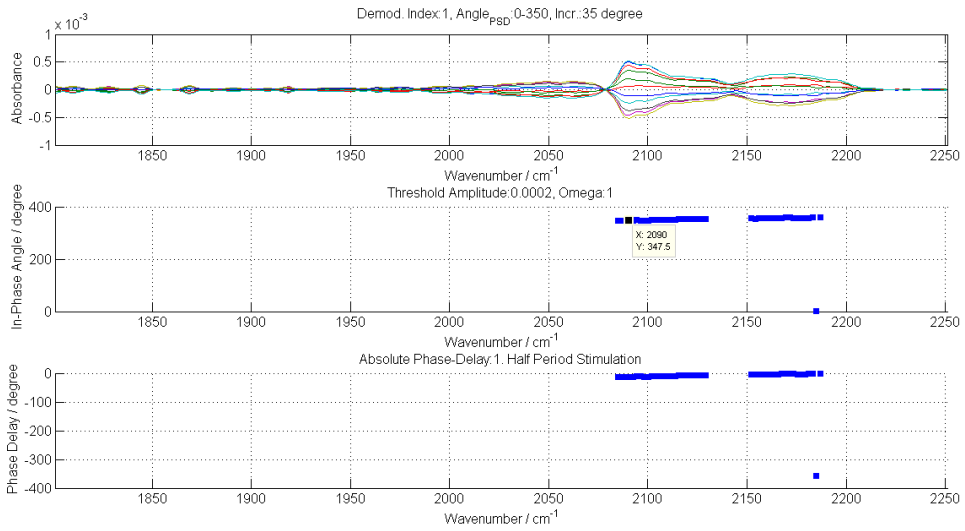

Figure 5.8 Phase-domain IR spectra during CO adsorption and desorption on Pt/Al-MCM-41-40

Figure 5.8 shows phase domain spectra of CO adsorption and desorption on Pt/Al-MCM-41-40. Absorption band at 2078cm^{-1} assignable to CO adsorption on Pt showed a phase-delay at around 12.5 º(360 º-347.5 º).

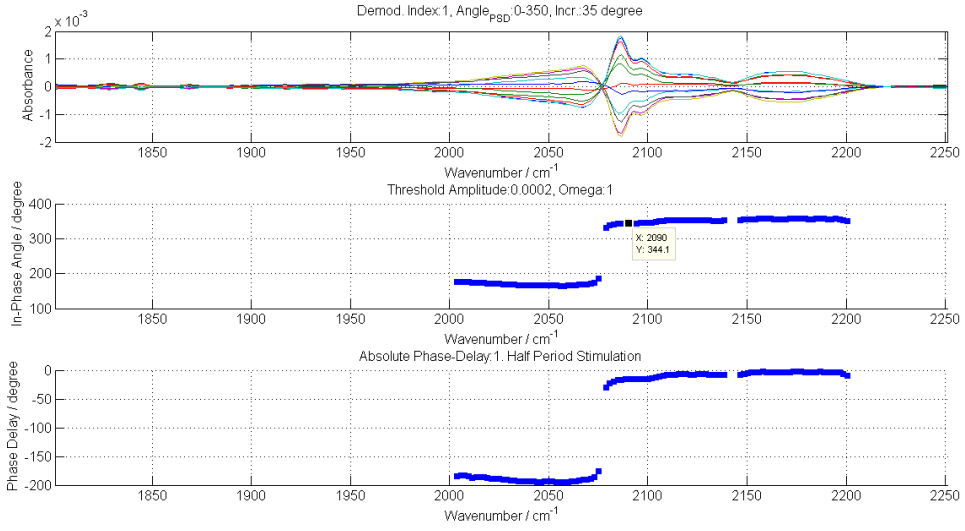

Figure 5.9 Phase-domain IR spectra during CO adsorption and desorption on Pt/Al-MCM-41-30

Figure 5.9 shows phase domain spectra of CO adsorption and desorption on Pt/Al-MCM-41-30. Absorption band at 2078cm^{-1} assignable to CO adsorption on Pt showed a phase-delay at around 15.9 º(360 º344.1 º).

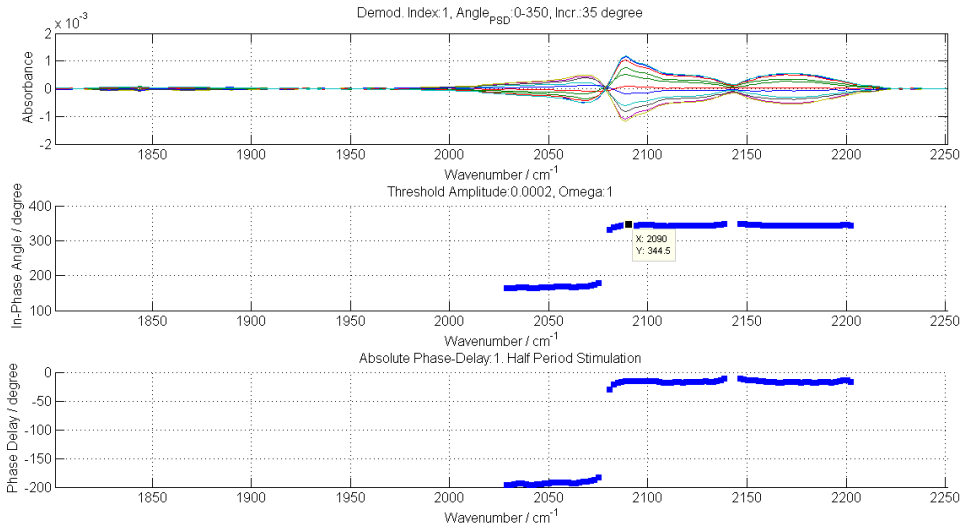

Figure 5.10 Phase-domain IR spectra during CO adsorption and desorption on Pt/Al-MCM-41-15

Figure 5.10 shows phase domain spectra of CO adsorption and desorption on Pt/Al-MCM-41-15. Absorption band at 2078cm^{-1} assignable to CO adsorption on Pt showed a phase-delay at around 15.5 º(360 º344.5 º).

From results in Figure 5.6-5.10, the rate of CO adsorption and desorption on Pt/Al-MCM-41 is Pt/Al-MCM-41-30 (15.9 ºdelay) < Pt/Al-MCM-41-15 (15.5 ºdelay) < Pt/Al-

MCM-41-40 (12.5 °delay) < Pt/Al-MCM-41-50 (11.9 °delay) < Pt/MCM-41 (10 °delay). It is obvious that with the increase of Al content from pure Si to Si/Al=30, the strength of CO adsorption on Pt/Al-MCM-41 was increased. Further increase Al content to Si/Al=15, CO adsorption strength on Pt/Al-MCM-41-15 was decreased in comparison with on Pt/Al-MCM-41-30. Therefore, the increase of Al content from pure Si to Si/Al=30 results in the increase of active sites on catalysts, which is explained by the effect of supports acidity on electronic properties of Pt particles.[69] The further increase of Al content on support leads to a decrease in the number of active sites because the overloading of Al can hinder the accessibility of CO to Pt particles inside MCM-41 pores.

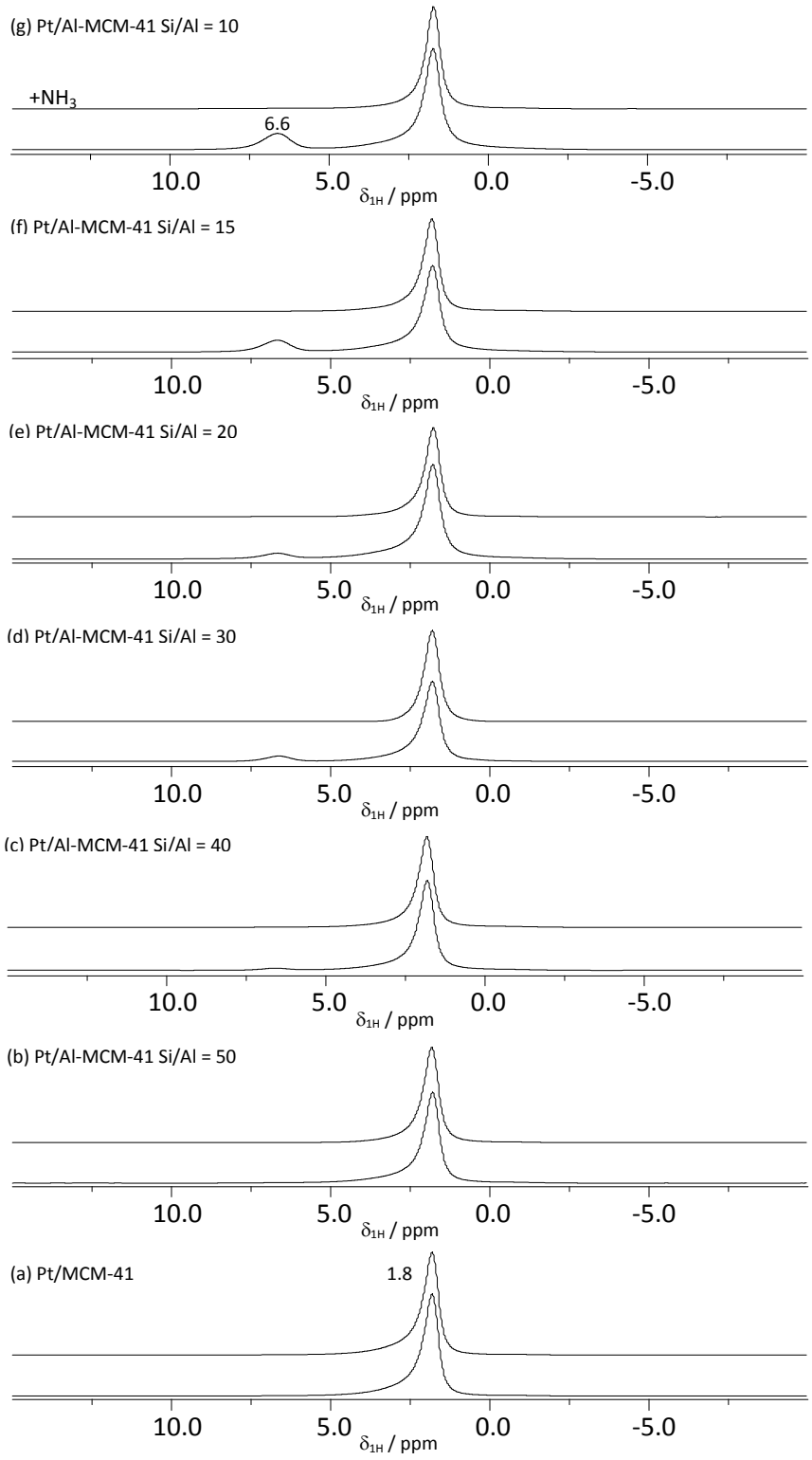

Figure 5.11 ^{1}H MAS NMR spectra of Pt/MCM-41 (a), Pt/Al-MCM-41 of Si/Al = 50 (b), Si/Al = 40 (c), Si/Al = 30 (d), Si/Al = 20 (e), Si/Al = 15 (f) and Si/Al = 10 (g) recorded after dehydrated at 723 K before and after loading with NH_3, subsequent evacuation at 393 K

^{1}H MAS NMR spectroscopy was employed to investigate the surface hydroxyl protons. The ^{1}H MAS NMR spectrum of Pt/Al-MCM-41 showed a strong peak at d_{1H} = 1.8 ppm which is due to silanol groups. Loading of NH_3 on the series of Pt/Al-MCM-41 catalysts, however, led to ^{1}H NMR signals of ammonium ions at 6.5-7.0 ppm (Figure. 5.11 c-g). This finding confirmed that the presence of SiOH groups with enhanced Brønsted acidity, caused by the incorporation of aluminum into the MCM-41 support material. The NMR intensities of the ammonium signals were utilized to quantify the number of Brønsted acid sites. The concentration and molar fraction of these Brønsted acid sites are summarized in Table 5.2. The results indicate total acid number decreases with the increase of Si/Al ratio. Specially, Pt/MCM-41 and Pt/Al-MCM-41-50 in Figure 5.11 (a) and (b) show almost no Brønsted acidity since small amounts of Brønsted acid sites were covered by Pt particles. With increasing Al content of Pt/Al-MCM-41, the surface acidity continuously increase up to Si/Al=10.

Table 5.2 Concentration of Brønsted acid sites of Pt/Al-MCM-41 with different Si/Al ratio

Pt/Al-MCM-41	Proportional of Brønsted acid sites/(mol %)	Population of Brønsted acid sites mmol/g	Population of Brønsted acid sites/nm^2	OH/Pt ratio
0Al	-	-	-	-
Si/Al=10	16	0.118	70.4×10^{-3}	23.7
Si/Al=15	14.22	0.127	81.3×10^{-3}	25.5
Si/Al=20	7.4	0.057	33.0×10^{-3}	11.4
Si/Al=30	7	0.048	29.7×10^{-3}	9.6
Si/Al=40	2.92	0.018	11.3×10^{-3}	3.6
Si/Al=50	-	-	-	-

Note: Brønsted acid sites (mol%) = (number of Brønsted acid sites/total number of OH sites on supports)×100%

5.2.2 Catalytic performances of catalysts

5.2.2.1 Conversion

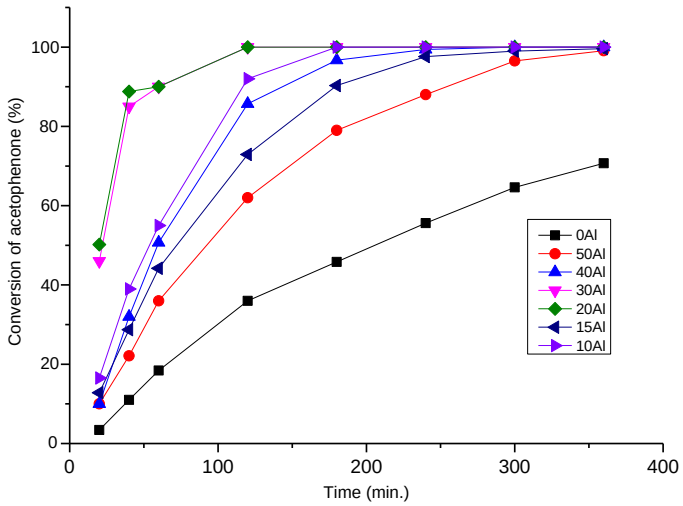

Figure 5.12 Catalytic conversion of AP hydrogenation on Pt/Al-MCM-41 at 1bar H_2 and room temperature, 360 min reaction time

To understand the effect of support acidity on acetophenone (AP) hydrogenation, AP hydrogenation was performed on a series of Pt/Al-MCM-41 catalysts with Si/Al= 10, 20, 30, 40, 50 and pure Si at 1bar H_2 pressure and room temperature. Figure 5.12 shows AP conversion on the series of Pt/Al-MCM-41. Pt/MCM-41 exhibits the lowest catalytic activity. The conversion of AP on Pt/MCM-41 only reaches 70.7% even after 360 min reaction time. Pt/Al-MCM-41-50 possesses slightly increasing acidity as summarized in Table 5.2, the conversion of AP on Pt/MCM-41-50 is higher than Pt/MCM-41 reaching 79% after only 180 min. Pt/Al-MCM-41-40 possesses even better catalytic activity than

Pt/Al-MCM-41-50 due to enhanced acidity by increasing Al content of support, with 85.7% conversion of AP after 120 min. With further increasing Al content, Pt/Al-MCM-41-20 shows the best catalytic performance with 88.8% conversion of AP only after 40 min. However, compared to Pt/Al-MCM-41-20, catalytic activity of Pt/Al-MCM-41-10 significantly decreased although the acidity of Pt/Al-MCM-41-10 is higher than that of Pt/Al-MCM-41-20. Notably, Pt/Al-MCM-41-15 with the highest Brønsted acid OH population as summarized in Table 5.2 shows even worse catalytic performance than Pt/Al-MCM-41-10.

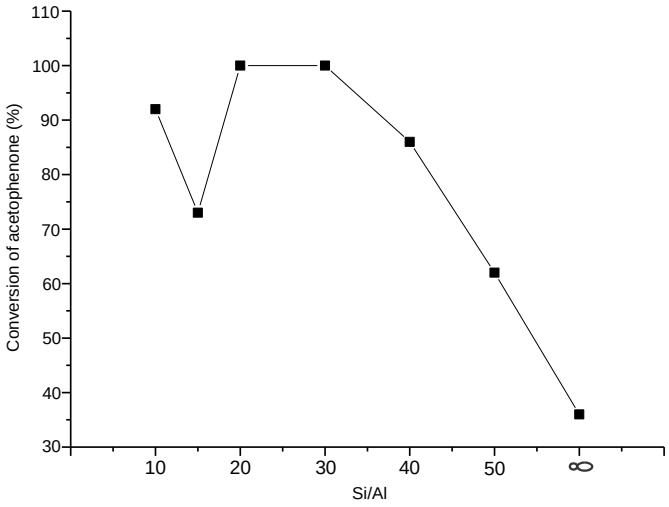

Figure 5.13 Effect of the Si/Al ratio of the support of Pt/Al-MCM-41 catalysts on the hydrogenation conversion of acetophenone at 1bar H_2 and room temperature, 120 mins reaction time

Figure 5.13 summarized the effect of Si/Al ratio of support on the catalytic conversion of AP. It can be clearly seen that the conversion of AP increases with Al content increasing up to Si/Al=20. Further increasing support Al content to Si/Al=15, the catalytic performance was decreased from 100% to 73%. When Si/Al content was increased to 10,

catalytic reactivity was increased again to 92%. As observed in Figure 5.3, Pt particles of Pt/Al-MCM-41 possess uniform distribution and similar particle size, therefore we assume the influence of particle size of Pt/Al-MCM-41 catalysts can almost be ruled out. Then, the catalytic behaviour clearly correlates with different properties of the supports when Pt particles are averagely distributed in MCM-41 supports. As summarized in Table 5.2, support composition difference lead to the change of proportional and population of Brønsted acid sites of Pt/Al-MCM-41. Notably, with increasing Al content from Si/Al=50 to Si/Al=20, population of Brønsted acid sites gradually increase from 11.3×10^{-3} OH/nm^2 to 33.0×10^{-3} OH/nm^2. This corresponds well with catalytic performance result because conversion of AP keep increasing with the increase of Al content to Si/Al=20. Further increasing Al content from Si/Al=20 to Si/Al=15, Brønsted acid sites significantly increased from 33.0×10^{-3}OH/nm^2 to 81.3×10^{-3} OH/nm^2. However, catalytic conversion significantly decreased from 100% to 73%. When Al content was increased from Si/Al=15 to Si/Al=10, Brønsted acid sites decreased from 81.3×10^{-3} OH/nm^2 to 70.4×10^{-3} OH/nm^2, catalytic performance increased again from 73% to 92%.

It has been proposed and proved that acidic and more covalent supports weaken Pt-H bond strength during hydrogenation, thereby improve catalytic activity of Pt or Pd-catalyzed hydrogenation.[69] Moreover, hydrogenation activity can generally be enhanced on Pt or Pd catalysts loading on acidic supports compared with that on non-acidic supports because molecules on acidic catalysts can absorb on both metal surface and acid sites in the metal–support interfacial regions and hydrogenate with the hydrogen spillover activated by metal sites.[179] Therefore, catalytic activity should increase with

the increasing of total acid sites of supports. However, from our observation, the catalytic activity of Pt/Al-MCM-41 was not totally parallel to acid sites of the catalysts when the particle size and distribution effect can almost be ruled out. We might think this can be caused by over loading of Al content into MCM-41 support. Since MCM-41 is nano-porous material, the relative accessibility of strong acid sites to reactants can be hindered with increasing contents of aluminium, thereby decrease the catalytic activity of supported Pt catalysts. In other words, a large proportion of the Al in Al-MCM-41-10 sample is buried deep within the pores where it offers the limited diffusion of reactants to accessible acid sites.[81]

5.2.2.2 Selectivity

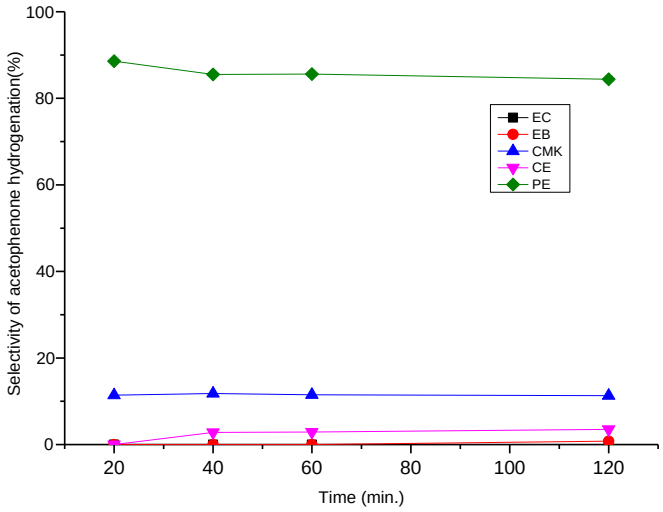

Figure 5.14 Selectivity of AP hydrogenation on Pt/MCM-41 at 1bar H_2 and room temperature, 120 min reaction time at conversion of 36%

Figure 5.14 shows the selectivity of AP hydrogenation on Pt/MCM-41 in 120 min. It can be seen from the above figure, the main product of AP hydrogenation on Pt/MCM-41 was 1-phenylethanol (PE). Small amounts of 1-cyclohexylmethylketone (CMK), 1-cyclohexylethanol (CE) and ethylbenzene (EB) were also generated. Structures of these compounds can be found in Scheme 3.1. The selectivity of PE was 88.6% after 20 min at conversion of 3.4% and only slightly decreased to 84.4% after 120 min when the conversion reached 36%. The selectivity of CMK kept almost stable at around 11%. In 20 min at conversion of 3.4%, no CE was produced. The selectivity of CE increased to 3.5% after 120 min at conversion of 36%. In 60 min, EB was not produced. After 60 min, EB began to appear and the selectivity of EB was 0.8% after 120 min at conversion of 36%. The product of ethylcyclohexane (EC) was not produced in 120 min.

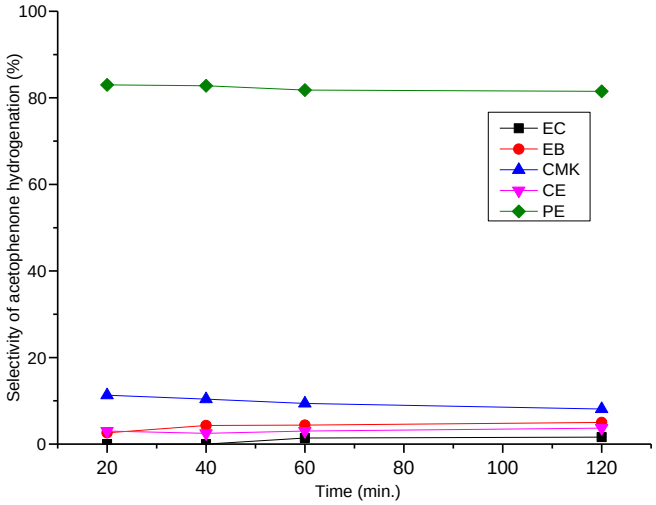

Figure 5.15 Selectivity of AP hydrogenation on Pt/Al-MCM-41 with Si/Al=50 at 1bar H_2 and room temperature, 120 min reaction time at conversion of 62%

To understand the acidity effect on the hydrogenation of AP, AP hydrogenation was performed on Pt/Al-MCM-41 with different amount of Al was incorporated into the framework. Starting with low Al content, we applied AP hydrogenation on Pt/Al-MCM-41 with Si/Al=50. As shown in Figure 5.15, PE, CMK, CE, EB and EC were produced. PE was the main product of AP hydrogenation on Pt/Al-MCM-41-50. The selectivity of PE was 83% after 20 min at conversion of 10% and slightly decreased to 81.5% after 120 min at conversion of 62%. The second main product was CMK. 11.3% of CMK was produced after 20 min at conversion of 10% and the selectivity of CMK slightly decreased to 8.1% after 120 min at conversion of 62%. CE, EB and EC only accounted for a small amount of products. The selectivity of CE, EB and EC all slightly increased over reaction time of 120 min. The selectivity of CE increased from 3% after 20 min at conversion of 10% to 3.7% after 120 min at conversion of 62%. The selectivity of EB increased from 2.6% after 20 min at conversion of 10% to 5% after 120 min at conversion of 62%. EC was not produced in 40min, the selectivity of EC was only 1.6% after 120 min at conversion of 62%.

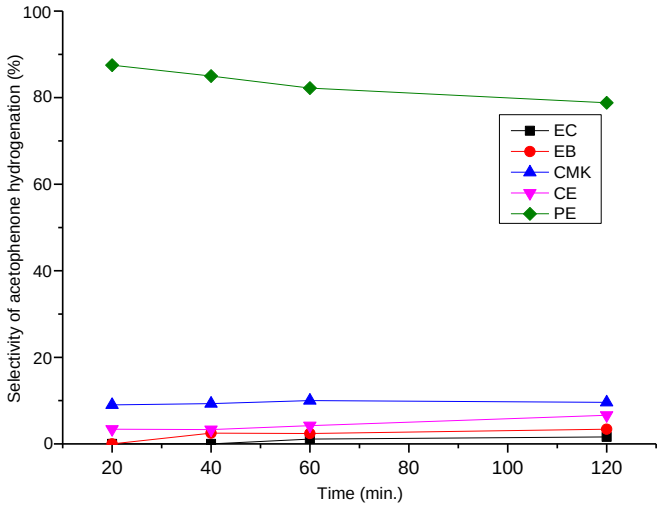

Figure 5.16 Selectivity of AP hydrogenation on Pt/Al-MCM-41 with Si/Al=40 at 1bar H_2 and room temperature, 120 min reaction time at conversion of 86%

AP hydrogenation was then performed on Pt/Al-MCM-41 with Si/Al=40. Figure 5.16 shows the selectivity of AP hydrogenation on Pt/Al-MCM-41-40. Similar to AP hydrogenation on Pt/MCM-41 and Pt/Al-MCM-41-50, PE was the main product over a reaction time of 120 min. However, the selectivity of PE decreased from 87.5% after 20 min reaction time at conversion of 10% to 78.8% after 120 min reaction time at conversion of 85.7%. The selectivity of PE decreased 8.7% on Pt/Al-MCM-41-40 over reaction time of 120 min. Notably, the selectivity of PE only decreased 1.5% on Pt/Al-MCM-41-50 in the same reaction time and condition. CMK appeared as the second main product, the selectivity of CMK kept almost the same at around 10% over the reaction time of 120 min. The selectivity of CE was 3.4% after 20 min at conversion of 10% and increased to 6.6% after 120 min at conversion of 85.7%. EB was not produced in 20 min, the selectivity of EB reached 3.4% after 120 min at conversion of 85.7%. In 40 min, EC

was not produced. The selectivity of EC slightly increased to 1.6% after 120 min at conversion of 87.5%.

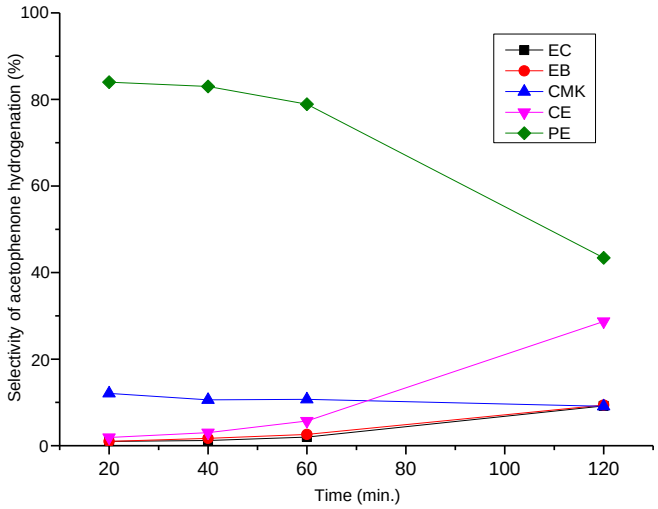

Figure 5.17 Selectivity of AP hydrogenation on Pt/Al-MCM-41 with Si/Al=30 at 1bar H_2 and room temperature, 120 min reaction time at conversion of 100%

AP hydrogenation showed significant difference when we further increased the support acidity. As shown in Figure 5.17, for the hydrogenation of AP on Pt/Al-MCM-41-30, PE, CMK, CE, EB and EC were produced. PE was the main product after 20 min at conversion of 46% with selectivity of 84%. However, the selectivity of PE significantly decreased to 43.4% after 120 min when conversion reached 100%. This indicates the selectivity of PE decreased 40.6% over reaction time of 120 min. In the meanwhile, the selectivity of CE significantly increased from 1.9% after 20 min at conversion of 46% to 28.7% after 120 min at conversion of 100%. The selectivity of CMK, EB and EC only slightly changed over the reaction time of 120 min. The selectivity of main product PE of

AP hydrogenation on Pt/Al-MCM-41-30 was only 43.4% after 120 min, which was much lower than that of AP hydrogenation on Pt/MCM-41, Pt/Al-MCM-41-50 and Pt/Al-MCM-41-40. It is interesting that the selectivity of CE achieved 28.7% after 120 min at conversion of 100% on Pt/Al-MCM-41-30, which was much higher that on Pt/MCM-41, Pt/Al-MCM-41-50 and Pt/Al-MCM-41-40. This phenomenon might indicate aromatic ring was more easily hydrogenated with increasing support acidity because the selectivity of PE significantly decreased whereas selectivity of CE increased to a high percentage. Due to the reaction pathway in Scheme 3.1, CE can either be produced from PE or CMK, CMK kept almost at constant amount. Thus, PE was most easily converted to CE on support acidity enhanced catalyst.

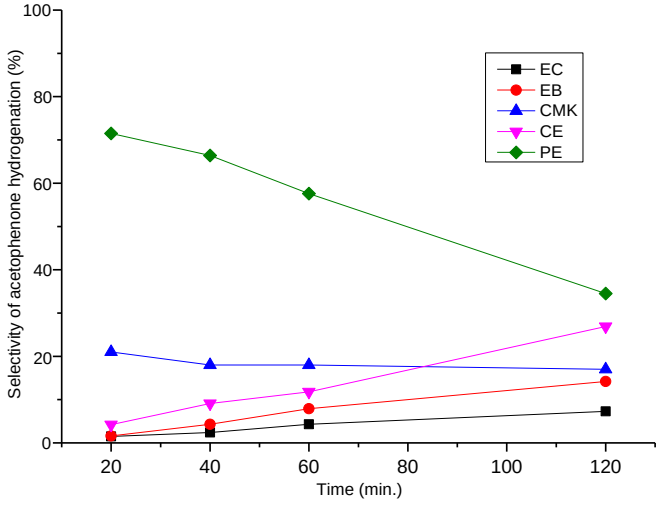

Figure 5.18 Selectivity of AP hydrogenation on Pt/Al-MCM-41 with Si/Al=20 at 1bar H_2 and room temperature, 120 min reaction time at conversion of 100%

Figure 5.18 shows AP hydrogenation on Pt/Al-MCM-41-20. It can be seen that products of PE, CE, CMK, EB and EC were detected over a reaction time of 120 min. PE was the

main product at the beginning with a selectivity of 71.5% after 20 min at conversion of 50.2%. Similar to AP hydrogenation on Pt/Al-MCM-41-30, the selectivity of PE significantly decreased to 34.5% after 120 min at conversion of 100%. Meanwhile, the selectivity of CE increased from 4.2% after 20 min at conversion of 50.2% to 26.9% after 120 min at conversion of 100%. The selectivity of CMK, EB and EC did not significantly change. Specially, the selectivity of CMK almost kept at the same over a reaction time of 120 min. The selectivity of EB increased from 1.6% after 20 min at conversion of 50.2% to 14.2% after 120 min at conversion of 100%. 1.5% EC was produced after 20 min (AP conversion of 50.2%), increasing to 7.3% after 120 min (AP conversion of 100%). This phenomenon confirms our deduction that PE was most easily converted to CE on support acidity enhanced catalyst.

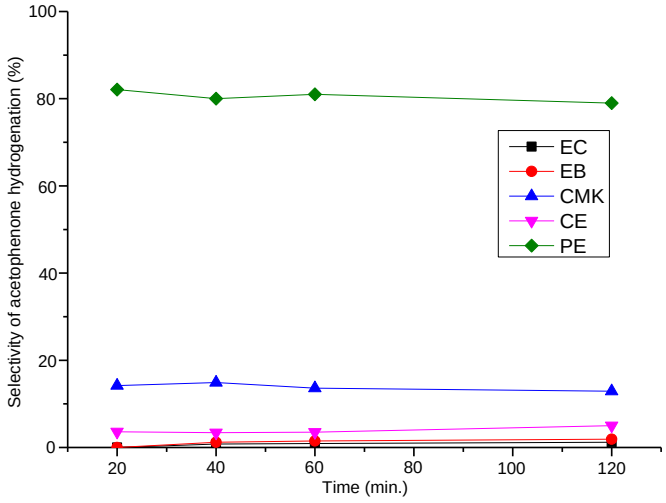

Figure 5.19 Selectivity of AP hydrogenation on Pt/Al-MCM-41 with Si/Al=15 at 1bar H_2 and room temperature, 120 min reaction time at conversion of 73%

With further increasing surface acidity, AP hydrogenation was performed on Pt/Al-MCM-41-15. As shown in Figure 5.19, PE appeared as dominant product over reaction time of 120 min. The selectivity of PE was 82.1% after 20 min (12.8% AP conversion), slightly decreased to 79.1% after 120 min (72.9% AP conversion). The selectivity of CMK kept almost unchanged at 13%-14% over 120 min. CE selectivity slightly increased from 3.6% after 20 min to 5% after 120 min. Almost no EB or EC was produced over120min.

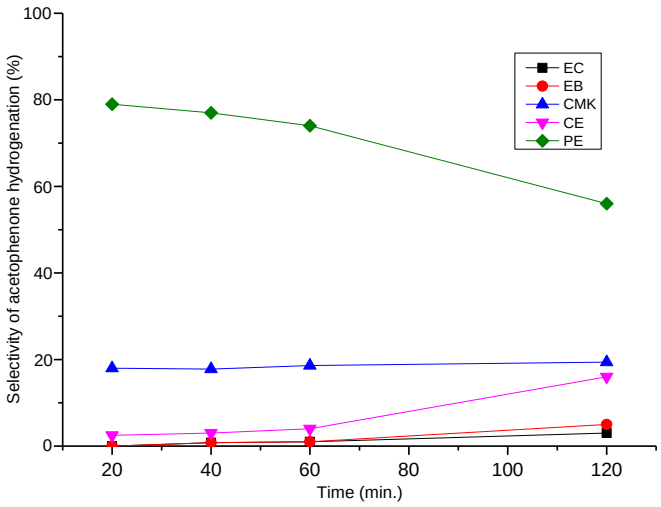

Figure 5.20 Selectivity of AP hydrogenation on Pt/Al-MCM-41 with Si/Al=10 at 1bar H_2 and room temperature, 120 min reaction time at conversion of 92%

AP hydrogenation was also performed on Pt/Al-MCM-41 with Si/Al=10. The selectivity of main product PE was 79% after 20 min (conversion of 16.5%) and decreased to 56% after reaction time of 120 min (conversion of 92%). On the other hand, CE selectivity increased from 2.5% after 20 min to 16% after 120 min. The selectivity of CMK kept

constant at 18%-19% over reaction time of 120 min. Only 3% EC and 5% EB were produced after 120min.

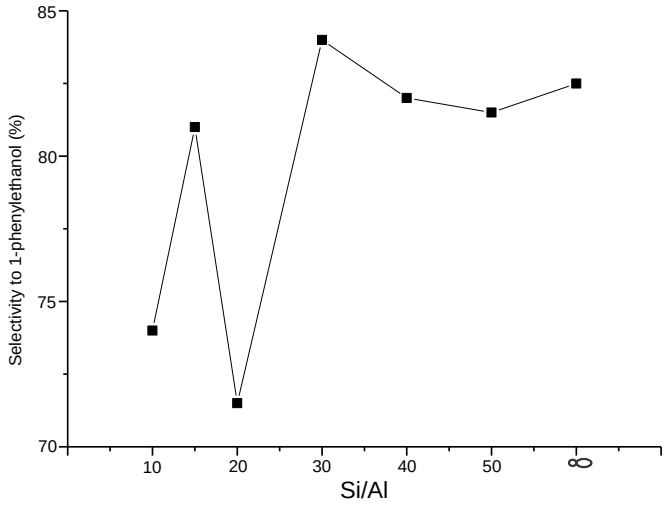

Figure 5.21 Effect of the Si/Al ratio of the support of Pt/Al-MCM-41 catalysts on the hydrogenation selectivity of acetophenone (AP) to the C=O hydrogenation product 1-phenylethanol PE at 1bar H_2 and room temperature at 50% conversion

Figure 5.21 shows the effect of Si/Al ratio of support on the catalytic selectivity to PE at conversion of 50%. With increasing support Al content from pure Si to Si/Al=30, AP hydrogenation showed high selectivity to produce PE (above 80%). However, when surface acidity was increased to Si/Al=20, the selectivity of PE significantly decreased to 71.5%. Further increasing Al content to Si/Al=10, the selectivity of PE slightly increased to 74%. PE selectivity on Pt/Al-MCM-41-15 (Si/Al=15) was higher than on Pt/Al-MCM-41-10 (Si/Al=10). Notably, Pt/Al-MCM-41-15 (81.3×10^{-3}OH/nm^2 Brønsted acid sites)

possesses higher acidity than Pt/Al-MCM-41-10 (71.4×10^{-33}OH/nm^2) as summarized in Table 5.2.

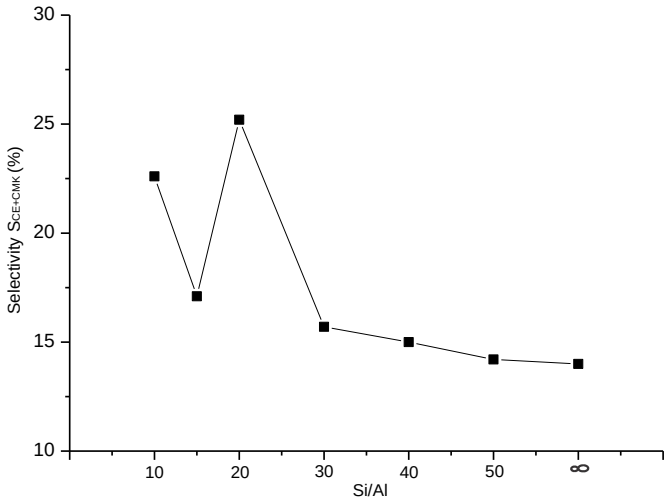

Figure 5.22 Effect of the Si/Al ratio of the support of Pt/Al-MCM-41 catalysts on the hydrogenation selectivity of acetophenone (AP) to the aromatic ring hydrogenation products 1-cyclohexylethanol and cyclohexylmethylketone (CE+CMK) at 1bar H_2 and room temperature at 50% conversion

On the contrary of C=O of AP hydrogenation to produce PE, selectivity to aromatic ring products of CE+CMK was low on Pt/MCM-41, Pt/Al-MCM-41-50, Pt/Al-MCM-41-40 and Pt/Al-MCM-41-30 (14% to 16%). It is worth noting that in Figure 5.22 with increasing Al content from pure Si to Pt/Al-MCM-41-30, selectivity to CE+CMK gradually increased from 14% to 15.7%. Further increasing Al content to Si/Al=20, selectivity to CE+CMK significantly increased to 25.2% and then decreased to 22.6% on Pt/Al-MCM-41-10. The selectivity to CE+CMK on Pt/Al-MCM-41-15 was decreased again in comparison with on Pt/Al-MCM-41-10. Notably, Pt/Al-MCM-41-15 ($81.3\times10^{-}$

^{3}OH/nm^{2} Brønsted acid sites) has higher acidity than Pt/Al-MCM-41-10 (71.4×10^{-33}OH/nm^{2}).

Due to results in Figure 5.21 and Figure 5.22, increasing surface acidity from pure SiO_2 to Si/Al=20 promotes the hydrogenation of aromatic ring to produce CE+CMK and weakens the hydrogenation toward carbonyl group to generate PE. However, excessive surface acidity (Si/Al=10 and Si/Al=15) decreases catalytic selectivity of aromatic ring hydrogenation products and increases the generation of carbonyl group hydrogenation products.

It has been reported that the tuning of support acidity can influence electronic properties of Pt particles, thereby weaken the bond strength of Pt-H and affect chemoselectivity of hydrogenation.[69] Moreover, Lin and Vannice[179-181] pointed out that the overall activity over the noble metal catalysts on acidic supports included two parts: one was the contribution of metal site, and the other was that of acid sites, where the spillover hydrogen could react with the adsorbed aromatic compound. In chapter 4, it is also proved that aromatic ring of PE can absorb on support acid sites. Therefore, it is reasonable the increase of surface acidity up to Si/Al=20 promotes the hydrogenation of aromatic ring to produce CE+CMK.

5.3 Conclusions

In this chapter, a series of Pt/Al-MCM-41 catalysts with different Si/Al ratio were successfully synthesized and characterized. The acidities of these uniform Pt/Al-MCM-

41 particles with high surface area were characterized by NMR spectroscopy. NMR spectroscopy indicates acid number of Pt/Al-MCM-41 catalysts generally decreases with the increase of Si/Al ratio. Acetophenone (AP) hydrogenation was tested on the series of Pt/Al-MCM-41 catalysts. Pt/Al-MCM-41 catalysts serve as bifunctional catalysts in the hydrogenation of AP. The overall activity over the noble metal catalysts on acidic supports can contribute to both metal sites and acid sites. On acid sites, the spillover hydrogen could react with the adsorbed compounds. The catalytic behaviour clearly correlates with different properties of the supports. Catalytic activity of Pt/Al-MCM-41 catalysts was not totally parallel to the number of strong acid sites of the catalysts when the particle size and distribution effect can almost be ruled out. Generally, overloading of Al into MCM-41 support decreases catalytic activity of Pt/Al-MCM-41 because the increase of aluminium contents can hinder the accessibility of strong acid sites to reactants due to nano-porous properties of MCM-41 material. Concerning catalytic selectivity of AP hydrogenation on Pt/Al-MCM-41, supports acidity affect electronic properties of Pt particles contributing to the chemoselectivity of AP hydrogenation. Moreover, acid sites in metal-support interfacial regions also influence AP hydrogenation chemoselectivity.

6 Hydrodeoxygenation of bio-oil model of benzaldehyde on acidic catalysts

6.1 Introduction

Hydrodeoxygenation (HDO) is an important reaction which can remove oxygenates from bio-oil (pyrolysis oil), thus improve the quality of bio-oil as a substitute of transportation fuel. Model compounds of HDO such as furans and phenols were widely studied.[28-31, 33, 36, 38] According to the work by Bridgwater, bio-oils produced from many pyrolysis included not only ketones (1-5 wt%) but also aldehydes (10-20 wt%).[182] It can be seen that aldehydes account for a large amount of bio-oils. Therefore, the hydrodeoxygenation of aldehydes is of great importance. However, few literatures addressed the hydrodeoxygenation of aldehydes.

Coventional metal sulfide catalysts such as sulfide $CoMo/Al_2O_3$ and $NiMo/Al_2O_3$ had good deoxygenation activity, but the sulfidation process of these catalysts was carried out at high temperature. The use of H_2S or CS_2 as sulfiding agent exhausted poisonous gas H_2S. Moreover, additional sulfiding agent was required to be added in the feed to maintain the sulfidation level of metal sulfide catalyst.[183]

Supported noble catalysts avoided the disadvantages of conventional sulfide catalyst and were used as promising catalysts for hydrodeoxygenation of bio-oil models. However, studies focused on the hydrodeoxygenation of aldehydes on supported noble catalysts

were still rather limited. Pt-catalyzed system is one of the most efficient for the hydrogenation reactions, it was also reported support acid-base properties can control the chemoselectivity in the hydrogenation and hydrogenolysis of carbonyl group on Pt.[133] The influence of support acid–base properties on the geometric and electronic properties of Pt has been extensively studied by Koningsberger's group.[152, 184] They tuned the ionicity of alumina by introducing different dopants (Si, W, F, Cl, K, Rb, and Cs).

Generally, Doping alumina with silica is a known procedure to increase the surface acidity of alumina.[133] Characterization techniques and DFT calculations have been used to elucidate the interaction between metal–support. They proved that the Pt–H bond strength is higher on ionic (basic) supports and lower on acidic and more covalent supports, which is the origin of the changes in the reactivity of Pt toward hydrogenation and hydrogenolysis.[152, 184] Procha´zkova´ et al.[108] investigated the hydrodeoxygenation of aldehydes on supported palladium catalysts, it is indicated that hydrodeoxygenation of aldehydes proceeded rapidly and selectively on tested supported palladium catalysts, results also showed the importance of acidity in this reaction selectivity.

It was proved in chapter 4 that support acidity can promote the transformation of carbonyl group of aromatic ketone to methylene one. The problem arises with whether this theory can be applied for the hydrodeoxygenation of aldehydes. Therefore, we performed hydrodeoxygenation of benzaldehyde hydrodeoxygenation on supported Pt catalysts with tunable acid properties in this chapter. Firstly, the hydrodeoxygenation of a

model aldehyde of benzaldehyde was performed on a noble reference catalyst of E4759 Pt/Al_2O_3 in a continuous flow reactor in the temperature from 80 ℃ to 200 ℃. Effect of temperature on the conversion and selectivity of this reaction was tested. Afterwards, the effect of acidity was investigated. We changed the support acidity of Pt/Al_2O_3 by doping SiO_2 using a flame spray pyrolysis (FSP) method as described in Chapter 2.2.2.4. The hydrodeoxygenation of benzaldehyde on Pt/SiO_2-Al_2O_3 with different Si/Al ratio was then performed to identify the reaction of benzaldehyde hydrodeoxygenation differing in the support acidity of Pt-based noble catalyst.

6.2 Results and discussion

6.2.1 Benzaldehyde hydrodeoxygenation on Pt/Al_2O_3

6.2.1.1 Conversion of benzaldehyde on Pt/Al_2O_3

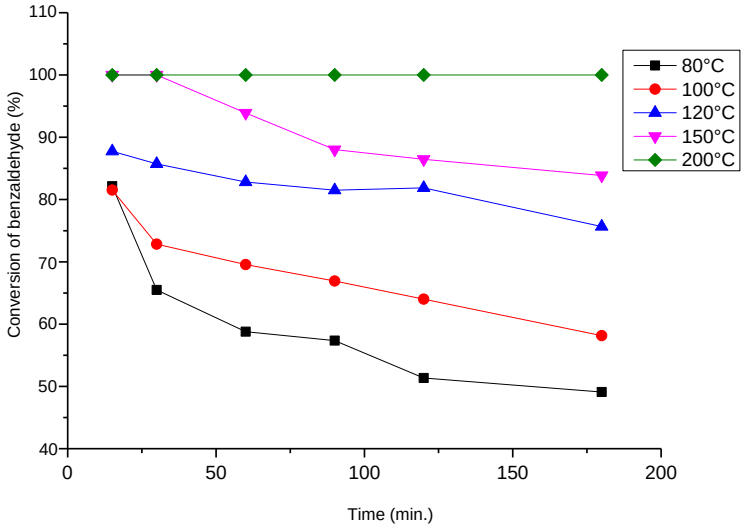

Figure 6.1 Conversion of hydrodeoxygenation of benzaldehyde on Pt/Al_2O_3 in continuous flow reactor at temperatures of 80 ℃, 100 ℃, 120 ℃, 150 ℃ and 200 ℃.

In order to study the temperature effect on hydrodeoxygenation of benzaldehyde, the reaction was carried out on a reference catalyst E4759 Pt/Al_2O_3 in a continuous flow reactor in the temperature range from 80 ℃ to 200 ℃ over a reaction time of 180 min. Catalytic activity results are shown in Figure 6.1. At 80 ℃, the conversion of benzaldehyde reached 82.1% after reaction time of 15 min, and decreased to 49.1% after 180 min. At 100 ℃, 81.5% of benzaldehyde was converted after 15 min and the conversion decreased to 58.2% after 180 min. When the reaction temperature was

increased to 120 ℃, conversion of benzaldehyde was 87.7% after 15 min and subsequently decreased to 75.7% after reaction time of 180 min. At 150 ℃, conversion of benzaldehyde achieved 100% at the beginning and still decreased to 83.9% after 180 min. when reaction temperature was increased to 200 ℃, conversion of benzaldehyde kept constant at 100% during reaction time of 180min. In Figure 6.1, the catalytic activity of Pt/Al_2O_3 gradually increased with the increasing of reaction temperature. Specially, with the increasing temperature from 80 ℃ to 100 ℃, the conversion of benzaldehyde increased from 49.1% to 58.2% after reaction time of 180 min. With further increasing temperature from 100 ℃ to 120 ℃, the conversion increased again from 58.2% to 75.7% after 180 min. Then, reaction at 150 ℃ showed higher conversion of 83.9% after 180 min. When temperature was increased to 200 ℃, the conversion of benzaldehyde achieved 100%.

6.2.1.2 Selectivity of benzaldehyde hydrodeoxygenation on Pt/Al_2O_3

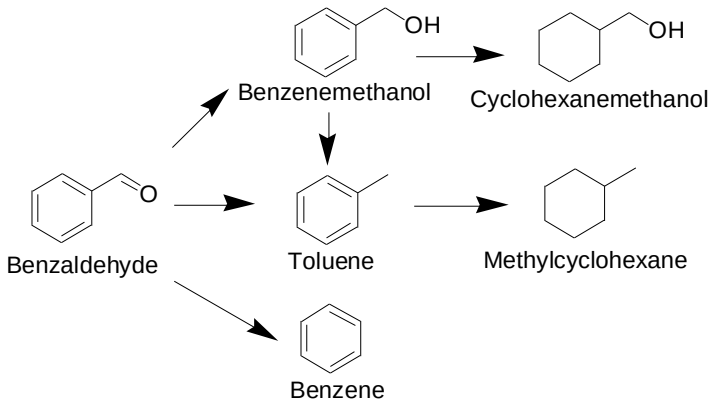

Scheme 6.1 Proposed benzaldehyde hydrodeoxygenation reaction pathway

Scheme 6.1 shows a possible reaction pathway for the hydrodeoxygenation of benzaldehyde accroding to literature.[185-187] As mentioned above, in bio-oil upgrading, it is desirable to only promote hydrogenolysis carbonyl groups to saturated C-C bonds and avoiding hydrogenation of aromatic rings because the latter decreases the octane number of the produced fuels and results in undesired hydrogen consumption.[69] Therefore, benzene and toluene are considered as the most valuable products of benzaldehyde hydrodeoxygenation.

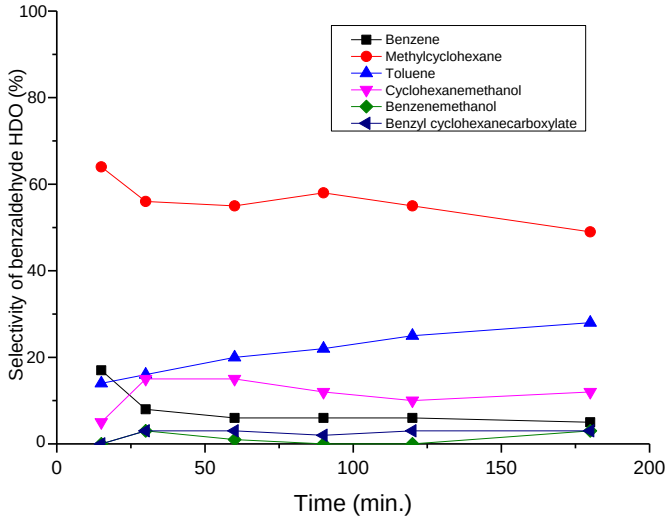

Figure 6.2 Selectivity of hydrodeoxygenation of benzaldehyde on Pt/Al_2O_3 at 80 ℃

Figure 6.2 shows the selectivity of benzaldehyde hydrodeoxygenation on Pt/Al_2O_3 at 80 ℃. Methylcyclohexane, toluene, cyclohexanemethanol, benzene, benzyl cyclohexanecarboxylate and benzenemethanol were produced. Methylcyclohexane was the main product over a reaction time of 180 min with the selectivity of 64% after 15 min at conversion of 82.1% and decreased to 49% after 180 min at conversion of 49.1%. The second main product was toluene with selectivity of 14% after 15 min (conversion of 82.1%) and increased to 28% after 180 min (conversion of 49.1%). The selectivity of benzene was 17% after 15 min (conversion of 82.1%) and decreased to 5% after 180 min (conversion of 49.1%). Cyclohexanemethanol was also produced, the selectivity of this product was 5% after 15 min (conversion of 82.1%) and increased to 12% after 180 min (conversion of 49.1%). The selectivity of benzyl cyclohexanecarboxylate and benzenemethanol was very low and kept almost constant at 0%.

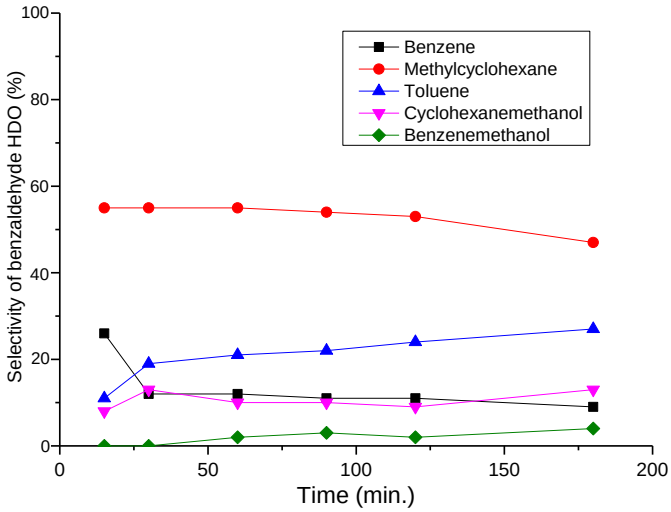

Figure 6.3 Selectivity of hydrodeoxygenation of benzaldehyde on Pt/Al_2O_3 at 100 ℃

Figure 6.3 shows the selectivity of benzaldehyde hydrodeoxygenation on Pt/Al_2O_3 at 100 ℃. The selectivity distribution of benzaldehyde hydrodeoxygenation on Pt/Al_2O_3 at 100 ℃ was similar to 80 ℃. Methylcyclohexane was still the main product over a reaction time of 180 min with a selectivity of 55% after 15 min (81.5% conversion) and decreased to 47% after 180 min (58.2% conversion). Toluene was the second main product with selectivity of 11% after 15 min (81.5% conversion) and increased to 27% after 180 min (58.2% conversion). The selectivity of benzene was 26% at the beginning (81.5% conversion) and decreased to 9% after 180 min (58.2% conversion). The selectivity of Cyclohexanemethanol increased from 8% after 15 min (81.5% conversion) to 13% after 180min (58.2% conversion). Only very small amount (2%) of benzenemethanol was produced after 60 min (69.6% conversion) and slightly increased to 4% after 180 min (58.2% conversion).

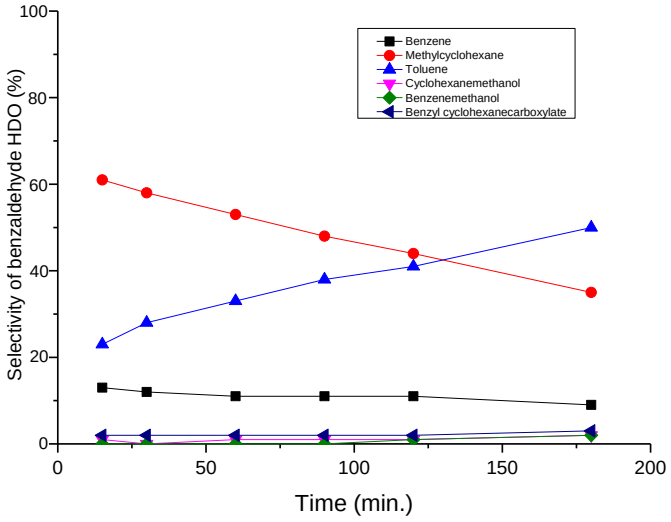

Figure 6.4 Selectivity of hydrodeoxygenation of benzaldehyde on Pt/Al_2O_3 at 120 ℃

The selectivity of benzaldehyde hydrodeoxygenation on Pt/Al_2O_3 at 120 ℃ showed some difference in comparison with those at 80 ℃ and 100 ℃. Methylcyclohexane was still the main product after 15 min with selectivity of 61% (87.7% conversion), but it decreased to 35% after 180 min (75.7% conversion). On the contrary, the selectivity of toluene significantly increased, toluene became the main product with selectivity of 50% after 180 min (75.7% conversion). The selectivity of benzene was not significantly changed during reaction time of 180 min. After 15 min, 13% benzene (87.7% conversion) was produced and decreased to 9% after 180 min (75.7% conversion). The selectivity of benzyl cyclohexanecarboxylate, cyclohexanemethanol and benzenemethanol was very low and kept near 0%.

It has been proposed earlier that the formation of benzal alcohol from benzaldehyde occur via a nucleophillic mechanism where carbonyl function is activated at the metal

support interface. Benzene is formed directly from benzaldehyde via the adsorption of benzaldehyde on acidic sites and subsequent dissociation of C-C band on metal sites while toluene can result from the subsequent conversion of the alcohol and hydrogenolysis of benzaldehyde, methylcyclohexane was suggested as a result of the further reduction of toluene.[185-187]

In Figure 6.2, 6.3 and 6.4, methylcyclohexane appeared as the primary main product. Since methylcyclohexane should be formed from further reduction of toluene. The reason of methylcyclohexane as the primary main products can be summarized as newly reduced catalysts carried large amount of adsorbed H at the Pt surface, so the benzaldehyde can be fully hydrogenated due to the high ratio of H to reactant at the beginning of the reaction. When more and more reactant or product adsorpbed on surface, competitive adsorption of C=O with aromatic ring will increase the chemoselectivity of C=O hydrogenation to toluene. The product of benzene was appeared at the beginning of the reaction. Benzene selectivity seems like kept at almost unchanged over reaction time of 180 min.

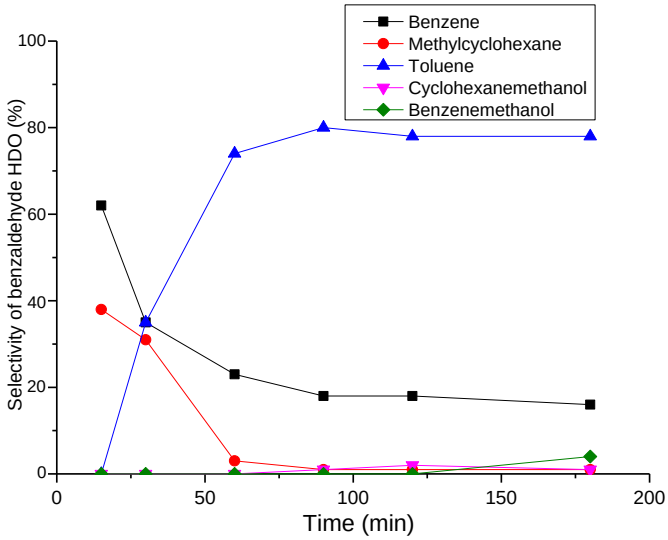

Figure 6.5 Selectivity of hydrodeoxygenation of benzaldehyde on Pt/Al_2O_3 at 150 ℃

For the hydrodeoxygenation of benzaldehyde on Pt/Al_2O_3 at 150 ℃, benzene was the main product at the beginning with selectivity of 62% after a reaction time of 15 min (100% conversion) and decreased to 16% after 180min (83.9% conversion). The selectivity of methylcyclohexane was 38% after 15 min and decreased to 1% after 180 min. The selectivity of toluene significantly increased, reaching 80% after 120 min (86.5% conversion) and slightly decreased to 78% after 180 min (83.9% conversion).

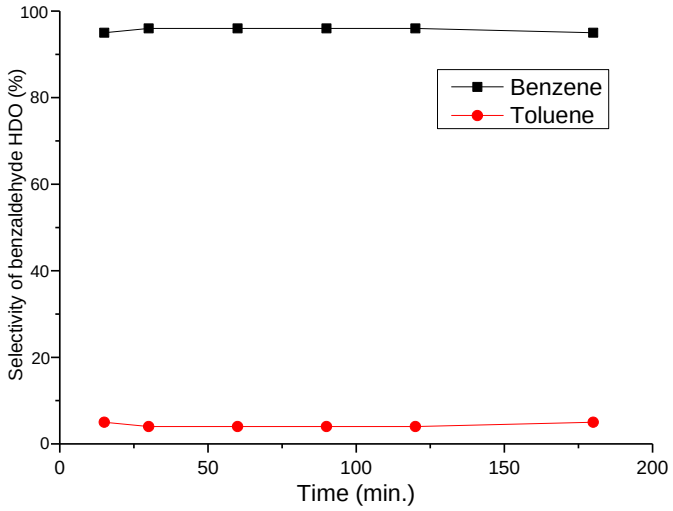

Figure 6.6 Selectivity of hydrodeoxygenation of benzaldehyde on Pt/Al_2O_3 at 200 ℃

Figure 6.6 shows hydrodeoxygenation of benzaldehyde on Pt/Al_2O_3 at 200 ℃. Interestingly, only benzene and toluene were produced. Benzene became the dominant product when the temperature was increased to 200 ℃. The selectivity of benzene kept almost constant at around 95% during reaction time of 180 min (100% conversion). The selectivity of toluene was also constant at around 5% (100% conversion). It is interesting to note that products of methylcyclohexane, cyclohexanemethanol and benzenemethanol disappeared when reaction temperature was increased to 200 ℃.

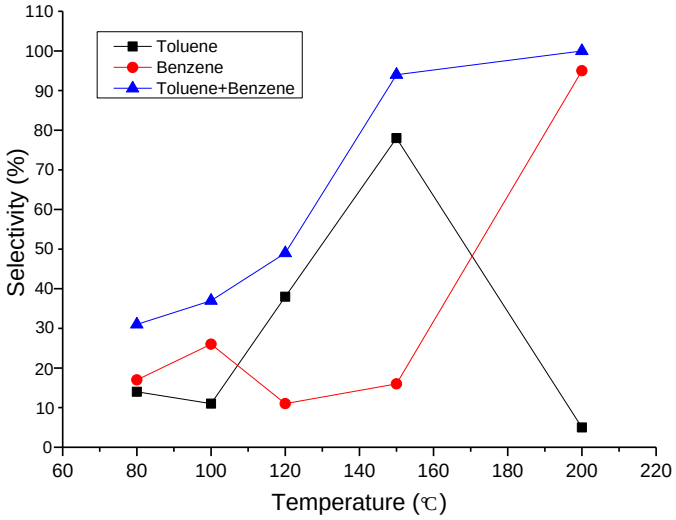

Figure 6.7 Influence of temperature on the hydrogenation of benzaldehyde: selectivity to produces benzene, toluene and (Benzene+Toluene) at 80% conversion of benzaldehyde

Figure 6.7 showed selectivity to benzene, toluene and Benzene+Toluene at 80% conversion. Increasing the temperature from 80 ℃ up to 200 ℃ enhanced the selectivity to products of Benzene+Toluene from 31% to 100%. Toluene selectivity increased from 14% at 80 ℃ to 78% at 150 ℃ and significantly decreased to 5% at 200 ℃. The selectivity of benzene continuously increased from 17% at 80 ℃ to 95% at 200 ℃. Previous study also showed benzene selectivity from dissociation of C-C bond of benzaldehyde increased with temperature increase from 150 ℃ to 350 ℃ because elevated temperature promoted the decomposition of C-C bond to produce benzene. [186]

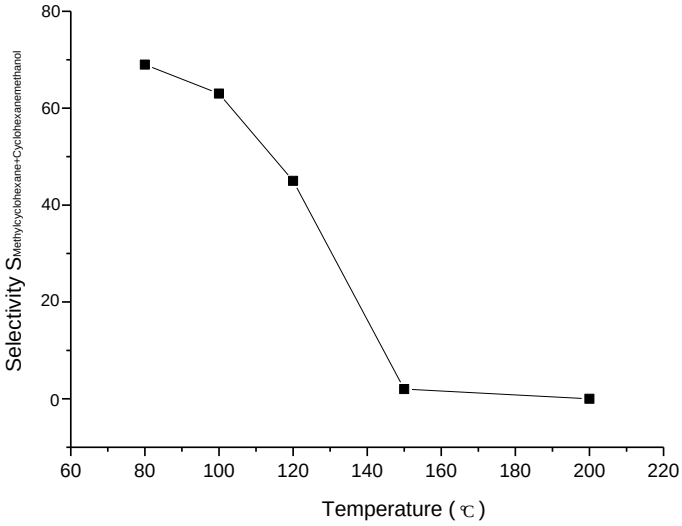

Figure 6.8 Influence of temperature on the hydrogenation of benzaldehyde: selectivity to phenyl ring hydrogenation to give the production of (Methylcyclohexane+Cyclohexanemethanol) at 80% conversion of benzaldehyde

On the contrary, in Figure 6.8 the selectivity to phenyl ring hydrogenation products (the sum of methylcyclohexane+cyclohexanemethanol) significantly decreased from 69% at 80℃ to 0% at 200℃. From above observation, it is concluded that the increase of reaction temperature promotes hydrogenolysis to produce toluene and to generate benzene, avoiding phenyl ring hydrogenation to give products of methylcyclohexane and cyclohexanemethanol because the dissociation of C-C bond to give production of benzene was enhanced at high temperatures.[186]

6.2.2 Benzaldehyde hydrodeoxygenation on Pt/SiO_2-Al_2O_3

6.2.2.1 Conversion on Pt/SiO_2-Al_2O_3

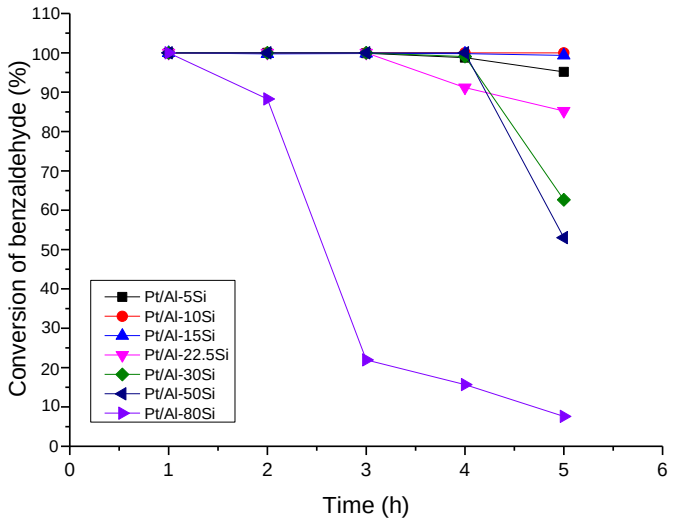

Figure 6.9 Conversion of hydrodeoxygenation of benzaldehyde at 140 ℃ over Pt/SiO_2-Al_2O_3

To understand acidity effect on benzaldehyde hydrodeoxygenation, we changed surface acidity by doping different amount of SiO_2 into Pt/Al_2O_3. Based on the study of benzaldehyde hydrodeoxygenation on Pt/Al_2O_3, we chose reaction temperature of 140 ℃ to test the catalytic activity and selectivity of Pt/SiO_2-Al_2O_3 because at reaction temperature of 150 ℃, toluene was produced in the highest amount. Details of characterization of Pt/SiO_2-Al_2O_3 with different Si/Al ratio can be found in the literature.[133] As can be seen in Figure 6.9, except Pt/SA-80 all the other catalysts including Pt/SA-5, Pt/SA-10, Pt/SA-15, Pt/SA-22.5, Pt/SA-30, Pt/SA-50 (Pt/SA-5, Pt/SA-10, Pt/SA-15, Pt/SA-22.5, Pt/SA-30, Pt/SA-50 and Pt/SA-80 represent Pt/Al-5Si,

Pt/Al-10Si, Pt/Al-15Si, Pt/Al-22.5Si, Pt/Al-30Si, Pt/Al-50Si and Pt/Al-80Si) show much higher catalytic activity than the reference catalyst of Pt/Al_2O_3 because the conversion of benzaldehyde on these catalysts kept at around 100% in reaction time of 3h. The conversion of benzaldehyde on Pt/SA-5 slightly decreased to 95% after 5h. On Pt/SA-10 and Pt/SA-15, the conversion kept almost constant at 100% during reaction time of 5h. The conversion of benzaldehyde on Pt/SA-22.5, Pt/SA-30 and Pt/SA-50 decreased to 85%, 62.6% and 53% after 5h. The low catalytic activity of Pt/SA-80 was probably caused by a fast growing of Pt particle size from relatively large amount of Al incorporated into the crystalline framework.[133] From above observation, the doping of SiO_2 improved catalytic performance in benzaldehyde hydrodeoxygenation in comparison with commercial E4759 Pt/Al_2O_3. Except for Pt/SA-80, all SiO_2-doped catalysts showed 10%-20% higher catalytic activity than E4759 Pt/Al_2O_3 under similar reaction condition.

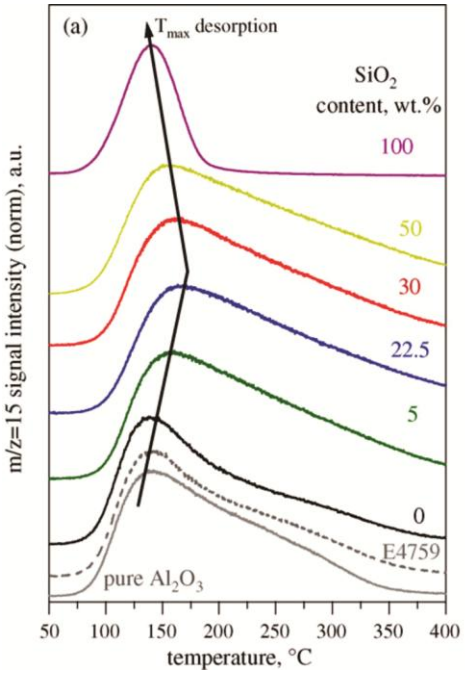

Figure 6.10 TPD patterns of NH_3 and the corresponding maximum desorption peak temperature

Figure 6.10 shows TPD patterns of NH_3 on Pt/SA catalysts, the acidity increased from 0 wt.% SiO_2 up to 22.5-30 wt.% SiO_2, above this range the acidity gradually decreased.[133]

6.2.2.2 Selectivity on Pt/SiO_2-Al_2O_3

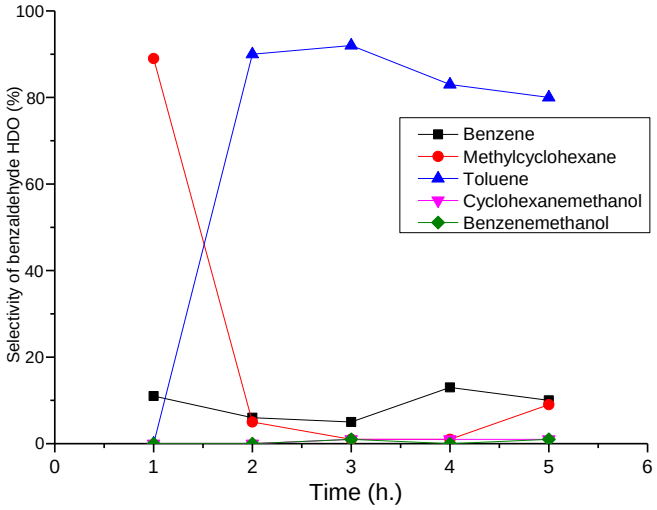

Figure 6.11 Selectivity of hydrodeoxygenation of benzaldehyde on Pt/SA-5 at 140 ℃

Figure 6.11 shows the selectivity of benzaldehyde hydrodeoxygenation on Pt/SA-5 at 140 ℃. Methylcyclohexane, toluene, cyclohexanemethanol, benzene and benzenemethanol were produced. Methylcyclohexane was the main product after 1h with selectivity of 89% (100% conversion), but the selectivity decreased to 5% after 2h (100% conversion). On the contrary, toluene was not produced in 1h (100% conversion), but the selectivity of toluene reached 90% after 2h (100% conversion). The selectivity of

benzene was not significantly changed during reaction time of 5h, 11% after 1h (100% conversion) decreased to10% after 5h (95% conversion).

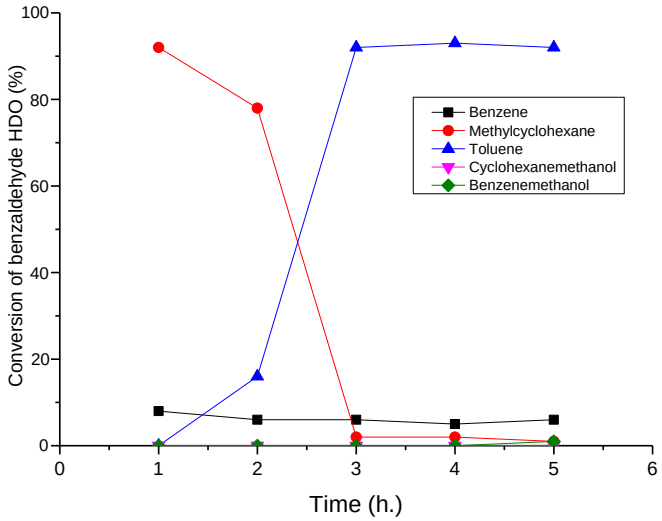

Figure 6.12 Selectivity of hydrodeoxygenation of benzaldehyde on Pt/SA-10 at 140 ℃

Figure 6.12 shows selectivity of benzaldehyde hydrodeoxygenation on Pt/SA-10 at 140 ℃. Methylcyclohexane was the main product at the beginning, with selectivity of 92% (100% conversion) after 1h, however, the selectivity of this product significantly decreased to 2% (100% conversion) after 3h. On the contrary, toluene was not produced after 1h, the selectivity of it significantly increased to 92% after 3h (100% conversion). The selectivity of toluene kept almost the same at 7% during reaction time of 5h. The selectivity of cyclohexanemethanol and benzenemethanol approached 0%.

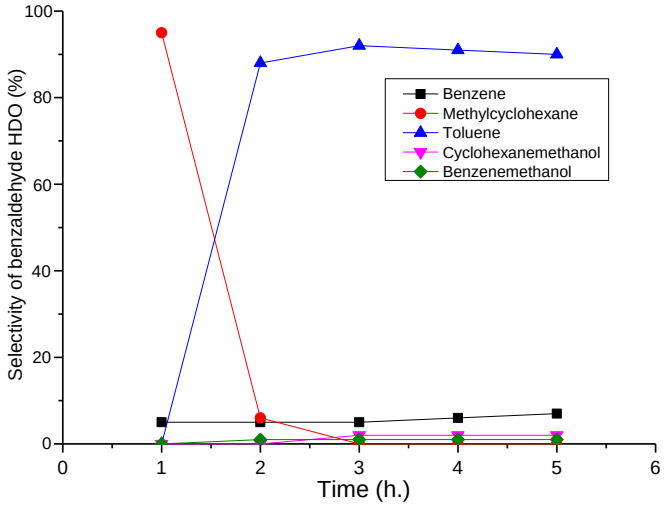

Figure 6.13 Selectivity of hydrodeoxygenation of benzaldehyde on Pt/SA-15 at 140 ℃

As shown in Figure 6.13, the catalytic selectivity distribution of benzaldehyde hydrodeoxygenation on Pt/SA-15 was similar to that on Pt/SA-5 and Pt/SA-10. Methylcyclohexane was the main product in the first place with selectivity at above 90% after 1h, followed by a significant decrease to around 0% after 3h whereas the selectivity to toluene significantly increased to around 90% after 3h and kept constant at above 90%. The selectivity of benzene almost kept at the same level (at around 6%) during reaction time of 5h. The selectivity of cyclohexanemethanol and benzenemethanol again approached 0%.

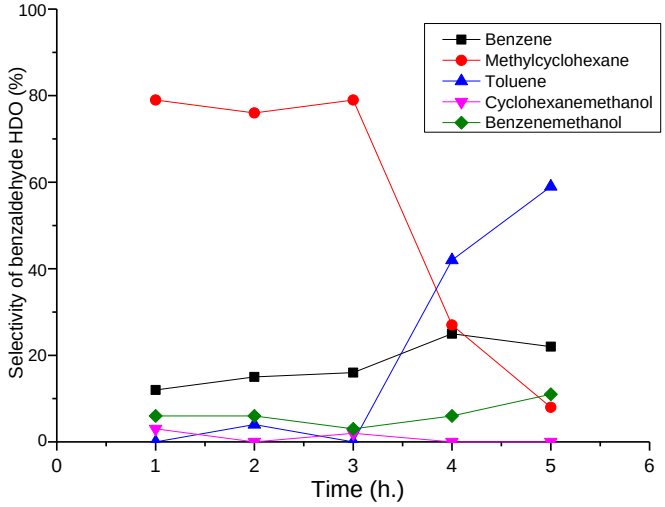

Figure 6.14 Selectivity of hydrodeoxygenation of benzaldehyde on Pt/SA-22.5 at 140 ℃

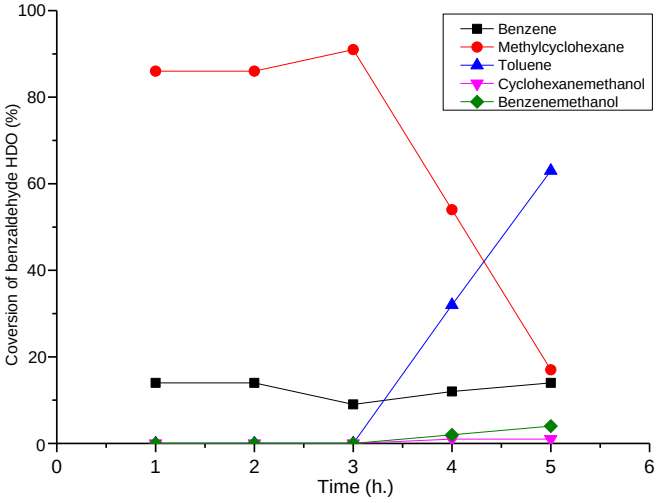

Figure 6.15 Selectivity of hydrodeoxygenation of benzaldehyde on Pt/SA-30 at 140 ℃

With increasing SiO_2 content to 22.5 wt.% and 30 wt.%, the selectivity distribution showed some difference in comparison with on Pt/SA-5, Pt/SA-10 and Pt/SA-15.

Methylcyclohexane was the main product with selectivity at constant around 80% in 3h. Then, after reaction time of 3h, the selectivity of methylcyclohexane began to decrease whereas the selectivity of toluene increased from 0% after 3h (100% conversion) to around 60% after 5h (85% conversion on Pt/SA-22.5, 63% conversion on Pt/SA-30). However, the increase in the selectivity of toluene on Pt/SA-22.5 and Pt/SA-30 was not as significant as on that of Pt/SA-5, Pt/SA-10 and Pt/SA-15. The selectivity of benzene was also not significantly changed. (10% to 20% during 5h)

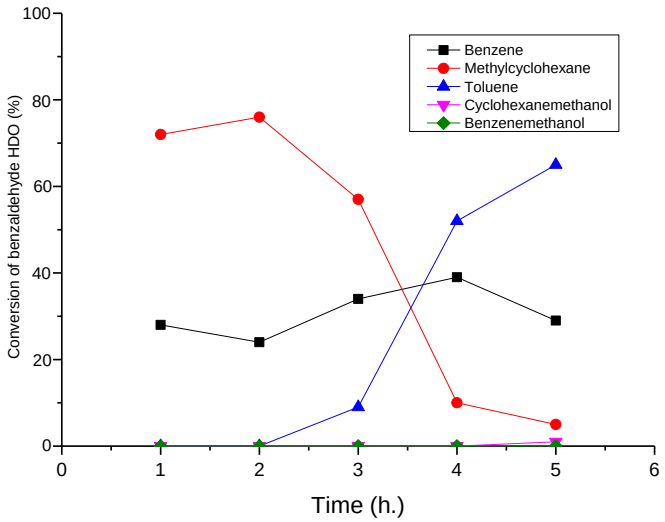

Figure 6.16 Selectivity of hydrodeoxygenation of benzaldehyde on Pt/SA-50 at 140 ℃

With increasing SiO_2 content to 50 wt.%, benzaldehyde hydrodeoxygenation was operated on Pt/SA-50 at 140 ℃. Products of methylcyclohexane, toluene and benzene were detected. Methylcyclohexane was the primary dominant product at the first with selectivity above 70% after 2h (100% conversion), and the selectivity gradually decreased to 5% after 5h (53% conversion). On the other hand, toluene was not appeared

in the first 2h. The selectivity of toluene gradually increased to 65% after 5h (53% conversion). The selectivity of benzene again was not significantly changed. (28% after 1h, 29% after 2h)

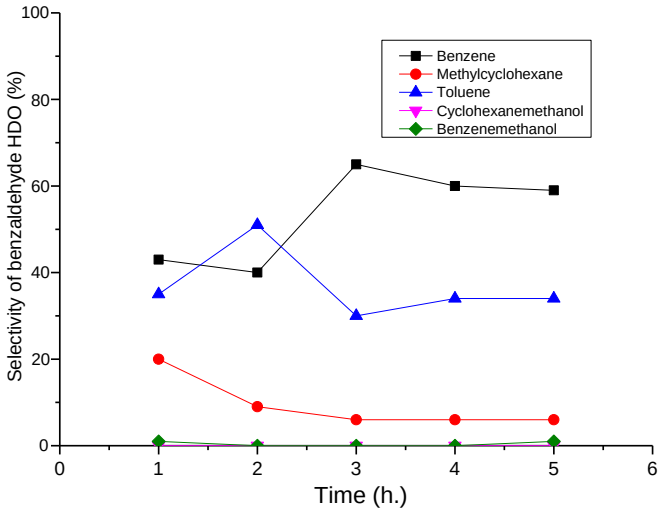

Figure 6.17 Selectivity of hydrodeoxygenation of benzaldehyde on Pt/SA-80 at 140 ℃

As shown in Figure 6.17, benzene became the main product of benzaldehyde hydrodeoxygenation on Pt/SA-80 with a selectivity of 43% after 1h (100% conversion), 59% after 5h (7.6% conversion). Toluene became the second main product. The selectivity to toluene after 1h was only 35% and slightly decreased to 34% after 5h. Selectivity to methylcyclohexane decreased from 20% after 1h to 6% after 5h.

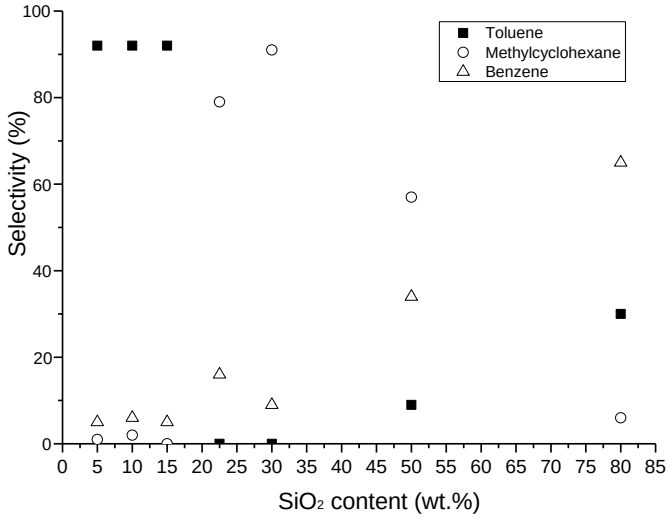

Figure 6.18 Influence of SiO_2 content of Pt/SiO_2-Al_2O_3 on the selectivity of benzaldehyde hydrodeoxygenation to produce toluene, methylcyclohexane and benzene after reaction time of 3h at 140 ℃

Figure 6.18 shows the influence of SiO_2 content on the products selectivity of toluene, methylcyclohexane and benzene at 3h and 140 ℃. Above 90% of toluene was produced on 5 wt.%, 10 wt.% and 15 wt.% SiO_2-doped Pt/SiO_2-Al_2O_3 whereas selectivity to methylcyclohexane and benzene were very low. When SiO_2 content was increased to 22.5 wt.% and 30 wt.%, almost no toluene was detected, but selectivity to methylcyclohexane significantly increased to around 80%, this trend suggests aromatic ring of toluene was more easily hydrogenated to produce methylcyclohexane on acidity enhanced catalyst. Interestingly, with increasing SiO_2 content to 80 wt.%, benzene selectivity began to grow and benzene became dominant product on Pt/SA-80 with selectivity achieving 65% after 3h. Previous temperature-programmed desorption (TPD) characterization (Figure 6.10) shows the strongest acidity was measured at 22.5-30 wt.% SiO_2, above this range the acidity decreased again.[133] Therefore, toluene prefers to form on relative low acidic

catalysts such as Pt/SA-5, Pt/SA-10 and Pt/SA-15. When acidity was increased, both carbonyl group and aromatic ring was reacted to give the product of methylcyclohexane on Pt/SA-22.5 and Pt/SA-30. Since toluene could be converted to methylcyclohexane, increasing the support acidity promoted the hydrogenation of aromatic ring of toluene to produce methylcyclohexane. There are two possible reasons: 1) On acidic catalysts, more active Pt surface hydrogenated both aromatic rings and C=O bonds; 2) more spillover hydrogen from more active Pt moved to the adsorbed reactants on supports to hydrogenate both aromatic rings and C=O bonds. Benzene was probably formed directly from benzaldehyde decomposition, the reaction pathways of benzaldehyde hydrogenolysis to benzene probably undergo a bifunctional site, the adsorption of reactant molecule on an acidic site, followed by dissociation of the aldehydic C-C bond on a metal site.[186]

6.3 Conclusions

Catalytic activity of reference E4759 Pt/Al_2O_3 in the hydrodeoxygenation of benzaldehyde gradually increased with the increasing of reaction temperature. The increase of reaction temperature also promoted the production of benzene and toluene and avoided phenyl ring hydrogenation to generate byproducts of methylcyclohexane and cyclohexanemethanol.

SiO_2-doped Pt/SiO_2-Al_2O_3 catalysts showed 10%-20% higher catalytic activity than E4759 Pt/Al_2O_3 under similar reaction condition. Acidity did influence catalytic

selectivity of benzaldehyde hydrodeoxygenation, toluene prefers to form on relative low acidic catalysts. Methylcyclohexane was more easily formed on high acidic catalysts. Benzene was probably formed by an independent way from the products of benzaldehyde reduction, it probably undergo a bifunctional site, the adsorption of reactant molecule on an acidic site, followed by dissociation of the aldehydic C-C bond on a metal site.[186]

7 Conclusions

In this thesis, the mechanisms of bio-oil model ketone hydrodeoxygenation on supported noble Pt or Pd catalysts were investigated. Then, the synthesis, characterization and catalytic performance of various catalysts for hydrodeoxygenation reactions of bio-oil model compounds were described.

The thesis addressed the understanding of bio-oil model ketone compound - acetophenone hydrodeoxygenation mechanism over alumina and silica-alumina supported Pt and Pd catalysts by in-situ attenuated total reflection infrared spectroscopy (ATR-IR) in combination with modulation excitation spectroscopy (MES) and phase sensitive detection (PSD). This approach allows proper detecting and analyzing active species at catalytic solid-liquid interfaces under working conditions. Key results can be summarized as below:

- On alumina supported platinum, AP was predominantly adsorbed on Pt in its η^1 (O) configuration and this species was hydrogenated with high chemoselectivity to PE. The produced PE was more strongly adsorbed on the Al_2O_3 support than on Pt.
- AP hydrodeoxygenation on silica-alumina Pd supported nanoparticles showed increasing EB selectivity with the increase of surface acidity.
- On silica-alumina supported Pd, hydrodeoxygenation of AP to EB involves the hydrogenation of AP to PE on metal surface, followed by dehydration of PE on

acid sites of supports to generate styrene. Styrene was then further hydrogenated on metal surface to produce EB.

- Then, according to the understanding of hydrodeoxygenation mechanism, catalysts of Pt/MCM-41 and Pt/SiO_2-Al_2O_3 were designed. Hydrodeoxygenation of acetophenone over mesoporous supported noble Pt catalysts with different surface acidity was applied. Hydrodeoxygenation of benzaldehyde on Pt/Al_2O_3 and Pt/SiO_2-Al_2O_3 with different surface acidity was also tested.
- Pt/MCM-41 catalysts with different Si/Al ratio possess high surface area and uniform particle size.
- The density of acid on Pt/Al-MCM-41 catalysts decreases with the increase of Si/Al ratio.
- Pt/Al-MCM-41 catalysts serve as bifunctional catalysts in the hydrogenation of AP. The catalytic behaviour was influenced by different properties of the supports. Generally, overloading of Al into MCM-41 support decreases catalytic activity of Pt/Al-MCM-41 due to the accessibility of nano-porous MCM-41 hindered by excessive Al.
- SiO_2-doped Pt/SiO_2-Al_2O_3 catalysts showed 10%-20% higher catalytic activity than E4759 Pt/Al_2O_3 under similar reaction condition.
- Acidity did influence catalytic selectivity of benzaldehyde hydrodeoxygenation, toluene prefers to form on low acidic catalysts. Methylcyclohexane more easily formed on high acidic catalysts.

Appendix

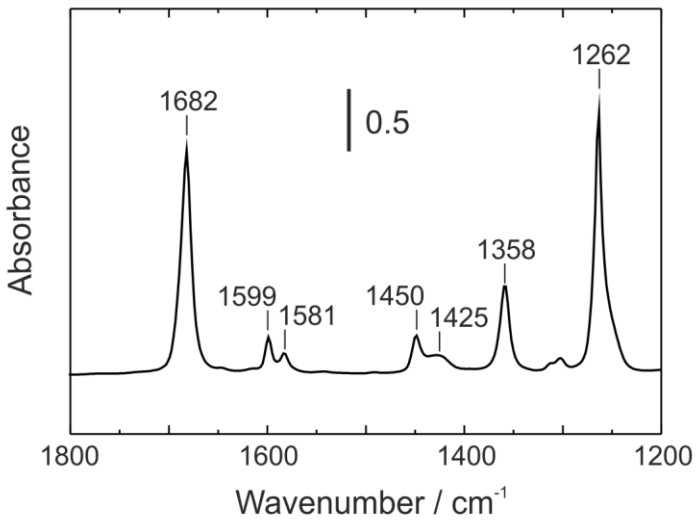

Figure A1. IR spectrum of pure AP in the liquid-phase.

The band at 1682 cm^{-1} is due to C=O stretching vibration, bands at 1450, 1581, and 1599 cm^{-1} are assigned to C=C stretching vibration of phenyl group, signal at 1358 cm^{-1} corresponds to the bending mode of CH_3. While signal at 1262 cm^{-1} is due to X-sensitive benzene mode.

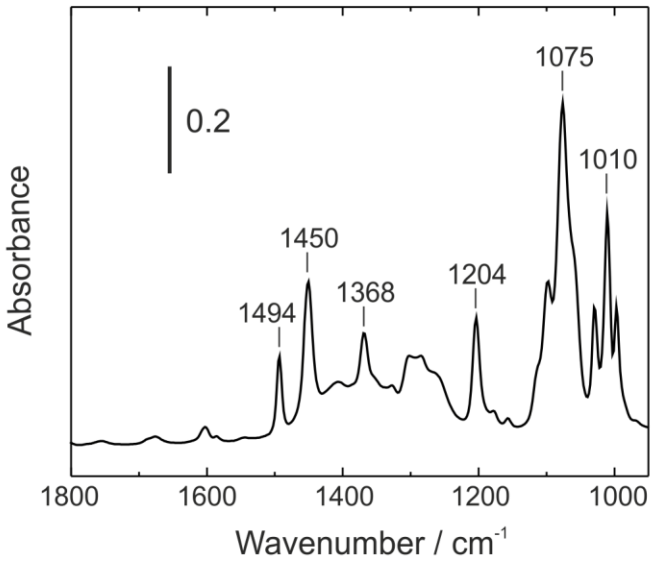

Figure A2. IR spectrum of pure PE in the liquid-phase.

The band at 1494 cm^{-1} is due to C=C stretching vibration of phenyl group1, 1204 cm^{-1} corresponds to deformation mode of phenyl group, band at 1010 cm^{-1} is due to C=C stretching vibration, band at 1075 cm^{-1} is assigned to C-O stretching vibration.

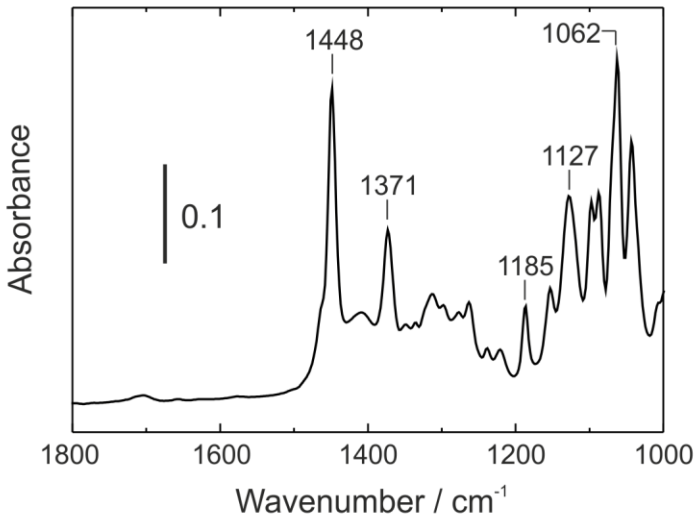

Figure A3. IR spectrum of pure CE in the liquid-phase.

Bands at 1448 and 1371 cm^{-1} are possibly assigned to bending mode of CH_2 and CH_3 group, respectively. Signal at 1062 cm^{-1} corresponds to C-O stretching vibration of CE.

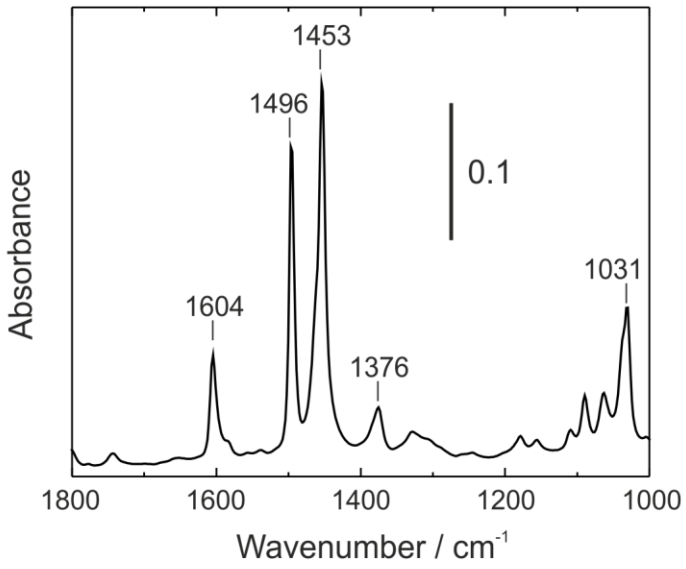

Figure A4. IR spectrum of pure EB in the liquid-phase.

Bands at 1604, 1496, and 1453 cm^{-1} are assigned to C=C stretching vibration of phenyl group, band at 1376 cm^{-1} correspond to bending mode of CH_3 group.

References

1. Iborra, S. and A. Corma, *Synthesis of transportation fuels from biomass: Chemistry, catalysts, and engineering.* Chem Rev, 2006. 106(9): p. 4044-4098.
2. Soares, R.R., D.A. Simonetti, and J.A. Dumesic, *Glycerol as a Source for Fuels and Chemicals by Low-Temperature Catalytic Processing.* Angewandte Chemie, 2006. 118(24): p. 4086-4089.
3. Chheda, J.N., G.W. Huber, and J.A. Dumesic, *Liquid-Phase Catalytic Processing of Biomass-Derived Oxygenated Hydrocarbons to Fuels and Chemicals.* Angewandte Chemie International Edition, 2007. 46(38): p. 7164-7183.
4. C. E. Wyman, S.R.D., M. E. Himmel, J.W. Brady, C. E. Skopec, L., *Viikari in Polysaccharides*. 2nd ed ed. 2005, New York, NY: Marcel Dekker.
5. Lin, Y.-C. and G.W. Huber, *The critical role of heterogeneous catalysis in lignocellulosic biomass conversion.* Energy & Environmental Science, 2009. 2(1): p. 68-80.
6. G .W. Huber, S.I., A. Corma, Chem. Rev., 2006. 106: p. 4044.
7. Yang, Y., A. Gilbert, and C. Xu, *Hydrodeoxygenation of bio-crude in supercritical hexane with sulfided CoMo and CoMoP catalysts supported on MgO: A model compound study using phenol.* Applied Catalysis A: General, 2009. 360(2): p. 242-249.
8. Bridgwater, A.V. and G.V.C. Peacocke, *Fast pyrolysis processes for biomass.* Renewable and Sustainable Energy Reviews, 2000. 4(1): p. 1-73.
9. Mohan, D., C.U. Pittman, and P.H. Steele, *Pyrolysis of Wood/Biomass for Bio-oil: A Critical Review.* Energy & Fuels, 2006. 20(3): p. 848-889.
10. Huber, G.W.a.C., A., *Synergies between Bio- and Oil Refineries for the Production of Fuels from Biomass.* Angew. Chem. Int. Ed., 2007. 46: p. 7184-7201.
11. Moraes, M.S.A., et al., *Qualitative analysis of bio oils of agricultural residues obtained through pyrolysis using comprehensive two dimensional gas chromatography with time-of-flight mass spectrometric detector.* Journal of Analytical and Applied Pyrolysis, 2012. 98(0): p. 51-64.
12. Maggi, R. and B. Delmon, *Characterization and upgrading of bio-oils produced by rapid thermal processing.* Biomass and Bioenergy, 1994. 7(1–6): p. 245-249.
13. Beckman, D. and D.C. Elliott, *Comparisons of the yields and properties of the oil products from direct thermochemical biomass liquefaction processes.* The Canadian Journal of Chemical Engineering, 1985. 63(1): p. 99-104.
14. Su-Ping, Z., *Study of Hydrodeoxygenation of Bio-Oil from the Fast Pyrolysis of Biomass.* Energy Sources, 2003. 25(1): p. 57-65.
15. Wildschut, J., et al., *Hydrotreatment of Fast Pyrolysis Oil Using Heterogeneous Noble-Metal Catalysts.* Industrial & Engineering Chemistry Research, 2009. 48(23): p. 10324-10334.
16. Bridgwater, A.V., *Renewable fuels and chemicals by thermal processing of biomass.* Chemical Engineering Journal, 2003. 91(2–3): p. 87-102.
17. L. Ingram, D.M., M. Bricka, P. Steele, D. Strobel, D. Crocker, B. Mitchell, J. Mohammad, K. Cantrell, and C.U. Pittman, Energy Fuels, 2007. 22: p. 614-625.
18. T.V. Choudhary, a.C.B.P., Appl. Catal., A, 2011. 397: p. 1-12.
19. Sealock, L.J., et al., *Chemical processing in high-pressure aqueous environments. 1. Historical perspective and continuing developments.* Industrial & Engineering Chemistry Research, 1993. 32(8): p. 1535-1541.

20. Li, N. and G.W. Huber, *Aqueous-phase hydrodeoxygenation of sorbitol with Pt/SiO2–Al2O3: Identification of reaction intermediates.* Journal of Catalysis, 2010. 270(1): p. 48-59.
21. Ingram, L., et al., *Pyrolysis of Wood and Bark in an Auger Reactor: Physical Properties and Chemical Analysis of the Produced Bio-oils.* Energy & Fuels, 2007. 22(1): p. 614-625.
22. Mullen, C.A., G.D. Strahan, and A.A. Boateng, *Characterization of Various Fast-Pyrolysis Bio-Oils by NMR Spectroscopy†.* Energy & Fuels, 2009. 23(5): p. 2707-2718.
23. Grange, P., et al., *Hydrotreatment of pyrolysis oils from biomass: reactivity of the various categories of oxygenated compounds and preliminary techno-economical study.* Catalysis Today, 1996. 29(1–4): p. 297-301.
24. Furimsky, E., *Catalytic hydrodeoxygenation.* Applied Catalysis A: General, 2000. 199(2): p. 147-190.
25. Elliott, D.C. and T.R. Hart, *Catalytic Hydroprocessing of Chemical Models for Bio-oil.* Energy & Fuels, 2008. 23(2): p. 631-637.
26. Elliott, D.C., *Historical Developments in Hydroprocessing Bio-oils.* Energy & Fuels, 2007. 21(3): p. 1792-1815.
27. Maggi, R. and B. Delmon, *A review of catalytic hydrotreating processes for the upgrading of liquids produced by flash pyrolysis*, in *Studies in Surface Science and Catalysis*, B.D. G.F. Froment and P. Grange, Editors. 1997, Elsevier. p. 99-113.
28. FURIMSKY, E., *THE MECHANISM OF CATALYTIC HYDRODEOXYGENATION OF FURAN.* Applied Catalysis, 1983. 6: p. 159-164.
29. Furimsky, E., *Mechanism of catalytic hydrodeoxygenation of tetrahydrofuran.* Industrial & Engineering Chemistry Product Research and Development, 1983. 22(1): p. 31-34.
30. LaVopa, V. and C.N. Satterfield, *Catalytic hydrodeoxygenation of dibenzofuran.* Energy & Fuels, 1987. 1(4): p. 323-331.
31. Bunch, A.Y., X. Wang, and U.S. Ozkan, *Hydrodeoxygenation of benzofuran over sulfided and reduced Ni–Mo/γ-Al2O3 catalysts: Effect of H2S.* Journal of Molecular Catalysis A: Chemical, 2007. 270(1–2): p. 264-272.
32. Bunch, A.Y., X. Wang, and U.S. Ozkan, *Adsorption characteristics of reduced Mo and Ni–Mo catalysts in the hydrodeoxygenation of benzofuran.* Applied Catalysis A: General, 2008. 346(1–2): p. 96-103.
33. Furimsky, E., et al., *On the mechanism of hydrodeoxygenation of ortho substituted phenols.* The Canadian Journal of Chemical Engineering, 1986. 64(6): p. 982-985.
34. Gevert, B.S., J.E. Otterstedt, and F.E. Massoth, *Kinetics of the HDO of methyl-substituted phenols.* Applied Catalysis, 1987. 31(1): p. 119-131.
35. Aubert, C., et al., *Factors affecting the hydrogenation of substituted benzenes and phenols over a sulfided NiO MoO3γ -Al2O3 catalyst.* Journal of Catalysis, 1988. 112(1): p. 12-20.
36. Laurent, E. and B. Delmon, *Influence of oxygen-, nitrogen-, and sulfur-containing compounds on the hydrodeoxygenation of phenols over sulfided cobalt-molybdenum/.gamma.-alumina and nickel-molybdenum/.gamma.-alumina catalysts.* Industrial & Engineering Chemistry Research, 1993. 32(11): p. 2516-2524.
37. Gevert, S.B., et al., *Direct hydrodeoxygenation and hydrogenation of 2,6- and 3,5-dimethylphenol over sulphided CoMo catalyst.* Applied Catalysis A: General, 1994. 117(2): p. 151-162.

38. Şenol, O.İ., et al., *Effect of hydrogen sulphide on the hydrodeoxygenation of aromatic and aliphatic oxygenates on sulphided catalysts.* Journal of Molecular Catalysis A: Chemical, 2007. 277(1–2): p. 107-112.
39. Romero, Y., F. Richard, and S. Brunet, *Hydrodeoxygenation of 2-ethylphenol as a model compound of bio-crude over sulfided Mo-based catalysts: Promoting effect and reaction mechanism.* Applied Catalysis B: Environmental, 2010. 98(3–4): p. 213-223.
40. Şenol, O.İ., T.R. Viljava, and A.O.I. Krause, *Hydrodeoxygenation of methyl esters on sulphided NiMo/γ-Al2O3 and CoMo/γ-Al2O3 catalysts.* Catalysis Today, 2005. 100(3–4): p. 331-335.
41. Maier, W.F., et al., *Heterogeneous deoxygenation of ketones.* Tetrahedron Letters, 1981. 22(42): p. 4227-4230.
42. Weiser, O.a.L., S., *Sulphide catalysts: Their Properties and Applications.* Pergamon, 1973.
43. Durand, R., et al., *Heterogeneous hydrodeoxygenation of ketones and alcohols on sulfided NiO MoO3γ–Al2O3 catalyst.* Journal of Catalysis, 1984. 90(1): p. 147-149.
44. Santori, G.F., et al., *Hydrogenation of aromatic ketones with Pt- and Sn-modified Pt catalysts.* Applied Catalysis A: General, 2004. 269(1–2): p. 215-223.
45. Chen, C.-S., H.-W. Chen, and W.-H. Cheng, *Study of selective hydrogenation of acetophenone on Pt/SiO2.* Applied Catalysis A: General, 2003. 248(1–2): p. 117-128.
46. Drelinkiewicza, A., et al., *Acetophenone Hydrogenation on Polymer–Palladium Catalysts. The Effect of Polymer Matrix.* Catalysis Letters, 2004. 94(3-4): p. 143-156.
47. Bonnier, J.M., J.P. Damon, and J. Masson, *New approach to skeletal nickel catalysts catalytic properties of the nickel-chromium system.* Applied Catalysis, 1988. 42(2): p. 285-297.
48. Masson, J., et al., *Selective hydrogenation of acetophenone on chromium promoted raney nickel catalysts: II. Catalytic properties in the hydrogenation of acetophenone, determination of the reactivity ratios as selectivity criteria.* Applied Catalysis A: General, 1993. 99(2): p. 147-159.
49. Masson, J., P. Cividino, and J. Court, *Selective hydrogenation of acetophenone on chromium promoted Raney nickel catalysts. III. The influence of the nature of the solvent.* Applied Catalysis A: General, 1997. 161(1–2): p. 191-197.
50. Masson, J., et al., *Selective Hydrogenation of Acetophenone on Unpromoted Raney Nickel : Influence of The Reaction Conditions*, in *Studies in Surface Science and Catalysis*, J.B.C.B.D.D.G.P.R.M. M. Guisnet and C. Montassier, Editors. 1991, Elsevier. p. 245-252.
51. Rylander, P.N., *Catalytic Hydrogenation over Pt Metals*. 1967, New York.
52. Merabti, R., et al., *Synthesis and characterization of activated carbon-supported copper or nickel and their catalytic behavior towards benzaldehyde hydrogenation.* Reaction Kinetics, Mechanisms and Catalysis, 2010. 101(1): p. 195-208.
53. Pinna, F., et al., *Consecutive hydrogenation of benzaldehyde over Pd catalysts: Influence of supports and sulfur poisoning.* Applied Catalysis A: General, 2001. 219(1–2): p. 195-200.
54. Vannice, M.A. and D. Poondi, *The Effect of Metal-Support Interactions on the Hydrogenation of Benzaldehyde and Benzyl Alcohol.* Journal of Catalysis, 1997. 169(1): p. 166-175.
55. Bridgwater, A.V., *Catalysis in thermal biomass conversion.* Applied Catalysis A: General, 1994. 116(1–2): p. 5-47.

56. Bridgwater, A.V., *Production of high grade fuels and chemicals from catalytic pyrolysis of biomass.* Catalysis Today, 1996. 29(1–4): p. 285-295.
57. Şenol, O.İ., T.R. Viljava, and A.O.I. Krause, *Effect of sulphiding agents on the hydrodeoxygenation of aliphatic esters on sulphided catalysts.* Applied Catalysis A: General, 2007. 326(2): p. 236-244.
58. Gutierrez, A., et al., *Hydrodeoxygenation of guaiacol on noble metal catalysts.* Catalysis Today, 2009. 147(3–4): p. 239-246.
59. Centeno, A., E. Laurent, and B. Delmon, *Influence of the Support of CoMo Sulfide Catalysts and of the Addition of Potassium and Platinum on the Catalytic Performances for the Hydrodeoxygenation of Carbonyl, Carboxyl, and Guaiacol-Type Molecules.* Journal of Catalysis, 1995. 154(2): p. 288-298.
60. de la Puente, G., et al., *Effects of Support Surface Chemistry in Hydrodeoxygenation Reactions over CoMo/Activated Carbon Sulfided Catalysts†.* Langmuir, 1999. 15(18): p. 5800-5806.
61. Foster, A., P.M. Do, and R. Lobo, *The Synergy of the Support Acid Function and the Metal Function in the Catalytic Hydrodeoxygenation of m-Cresol.* Topics in Catalysis, 2012. 55(3-4): p. 118-128.
62. Lin, Y.-C., et al., *Catalytic Hydrodeoxygenation of Guaiacol on Rh-Based and Sulfided CoMo and NiMo Catalysts.* Energy & Fuels, 2011. 25(3): p. 890-896.
63. Liu, C., et al., *Hydrodeoxygenation of Benzofuran over Silica–Alumina-Supported Pt, Pd, and Pt–Pd Catalysts.* Energy & Fuels, 2012. 26(7): p. 4205-4211.
64. J. Weitkamp, L.P., *Catalysis and Zeolites – Fundamentals and Application*: Springer-Verlag.
65. Nishimura, S., *Handbook of Heterogeneous Catalytic Hydrogenation for Organic Synthesis*. 2001, New York: John Wiley & Sons.
66. Davda, R.R., et al., *A review of catalytic issues and process conditions for renewable hydrogen and alkanes by aqueous-phase reforming of oxygenated hydrocarbons over supported metal catalysts.* Applied Catalysis B: Environmental, 2005. 56(1–2): p. 171-186.
67. Shabaker, J.W.H., G. W.; Davda, R. R.; Cortright, R. D.; Dumesic, J. A., *Aqueous-phase reforming of ethylene glycol over supported platinum catalysts.* Catal. Lett., 2003. 88 p. 1-8.
68. Lin, S.D., D.K. Sanders, and M. Albert Vannice, *Influence of metal-support effects on acetophenone hydrogenation over platinum.* Applied Catalysis A: General, 1994. 113(1): p. 59-73.
69. Huang, J., et al., *Tuning the support acidity of flame-made Pd/SiO2–Al2O3 catalysts for chemoselective hydrogenation.* Journal of Catalysis, 2011. 281(2): p. 352-360.
70. Beck, J.S., et al., *A new family of mesoporous molecular sieves prepared with liquid crystal templates.* Journal of the American Chemical Society, 1992. 114(27): p. 10834-10843.
71. C.T. Kresge, M.E.L., W.J. Roth, J.C. Vartuli and J.S. Beck, Nature, 1992. 359: p. 710.
72. Kosslick, H., et al., *Acidity and active sites of Al-MCM-41.* Applied Catalysis A: General, 1999. 184(1): p. 49-60.
73. R. Schmidt, D.A., M. Stocker and O.H. Ellestad, J. Chem. Soc. Chem. Commun, 1994: p. 1493.
74. Chen, X., et al., *Characterization and catalytic performance of mesoporous molecular sieves Al-MCM-41 materials.* Catalysis Letters, 1997. 44(1-2): p. 123-128.

75. **Kosslick, H., H. Landmesser, and R. Fricke, *Acidity of substituted MCM-41-type mesoporous silicatesprobed by ammonia.* J. Chem. Soc., Faraday Trans., 1997. 93(9): p. 1849-1854.**
76. **Janicke, M., et al., *Aluminum Incorporation in Mesoporous Molecular Sieves*, in *Studies in Surface Science and Catalysis*, H.G.K.H.P. J. Weitkamp and W. Hölderich, Editors. 1994, Elsevier. p. 243-250.**
77. **Roos, K., et al., *Catalytic properties of mesoporous crystalline MCM-41 and related materials forhydrocarbon cracking*, in *Studies in Surface Science and Catalysis*, H.G.K.I.K. H.K. Beyer and J.B. Nagy, Editors. 1995, Elsevier. p. 389-396.**
78. **Borade, R. and A. Clearfield, *Synthesis of aluminum rich MCM-41.* Catalysis Letters, 1995. 31(2-3): p. 267-272.**
79. **Kloetstra, K.R., H.W. Zandbergen, and H. Bekkum, *MCM-41 type materials with low Si/Al ratios.* Catalysis Letters, 1995. 33(1-2): p. 157-163.**
80. **Park, K.-C., D.-J. Yim, and S.-K. Ihm, *Characteristics of Al-MCM-41 supported Pt catalysts: effect of Al distribution in Al-MCM-41 on its catalytic activity in naphthalene hydrogenation.* Catalysis Today, 2002. 74(3–4): p. 281-290.**
81. **Mokaya, R., *Al Content Dependent Hydrothermal Stability of Directly Synthesized Aluminosilicate MCM-41.* The Journal of Physical Chemistry B, 2000. 104(34): p. 8279-8286.**
82. **Weglarski, J., et al., *IR spectroscopic studies of the acidic properties of the mesoporous molecular sieve MCM-41.* Journal of the Chemical Society, Faraday Transactions, 1996. 92(24): p. 5161-5164.**
83. **Mokaya, R. and W. Jones, *Synthesis of acidic aluminosilicate mesoporous molecular sieves using primary amines.* Chemical Communications, 1996(8): p. 981-982.**
84. **Jacquin, M., et al., *Novel supported Rh, Pt, Ir and Ru mesoporous aluminosilicates as catalysts for the hydrogenation of naphthalene.* Applied Catalysis A: General, 2003. 251(1): p. 131-141.**
85. **Wang, J., et al., *Acid function of Al‐MCM‐41 supported platinum catalysts in hydrogenation of benzene, toluene o‐xylene.* Catalysis Letters, 1998. 55(3-4): p. 157-163.**
86. **Chatterjee, M., et al., *Hydrogenation of Phenol in Supercritical Carbon Dioxide Catalyzed by Palladium Supported on Al-MCM-41: A Facile Route for One-Pot Cyclohexanone Formation.* Advanced Synthesis & Catalysis, 2009. 351(11-12): p. 1912-1924.**
87. **Bejblová, M., et al., *Hydrodeoxygenation of benzophenone on Pd catalysts.* Applied Catalysis A: General, 2005. 296(2): p. 169-175.**
88. **Zhao, C., et al., *Highly Selective Catalytic Conversion of Phenolic Bio-Oil to Alkanes.* Angewandte Chemie, 2009. 121(22): p. 4047-4050.**
89. **Laurent, E. and B. Delmon, *Study of the hydrodeoxygenation of carbonyl, car□ylic and guaiacyl groups over sulfided CoMo/γ-Al2O3 and NiMo/γ-Al2O3 catalysts: I. Catalytic reaction schemes.* Applied Catalysis A: General, 1994. 109(1): p. 77-96.**
90. **Laurent, E. and B. Delmon, *Study of the hydrodeoxygenation of carbonyl, car□ylic and guaiacyl groups over sulfided CoMo/γ-Al2O3 and NiMo/γ-Al2O3 catalyst: II. Influence of water, ammonia and hydrogen sulfide.* Applied Catalysis A: General, 1994. 109(1): p. 97-115.**

91. Topsøe, N.-Y. and H. Topsøe, *Characterization of the structures and active sites in sulfided Co MoAl2O3 and Ni MoAl2O3 catalysts by NO chemisorption.* Journal of Catalysis, 1983. 84(2): p. 386-401.
92. Ferrari, M., et al., *Influences of the Hydrogen Sulfide Partial Pressure and of a Nitrogen Compound on the Hydrodeoxygenation Activity of a CoMo/Carbon Catalyst.* Journal of Catalysis, 2001. 198(1): p. 47-55.
93. Lee, C.-L. and D.F. Ollis, *Catalytic hydrodeoxygenation of benzofuran and o-ethylphenol.* Journal of Catalysis, 1984. 87(2): p. 325-331.
94. Weisser, O. and S. Landa, *Sulphide Catalysts.* Their Properties and Applications, 1973: p. 268.
95. Chen, C.-S. and H.-W. Chen, *Enhanced selectivity and formation of ethylbenzene for acetophenone hydrogenation by adsorbed oxygen on Pd/SiO2.* Applied Catalysis A: General, 2004. 260(2): p. 207-213.
96. Drelinkiewicza, A.W., A.; Makowski, W.; Sobczak, J. W.; Kroĺ , A.; Zieba, A., Catal. Lett., 2004. 94: p. 143.
97. Jutz, F.A., J.-M.; Baiker, A., J. Catal., 2009. 268: p. 356.
98. Malyala, R.V.R., C. V.; Arai, M.; Hegde, S. G.; Chaudhari, R. V., Appl. Catal., A, 2000. 193: p. 71.
99. Lin, S.D.S., D. K.; Albert Vannice, M., Appl. Catal., A, 1994. 113: p. 59.
100. Huck, W.-R.M., T.; Baiker, A., Adv. Synth. Catal., 2003. 345: p. 255.
101. Schmidt, E.V., A.; Mallat, T.; Baiker, A., J. Am. Chem. Soc., 2009. 131: p. 12358.
102. Rajashekharam, M.V.B., I.; Fouilloux, P.; Schweich, D.; Delmas, H.; Chaudhari, R. V., Catal. Today, 1999. 48: p. 83.
103. Gao, F.A., A. D.; Zhang, H.; Cheng, S.; Garland, M., J. Catal., 2006. 241: p. 189.
104. Bergault, I.R., M. V.; Chaudhari, R. V.; Schweich, D.; Delmas, H., Chem. Eng. Sci., 1997. 52: p. 4033.
105. Bergault, I.F., P.; Joly-Vuillemin, C.; Delmas, H., J. Catal., 1998. 175: p. 328.
106. Bergault, I.J.-V., C.; Fouilloux, P.; Delmas, H., Catal. Today, 1999. 48: p. 161.
107. Alotaibi, M., E. Kozhevnikova, and I. Kozhevnikov, *Efficient hydrodeoxygenation of biomass-derived ketones over bifunctional Pt-polyoxometalate catalyst.* Chemical Communications, 2012.
108. Procházková, D., et al., *Hydrodeoxygenation of aldehydes catalyzed by supported palladium catalysts.* Applied Catalysis A: General, 2007. 332(1): p. 56-64.
109. Ferri, D., T. Bürgi, and A. Baiker, *Pt and Pt/Al2O3 Thin Films for Investigation of Catalytic Solid–Liquid Interfaces by ATR-IR Spectroscopy: CO Adsorption, H2-Induced Reconstruction and Surface-Enhanced Absorption.* The Journal of Physical Chemistry B, 2001. 105(16): p. 3187-3195.
110. Somorjai, G.A. and G. Rupprechter, *Molecular studies of catalytic reactions on crystal surfaces at high pressures and high temperatures by infrared-visible sum frequency generation (SFG) surface vibrational spectroscopy.* The Journal of Physical Chemistry B, 1999. 103(10): p. 1623-1638.
111. Somorjai, G.A., Introduction to Surface Chemistry and Catalysis (John Wiley), 1994.
112. Meier, R.J., *Vibrational spectroscopy: a 'vanishing' discipline?* Chemical Society Reviews, 2005. 34(9): p. 743-752.
113. Stavitski, E. and B.M. Weckhuysen, *Infrared and Raman imaging of heterogeneous catalysts.* Chemical Society Reviews, 2010. 39(12): p. 4615-4625.
114. Wachs, I.E. and C.A. Roberts, *Monitoring surface metal oxide catalytic active sites with Raman spectroscopy.* Chemical Society Reviews, 2010. 39(12): p. 5002-5017.

115. Hunger, M. and J. Weitkamp, *In situ IR, NMR, EPR, and UV/Vis Spectroscopy: Tools for New Insight into the Mechanisms of Heterogeneous Catalysis.* Angewandte Chemie International Edition, 2001. 40(16): p. 2954-2971.
116. Lesage, T., et al., *Studying the NOx-trap mechanism over a Pt-Rh/Ba/Al2O3 catalyst by operando FT-IR spectroscopy.* Phys. Chem. Chem. Phys., 2003. 5(20): p. 4435-4440.
117. Saussey, J. and J.C. Lavalley, *An in situ FT-IR study of adsorbed species on a Cu-ZnAl2O4 methanol catalyst under 1 MPa pressure and at 525 K: effect of the H2/CO/CO2 feed stream composition.* Journal of Molecular Catalysis, 1989. 50(3): p. 343-353.
118. Urakawa, A., N. Maeda, and A. Baiker, *Space- and Time-Resolved Combined DRIFT and Raman Spectroscopy: Monitoring Dynamic Surface and Bulk Processes during NOx Storage Reduction.* Angewandte Chemie, 2008. 120(48): p. 9396-9399.
119. Grunwaldt, J.-D., et al., *Comparative Study of Au/TiO2 and Au/ZrO2 Catalysts for Low-Temperature CO Oxidation.* Journal of Catalysis, 1999. 186(2): p. 458-469.
120. Schild, C., et al., *Carbon dioxide hydrogenation over nickel/zirconia catalysts from amorphous precursors: on the mechanism of methane formation.* The Journal of Physical Chemistry, 1991. 95(16): p. 6341-6346.
121. Maeda, N., A. Urakawa, and A. Baiker, *Support Effects and Chemical Gradients along the Catalyst Bed in NOx Storage-Reduction Studied by Space- and Time-Resolved In Situ DRIFTS.* The Journal of Physical Chemistry C, 2009. 113(38): p. 16724-16735.
122. Weigel, J., et al., *Surface Species in CO and CO2 Hydrogenation over Copper/Zirconia: On the Methanol Synthesis Mechanism.* Langmuir, 1996. 12(22): p. 5319-5329.
123. Ryczkowski, J., *IR spectroscopy in catalysis.* Catalysis Today, 2001. 68(4): p. 263-381.
124. Andanson, J.-M. and A. Baiker, *Exploring catalytic solid/liquid interfaces by in situ attenuated total reflection infrared spectroscopy.* Chemical Society Reviews, 2010. 39(12): p. 4571-4584.
125. Bürgi, T. and A. Baiker, *Attenuated Total Reflection Infrared Spectroscopy of Solid Catalysts Functioning in the Presence of Liquid-Phase Reactants*, in *Advances in Catalysis*, C.G. Bruce and K. Helmut, Editors. 2006, Academic Press. p. 227-283.
126. Urakawa, A., et al., *ATR-IR Flow-Through Cell for Concentration Modulation Excitation Spectroscopy: Diffusion Experiments and Simulations.* The Journal of Physical Chemistry B, 2003. 107(47): p. 13061-13068.
127. Baurecht, D.F., U. P., ReV. Sci. Instrum., 2001. 72: p. 3782.
128. Urakawa, A., T. Bürgi, and A. Baiker, *Sensitivity enhancement and dynamic behavior analysis by modulation excitation spectroscopy: Principle and application in heterogeneous catalysis.* Chemical Engineering Science, 2008. 63(20): p. 4902-4909.
129. Maeda, N., K. Hungerbühler, and A. Baiker, *Asymmetric Hydrogenation on Chirally Modified Pt: Origin of Hydrogen in the N–H–O Interaction between Cinchonidine and Ketone.* Journal of the American Chemical Society, 2011. 133(49): p. 19567-19569.
130. Maeda, N., et al., *Heterogeneous Asymmetric Hydrogenation of Activated Ketones: Mechanistic Insight into the Role of Alcohol Products by in Situ Modulation-Excitation IR Spectroscopy.* The Journal of Physical Chemistry C, 2012. 116(6): p. 4182-4188.
131. Meemken, F., et al., *Heterogeneous Asymmetric Hydrogenation of Prochiral Alkenoic Acid: Origin of Rate and Enantioselectivity Enhancement by Amine Addition.* ACS Catalysis, 2012. 2(3): p. 464-467.
132. Meemken, F., et al., *Platinum-Catalyzed Asymmetric Hydrogenation: Spectroscopic Evidence for an O-H-O Hydrogen-Bond Interaction between Substrate and Modifier.* Angewandte Chemie International Edition, 2012. 51(33): p. 8212-8216.

133. **Schimmoeller, B., et al., *Fine tuning the surface acid/base properties of single step flame-made Pt/alumina.* Applied Catalysis A: General, 2010. 374(1–2): p. 48-57.**
134. **Schimmoeller, B., et al., *Structure of flame-made vanadia/titania and catalytic behavior in the partial oxidation of o-xylene.* Journal of Catalysis, 2008. 256(1): p. 74-83.**
135. **Chen, C.-S.C., H.-W.; Cheng, W.-H., Appl. Catal., A, 2003. 248: p. 117.**
136. **Andanson, J.-M.B., A., Chem. Soc. Rev., 2010. 39: p. 4517.**
137. **Bürgi, T.B., A., Adv. Catal., 2006. 50: p. 227.**
138. **Bürgi, T.B., A., J. Phys. Chem. B, 2002. 106: p. 10649.**
139. **Maeda, N.H.h., K.; Baiker, A., J. Am. Chem. Soc., 2011. 133: p. 19567.**
140. **Maeda, N.S., S.; Mallat, T.; Hungerbühler, K.; Baiker, A., J. Phys. Chem. C, 2012. 116: p. 4182.**
141. **Gambi, A., et al., *Infrared studies of acetophenone and its deuterated derivatives.* Spectrochimica Acta Part A: Molecular Spectroscopy, 1980. 36(10): p. 871-878.**
142. **Huang, H.G., et al., *Vibrational studies of the reactions of acetophenone with Si(100)-2×1.* Chemical Physics Letters, 2005. 414(1–3): p. 143-147.**
143. **Raskó, J. and J. Kiss, *Adsorption and surface reactions of acetaldehyde on TiO2, CeO2 and Al2O3.* Applied Catalysis A: General, 2005. 287(2): p. 252-260.**
144. **Greenler, R.G., *Infrared study of adsorbed molecules on metal surfaces by reflection techniques.* The Journal of Chemical Physics, 1966. 44: p. 310.**
145. **Shin-ya, K., et al., *Absolute Configuration and Conformation Analysis of 1-Phenylethanol by Matrix-Isolation Infrared and Vibrational Circular Dichroism Spectroscopy Combined with Density Functional Theory Calculation.* The Journal of Physical Chemistry A, 2007. 111(35): p. 8598-8605.**
146. **Basset, J.M., et al., *A study of benzene hydrogenation and identification of the adsorbed species with PtAl2O3 catalysts.* Journal of Catalysis, 1975. 37(1): p. 22-36.**
147. **Lebedeva, N.P., et al., *Role of Crystalline Defects in Electrocatalysis: CO Adsorption and Oxidation on Stepped Platinum Electrodes As Studied by in situ Infrared Spectroscopy.* The Journal of Physical Chemistry B, 2002. 106(38): p. 9863-9872.**
148. **Schmidt, E., et al., *Metal–support interaction in Pt/alumina: Inversion of diastereoselectivity by tuning the acid–base properties of the support.* Journal of Catalysis, 2010. 274(2): p. 117-120.**
149. **Remans, T., et al., *Handbook of Heterogeneous Catalysis*. 2008, Wiley-VCH Verlag GmbH & Co. KGaA, Weinheim, Germany.**
150. **Stakheev, A.Y. and L.M. Kustov, *Effects of the support on the morphology and electronic properties of supported metal clusters: modern concepts and progress in 1990s.* Applied Catalysis A: General, 1999. 188(1–2): p. 3-35.**
151. **Hoxha, F., et al., *Influence of support acid–base properties on the platinum-catalyzed enantioselective hydrogenation of activated ketones.* Journal of Catalysis, 2010. 271(1): p. 115-124.**
152. **Oudenhuijzen, M.K., et al., *Three-Site Model for Hydrogen Adsorption on Supported Platinum Particles: Influence of Support Ionicity and Particle Size on the Hydrogen Coverage.* Journal of the American Chemical Society, 2005. 127(5): p. 1530-1540.**
153. **Johannessen, T., et al., *Flame Synthesis of Nanoparticles: Applications in Catalysis and Product/Process Engineering.* Chemical Engineering Research and Design, 2004. 82(11): p. 1444-1452.**

154. Schimmoeller, B., et al., *Structure of flame-made vanadia/silica and catalytic behavior in the oxidative dehydrogenation of propane.* Journal of Catalysis, 2010. 274(1): p. 64-75.
155. Baurecht, D., I. Porth, and U.P. Fringeli, *A new method of phase sensitive detection in modulation spectroscopy applied to temperature induced folding and unfolding of RNase A.* Vibrational Spectroscopy, 2002. 30(1): p. 85-92.
156. de Mallmann, A. and D. Barthomeuf, *Change in benzene adsorption with acidobasicity of (Cs,Na)X zeolites studied by i.r. spectroscopy.* Zeolites, 1988. 8(4): p. 292-301.
157. Condirston, D. and J. Laposa, *Vibrational spectra of styrene-H8,-D3,-D5, and-D8.* Journal of Molecular Spectroscopy, 1976. 63(3): p. 466-477.
158. Hong, D.-Y., et al., *Hydrodeoxygenation and coupling of aqueous phenolics over bifunctional zeolite-supported metal catalysts.* Chemical Communications, 2010. 46(7): p. 1038-1040.
159. Hicks, J.C., *Advances in C–O Bond Transformations in Lignin-Derived Compounds for Biofuels Production.* The Journal of Physical Chemistry Letters, 2011. 2(18): p. 2280-2287.
160. Ruiz, P.E., et al., *Relevance of sulfiding pretreatment on the performance of Re/ZrO2 and Re/ZrO2-sulfated catalysts for the hydrodeoxygenation of guayacol.* Applied Catalysis A: General, 2010. 384(1–2): p. 78-83.
161. Chakraborty, B. and B. Viswanathan, *Surface acidity of MCM-41 by in situ IR studies of pyridine adsorption.* Catalysis Today, 1999. 49(1–3): p. 253-260.
162. Mokaya, R., et al., *Acidity and catalytic activity of the mesoporous aluminosilicate molecular sieve MCM-41.* Catalysis Letters, 1996. 37(1-2): p. 113-120.
163. Jentys, A., N.H. Pham, and H. Vinek, *Nature of hydroxy groups in MCM-41.* Journal of the Chemical Society, Faraday Transactions, 1996. 92(17): p. 3287-3291.
164. Corma, A., A. Martínez, and V. Martínez-Soria, *Hydrogenation of Aromatics in Diesel Fuels on Pt/MCM-41 Catalysts.* Journal of Catalysis, 1997. 169(2): p. 480-489.
165. Mathew, N.T., et al., *Rearrangement of allyl phenyl ether over Al-MCM-41.* Journal of Catalysis, 2005. 229(1): p. 105-113.
166. Luan, Z., et al., *Mesopore Molecular Sieve MCM-41 Containing Framework Aluminum.* The Journal of Physical Chemistry, 1995. 99(3): p. 1018-1024.
167. Chen, C.-Y., H.-X. Li, and M.E. Davis, *Studies on mesoporous materials: I. Synthesis and characterization of MCM-41.* Microporous Materials, 1993. 2(1): p. 17-26.
168. Solymosi, F., *Importance of the Electric Properties of Supports in the Carrier Effect.* Catalysis Reviews, 1968. 1(1): p. 233-255.
169. Barshad, Y., X. Zhou, and E. Gulari, *Carbon monoxide oxidation under transient conditions: A fourier-transform infrared transmission spectroscopy study.* Journal of Catalysis, 1985. 94(1): p. 128-141.
170. Barth, R. and A. Ramachandran, *Temperature effects on the infrared spectrum of carbon monoxide adsorbed by supported platinum.* Journal of Catalysis, 1990. 125(2): p. 467-471.
171. Barth, R., et al., *Thermal desorption-infrared study of carbon monoxide adsorption by alumina-supported platinum.* Journal of Catalysis, 1989. 116(1): p. 61-70.
172. Primet, M., *Electronic transfer and ligand effects in the infrared spectra of adsorbed carbon monoxide.* Journal of Catalysis, 1984. 88(2): p. 273-282.
173. Zafeiratos, S., et al., *The effect of Mo oxides and TiO2 support on the chemisorption features of linearly adsorbed CO on Pt crystallites: an infrared and photoelectron spectroscopy study.* Journal of Catalysis, 2005. 232(1): p. 127-136.

174. **Tanaka, K. and J.M. White, *Infrared studies of CO adsorption on reduced and oxidized PtTiO2.* Journal of Catalysis, 1983. 79(1): p. 81-94.**
175. **Kitamura, F., et al., *CO adsorption on Pt(111) and Pt(100) single crystal surfaces in aqueous solutions studied by infrared reflection-absorption spectroscopy.* Chemical Physics Letters, 1987. 142(5): p. 318-322.**
176. **Stakheev, A.Y., et al., *Evidence for Monatomic Platinum Species in H-ZSM-5 from FTIR Spectroscopy of Chemisorbed CO.* Journal of Catalysis, 1997. 169(1): p. 382-388.**
177. **Sachtler, W.M.H., and Stakheev, A. Yu., Catal. Today, 1992. 12: p. 283.**
178. **Sachtler, W.M.H., *Metal clusters in zeolites: an intriguing class of catalysts.* Accounts of Chemical Research, 1993. 26(7): p. 383-387.**
179. **Lin, S.D. and M.A. Vannice, *Hydrogenation of Aromatic Hydrocarbons over Supported Pt Catalysts .I. Benzene Hydrogenation.* Journal of Catalysis, 1993. 143(2): p. 539-553.**
180. **Lin, S.D. and M.A. Vannice, *Hydrogenation of Aromatic Hydrocarbons over Supported Pt Catalysts .II. Toluene Hydrogenation.* Journal of Catalysis, 1993. 143(2): p. 554-562.**
181. **Lin, S.D. and M.A. Vannice, *Hydrogenation of Aromatic Hydrocarbons over Supported Pt Catalysts .III. Reaction Models for Metal Surfaces and Acidic Sites on Oxide Supports.* Journal of Catalysis, 1993. 143(2): p. 563-572.**
182. **Bridgwater, A.V., Czernik, S., Piskorz, J., in: A.V. Bridgwate (Ed.), ed. *Fast pyrolysis of biomass: A handbook*. CPL Press ed. Vol. Volume 2. 2002: Newbury. 1-19.**
183. **Wang, W., et al., *Amorphous Co–Mo–B catalyst with high activity for the hydrodeoxygenation of bio-oil.* Catalysis Communications, 2011. 12(6): p. 436-440.**
184. **Oudenhuijzen, M.K., et al., *Theoretical Study on Pt Particle Adsorbate Bonding: Influence of Support Ionicity and Implications for Catalysis.* The Journal of Physical Chemistry B, 2004. 108(52): p. 20247-20254.**
185. **Haffad, D., et al., *Reduction of Benzaldehyde on Metal Oxides.* Journal of Catalysis, 1997. 172(1): p. 85-92.**
186. **Saadi, A., et al., *Benzaldehyde hydrogenation over supported nickel catalysts.* Journal of Molecular Catalysis A: Chemical, 2006. 253(1–2): p. 79-85.**
187. **Perret, N., F. Cárdenas-Lizana, and M.A. Keane, *Selective hydrogenation of benzaldehyde to benzyl alcohol over Au/Al2O3.* Catalysis Communications, 2011. 16(1): p. 159-164.**